

**EXPLORING THE ENIGMATIC ROLE OF
EPSTEIN-BARR VIRUS IN
NEUROINFLAMMATION AND
NEURODEGENERATION ASSOCIATED
WITH ALZHEIMER'S DISEASE**

Ph.D. Thesis

By
DEEKSHA TIWARI



**DEPARTMENT OF BIOSCIENCES AND BIOMEDICAL
ENGINEERING
INDIAN INSTITUTE OF TECHNOLOGY INDORE
APRIL 2022**

EXPLORING THE ENIGMATIC ROLE OF EPSTEIN-BARR VIRUS IN NEUROINFLAMMATION AND NEURODEGENERATION ASSOCIATED WITH ALZHEIMER'S DISEASE

A THESIS

*Submitted in partial fulfillment of the
requirements for the award of the degree
of*
DOCTOR OF PHILOSOPHY

by
DEEKSHA TIWARI



**DEPARTMENT OF BIOSCIENCES AND BIOMEDICAL
ENGINEERING
INDIAN INSTITUTE OF TECHNOLOGY INDORE
APRIL 2022**



INDIAN INSTITUTE OF TECHNOLOGY INDORE

I hereby certify that the work which is being presented in the thesis entitled **EXPLORING THE ENIGMATIC ROLE OF EPSTEIN-BARR VIRUS IN NEUROINFLAMMATION AND NEURODEGENERATION ASSOCIATED WITH ALZHEIMER'S DISEASE** in the partial fulfillment of the requirements for the award of the degree of **DOCTOR OF PHILOSOPHY** and submitted in the **DEPARTMENT OF BIOSCIENCES AND BIOMEDICAL ENGINEERING, Indian Institute of Technology Indore**, is an authentic record of my own work carried out during the time period from July 2017 to April 2022 under the supervision of **Dr. Hem Chandra Jha**, Assistant Professor, Department of Biosciences and Biomedical Engineering.

The matter presented in this thesis has not been submitted by me for the award of any other degree of this or any other institute.

Deeksha Tiwari
13.6.2022

**Signature of the student with date
(DEEKSHA TIWARI)**

This is to certify that the above statement made by the candidate is correct to the best of my/our knowledge.

Hem Chandra Jha

(13.06.2022)

Signature of Thesis Supervisor with date

(HEM CHANDRA JHA)

DEEKSHA TIWARI has successfully given his/her Ph.D. Oral Examination held on **16.11.2022**.

Signature of Thesis Supervisor with date

(HEM CHANDRA JHA)



INDIAN INSTITUTE OF TECHNOLOGY INDORE

REPORT OF PH.D. THESIS ORAL EXAMINATION (Form PTS 6)

Name of Student: Deeksha Tiwari Roll No.: 1701171004

Discipline: Biosciences and Biomedical Engineering

Date of Joining the PhD Program: 07-07-2017

Date of Confirmation to the PhD Program: 25-07-2017

Date of OPEN SEMINAR: 29-04-2022

Date of ORAL EXAMINATION*: 16-11-2022

Thesis Title: Exploring the enigmatic role of Epstein-Barr virus (EBV) in mediating neuroinflammation and neurodegeneration associated with Alzheimer's Disease (AD)

Thesis Supervisor(s): 1. Dr. Hem Chandra Jha

Report of the Board:

1. Necessary modifications suggested by the thesis examiners have been incorporated.

YES/ NO

2. Authenticate the work as the students' own:

YES/ NO

3. Comments (elicit the candidate's replies to the questions raised by the thesis examiners and judge if the presentation of the work by the student and the answers to the questions asked have been satisfactory):
(Continue on reverse, if necessary)

The seminar presentation was very good. Slides were very good too.

The question - answering session went well. The answers were satisfactory.

4. The candidate has PASSED/ FAILED in the PhD ORAL EXAMINATION

ORAL EXAMINATION BOARD

Name and Affiliation of the Examiners	Signature with date
1. DR. SUDIP K. GHOSH PROFESSOR, DEPT. OF BIOTECHNOLOGY IIT KHARAGPUR	<i>Sudip Ghosh</i> 18.11.2022
2. DR. HEM CHANDRA JHA Associate Prof, BSBE, IIT Indore	<i>H Jha</i> 18/11/2022
3. DR. SANDEEP CHAUDHARY PROFESSOR, CIVIL ENGG DEPTT, IIT INDORE	<i>S Chg</i> 18.11.2022
4. Dr. Rajesh Kumar Professor, physics, PSpC member.	<i>R Kumar</i> 18/11/2022
5. Dr Abhijeet Joshi Associate Professor, PSpC member, BSBE	<i>Ab Joshi</i> 18/11/22
6. DR. M. Tanveer Associate Professor, PSpC member, Maths	<i>M Tanveer</i> 18/11/2022
7.	
8.	

Schaughy
18.11.2022

(Signature of Chairman, PhD ORAL EXAMINATION BOARD with date)

For Office Use Only

Course Units:

CPI:

The candidate has met all the requirements for the award of the PhD degree and be issued provisional Degree after submission of Hard bound copies of the Thesis and the No Dues Certificate.

Date:

Deputy / Assistant Registrar (Academic)

ACKNOWLEDGEMENTS

“If you are on the right path, it will always be uphill.”

If my Ph.D. journey has taught me anything, it is not to give up when the going gets tough. Naturally, these five years of Ph.D. accompanied a fair share of highs and lows, but I was able to trudge the path with ease due to the unconditional support of my family and friends. Hence, through this acknowledgment section of “the fruit of my five years' worth of efforts,” I would first like to thank them for their unwavering faith in me. I would especially like to acknowledge the efforts of my parents; my mother, Mrs. Deepa Tiwari, who has always inspired me to make a mark of my own in this world, and my father, Mr. Pradeep Tiwari, whose unshakable optimism is infectious. A special mention to “my support system” and my partner in crime, my brother, Mr. Balark Tiwari, is a must, who kept me on my toes and always encouraged me to push beyond my limits. Being a research scholar himself, he has always pushed me to look at things from another angle. It would not have been possible for me to see the end of this journey without you people. It is rightly said that children inherit the intellect and integrity passed down through the generations. On that note, I would like to thank my grandparents for always being there and lifting my spirits by sharing their experiences. I want to make a special mention of my grandfather, Mr. Shiv Mangal Tiwari (baba), who being an academician himself, was my first introduction to the world of books and education. He has always supported my endeavors and applauded even the tiniest of my victories. Thank you, baba, for celebrating those wins with me and creating memories that strengthened me during my lows. Above all, I would like to acknowledge Mr. Rahul Kakani for being my “Hanuman Ji” and reminding me of my capabilities when I was doubtful and unsure about what I could accomplish.

I want to express my deep gratitude toward my extended family: my friends. First, I would like to thank my closest confidants, lab mates, and my first collaborators, Dr. Shweta Jakhmola and Dr. Omkar Indari for being my pillars of strength and my critiques. I learned a lot from you guys and will always cherish the times spent with you two. The journey of five years was a delight because of your company in and out of the lab. Apart from these two, I would like to thank all my juniors in the Infection Bioengineering Group for creating a lively and conducive environment in the lab that helped me grow as a researcher. Mr. Dharmendra Kashyap, Mr. Budhadev Baral, Miss. Nidhi Varshney, Miss. Annu Rani, Mr. Tarun Prakash Verma, I thank all of you for being a part of this enlightening journey. Though, I got very little time with the new additions to the family Miss. Meenakshi Kandpal, and Mr. Prateek Kundu, it was a pleasure interacting with you. My list of friends to be appreciated would be incomplete without mentioning Mr. Sumit Kundu, Mrs. Chanchal Rana Kundu, and the adorable bundle of joy Avni Kundu. Their abode was a place of comfort for me on the campus, a home away from home. I thank you all for the homely food and feeling I got to share there. Some people make your life fun by just being around, and I like to thank all my Ph.D. batchmates for that. Miss. Kanchan Samadhia, Dr. Mrinal Kashyap, Mr. Arjun Meda, Dr. Rajoshree Roy, Dr. M.D. Fulbabu are just a few crucial names on the list to be acknowledged. However, the list does not end with them, and I would particularly like to acknowledge all the support and motivation I received during this tenure from

Mr. Dhananjay Mishra and Mr. Bhaskar Sharma. These two have always been the ones to lift my spirits when the road seems gloomy and dark. Last but not least, I also have to thank Miss. P.V. Soumya, and Dr. Shephali Bansod for being “my person” now and forever.

I shall extend my gratitude, especially to my Ph.D. supervisor Dr. Hem Chandra Jha, who gave me the opportunity to go through this beautiful journey towards enlightenment. I feel fortunate to have such a guide with infectious enthusiasm and dedication toward work. I cannot thank him enough for always inspiring and pushing me to think beyond the obvious. Developing my research acumen would have been inefficient without his out-of-the-box insights, which drove me to break the bounds of convention and think the unthinkable. In this scholarly adventure, I also got to interact and learn from numerous collaborators at various institutes in and out of the country. I would particularly like to appreciate the efforts of Dr. Rajesh Kumar (HOD, Physics, IIT Indore), Dr. Suman Tapryal, Dr. Vikas Kumar (Central University of Rajasthan), Dr. Gaurava Srivastava, and Dr. Imran Siddiqi (CDRI, Lukhnow), Dr. Nitish Mittal (University of Basel), and Dr. Jayabalan Jesumony (RRCAT, Indore) for helping me on the path to producing meaningful research outputs. I am genuinely grateful for the constant critical and insightful inputs given by the members of my PSPC committee here at IIT Indore, Dr. Rajesh Kumar, Dr. M. Tanveer, and Dr. Abhijeet Joshi.

Further, I would like to extend my gratitude to the entire BSBE family, Dr. Amit Kumar (HOD, BSBE), and the office staff for supporting me throughout my tenure and making it comfortable and convenient. My sincerest thanks to the Sophisticated Instrumentation Centre (IIT Indore) for providing the facilities for my research endeavors. I would also like to acknowledge the Ministry of Human Resources Development (MHRD), Govt. of India, for providing me the financial assistance during the entire tenure of my Ph.D.

At last, I would like to thank the Almighty for giving me the chance and fortitude to bring this journey to fruition and pray for his guidance throughout the life ahead.

Besides this, I have to thank the innumerable people who supported my adventure directly or indirectly. I wish I could thank each of you individually for all your efforts, but time and space compel me to stop here.

-Deeksha Tiwari

Dedicated
to
the first spark of exploration
ever ignited in me

SYNOPSIS

1.1. Introduction

1.1.1. Epstein-Barr virus (EBV) and associated spectrum of diseases

The members of the *Herpesviridae* family have long been known for their neuroinvasive potential and are linked with various disorders of the Central nervous system (CNS), such as encephalitis, neuritis, cerebral lymphoma, myelitis, etc. [1]. However, the neurotropic potential of the Human Herpesvirus 4 (HHV-4) in particular has only been recently established *in-vitro* [2], [3]. HHV-4, also known as Epstein-Barr virus (EBV), is primarily considered an oncogenic lymphotropic virus that infects B-cells and epithelial cells to establish lifelong latency. It has been prominently associated with a heterogeneous group of malignancies such as Burkitt's, Hodgkin's, non-Hodgkin's lymphoma, nasopharyngeal carcinoma, gastric cancer adenocarcinomas, etc. [4]. Though EBV's ability to cause neurodegeneration has been debated for decades, multiple clinical and *in-vivo* studies have recently provided convincing evidence of its involvement in neurodegenerative disorders (NDDs) like multiple sclerosis (MS), Alzheimer's (AD), Parkinson's disease (PD), chronic fatigue syndrome (CFS), and so on [5]. Various studies have reported a robust anti-EBV antibody response in the serological and cerebrospinal fluid (CSF) samples collected from patients suffering from NDDs, thus indicating a strong association between EBV and NDDs [6], [7].

Neurotropic herpesviruses such as EBV are believed to gain entry into the CNS via hematogenous dissemination or directly crossing through the blood-brain barrier (BBB) by infecting the peripheral nerve endings and disseminating in the brain in a retrograde fashion [5]. Interestingly, our latest findings corroborated the EBV's capability to infect neurons, glial cells, and the endothelial cells of the BBB [2], [3], [8], [9]. Either way, the entry of EBV into the CNS elicits a neuroinflammatory response mediated by glial cells as the first step towards neurodegeneration which goes on to incur neuronal damage, thereby leading to

the characteristic pathology of the NDDs. Though EBV is a ubiquitous virus infecting ~90% of the global adult population, only a handful develop fatal consequences such as NDDs. An individual's native immune status is crucial in susceptibility to such severe outcomes. However, what triggers the onset of these cataclysmic events is still not fully understood [10], [11]. Therefore, it is imperative to understand how EBV could lead to neurodegeneration. In our study, we tried to address the involvement of EBV in AD, a NDD with the highest global burden so far.

1.1.2. The viral hypothesis in Alzheimer's disease

Alois Alzheimer first characterized AD as a progressive brain deterioration resulting in cognitive impairment [12]. Pathological signs, among many others, such as the formation of proteinaceous aggregate (of amyloid- β , τ -protein, and α -synuclein) in the brain and a gradual decline in cognitive abilities, including memory, are now considered the hallmarks of AD [13]. Though the disease pathophysiology is well established, its initiation and development mechanisms are still under investigation. Various hypotheses were put forward to explain the disease's causation through the decades. One of the most notable and controversial is viral infections in the brain as an inducer of degenerative changes associated with AD [14]. Multiple *in-vivo* and *in-vitro* studies, along with clinical records of population cohorts, indicating a strong probable association between the two, have reignited the enthusiasm of the scientific community for the hypothesis [7], [15], [16]. These observations collectively advocate that many AD hallmarks, such as neuroinflammation and aggregate formation, are initiated as a defensive measure against acute viral infection in the brain [17]. In fact, several studies have suggested that certain peptides generated from proteasomal cleavage of viral proteins possess amyloidogenic tendencies [18], [19]. However, a chronic infection could lead to a maladaptive response causing self-harm, presenting as NDDs [20]. Further, certain host genetic factors, such as the presence of a specific variant of apolipoproteins, ApoE, which is considered a risk factor for AD development [21], also deem an individual highly susceptible to herpesvirus infections [22], [23].

Interestingly, contemporary research has suggested cell-cycle dysregulation in neurons is integral to AD [24]. Terminally differentiated neurons in the adult human brain are supposed to be resting in the G₀ phase of the cell cycle. However, reports have shown that if somehow triggered to re-enter the cell cycle, they die instead of duplicating due to the abortive cell cycle [25]. Multiple *in-vitro* and *in-vivo* studies on AD models have demonstrated the presence of markers indicating the ongoing cell cycle in the adult neuron [26]–[29]. Furthermore, being an oncogenic virus, EBV has an indisputable capability to manipulate the host cell cycle. Various EBV proteins such as EBV nuclear antigens (EBNA-1, 2, 3) [30], [31], latent membrane proteins (LMP-1, 2a, 2b) [32]–[35], and several other viral transcripts (EBER, BZLF1, etc.) [36] are implicated in modulating the host cell cycle at different stages. Latest experimental evidence of EBV’s capability to infect neuronal cells can be extrapolated to imply a probable link between EBV-mediated cell cycle dysregulation in neurons and AD.

Though the association of EBV with AD has constantly been under question, our research findings and literature-based reports suggest otherwise. Therefore, there is a pressing need to elucidate the details of EBV’s involvement in mediating AD pathophysiology.

1.2. Scope and Objectives of the Research

1.2.1. Scope

EBV infection in the neural milieu could lead to a number of pathophysiologies. Neurons subjected to the viral infection could either undergo abortive cell-cycle re-entry leading to neurodegeneration or die following another pathway. Whereas infection in the glial cells might incur inflammatory response causing aggravation of degenerative conditions, thereby facilitating neuronal insult. However, the association of EBV with AD has been debated and remains underexplored. Therefore, it is crucial to understand the response of the CNS cells to EBV infection and what sequential events occur afterward that result in degenerative pathophysiologies associated with AD. The objectives listed below are formulated to address the hypothesis mentioned above to unravel the mechanistic role of EBV infection in AD.

1.2.2. Objectives

- Understanding the involvement of EBV in aggregate formation: a characteristic pathology of AD
- Investigating the biochemical effect of EBV infection in glial cells, which may mediate indirect insult to the neurons causing degeneration
- Employing an *in-silico* approach to study probable interaction between viral and host proteins conspiring to create a deleterious microenvironment in neuronal milieu culminating in AD
- Attempting to target various aspects of EBV infection in the neural milieu to hinder the progression of neurodegeneration using computational tools

1.2.3. Chapters

Chapter 1: Does the Epstein-Barr virus has the potential to initiate the neurodegenerative pathology (aggregate formation) associated with Alzheimer's disease?

Chapter 2: Investigating the biochemical response in microglial cells upon EBV infection through Raman microspectroscopy

Chapter 3: Examining the probable interaction of apolipoprotein variant E (ApoE) with Epstein-Barr virus proteins

Chapter 4: Identification of potential phytochemical inhibitors of EBV-*dUTPase* to target EBV mediated neuropathologies: a potential therapeutic approach

1.3. Summary of the Results and Conclusions

The study from Chapter 1 of this work illustrates the possibility of EBV infection playing a crucial role in developing AD pathophysiology via the viral peptides generated through cellular proteasomal activity in amalgamation with other infection-induced events. Initial *in-silico* analysis of ~100 viral proteins using online aggregation prediction servers like AGGRESCAN and TANGO identified multiple candidates with aggregate formation tendency. The protein candidates were further screened based on their comparative aggregation score with positive control amyloid- β (A β) and hydrophobicity values. The screened proteins were then subjected to online servers such as NetChop3.0 and PCleavage, predicting cleavage sites present on the entire protein. The individual peptides thus formed were again evaluated for their aggregation score using AGGRESCAN and TANGO, which gave us a 12 amino-acid long peptide generated from glycoprotein-M (EBV-gM₁₄₆₋₁₅₇) of the EBV as a potential candidate having higher aggregation tendencies compared to A β .

The follow-up *in-vitro* experiments performed on EBV-gM₁₄₆₋₁₅₇ corroborated the hypothesis. A correlation between aggregate formation and viral infection is strongly depicted by Congo-red staining along with concentration and time-dependent evolution of fluorescence seen through Thioflavin-S staining of the aggregates. The Raman signals displaying the presence of higher β -sheet conformation and cytotoxicity of aggregates against neurons (IMR-32) support the above-mentioned claim. Based on these results, a mechanism for viral protein processing inside the host cell leading to the formation of proteinaceous aggregates has been proposed and explained in this study. This operational insight provides a novel outlook on how the infection of EBV could lead to the characteristic neurodegenerative pathology of AD. However, the conjecture needs to be explored further in detail with more *in-vitro* and *in-vivo* studies.

After establishing the effect of EBV on the neuronal microenvironment, in Chapter 2, we went on to study the effects of EBV infection in glial cells using Raman spectroscopy (RS). Previous reports have indicated that the RS could be utilized as an efficient tool to discern the altered biochemistry of the cell upon infection. We carried out time-dependent (early: 2, 4, 6, hours post-infection; late: 12, 24, 36 hpi) *in-vitro* spatial Raman spectroscopy on microglial cells

(HMC-3) at different cellular locations, namely nuclear and peripheral. Our analysis showed the temporal evolution of EBV infection, enabling us to understand the virus's influencing mechanism. In brief, the investigation directed us to believe that EBV enters the microglial cells probably in the first 2 hpi by utilizing PIP-dependent signalling pathways. The Raman spectrum data obtained shows that it probably takes up to 6 hpi for the virus to reach inside and manipulate the nuclear microenvironment of microglial cells. Moreover, during its nuclear hijack process from 6 to 12 hpi, our data shows signs of glycogen and amino acid metabolism manipulation by the virus. Later, the Raman signals recorded during 12–24 hpi indicate that the virus's replication and cellular transport processes are still being carried on in microglial cells. It is only after 24 hpi that viral packaging and egress are initiated. Thus, the study aided us in furthering our understanding of the involvement of different biomolecules at various stages of EBV infection progression in microglial cells. With further advances in technology in the future, the application of RS could extend to differentiating the viral infection stages in clinical settings and help in non-invasive and early disease diagnosis. The temporal and spatial Raman spectroscopic technique appears to be a forward step toward understanding the viral biology after infection in host cells and assisting in a comparative analysis of replication kinetics in different cells on infection with multitrophic viruses such as EBV.

Further, in Chapter 3, we examined how EBV could interact with host proteins strongly associated with an individual's increased susceptibility to AD. The most prevailing disease hypothesis implicated Apolipoprotein E (ApoE) as a risk factor in the disease pathology. ApoE essentially carries out the lipid transport across the cell and is believed to be involved in A β aggregation and clearance. Interestingly, humans possess multiple isoforms of the ApoE, namely, ApoE2, ApoE3, and ApoE4. Among these variants, ApoE3 is the healthy isoform found in ~78% of the population, which most efficiently binds and sequester A β fragments. Therefore, we hypothesized that a possible interaction of ApoE3 in healthy individuals with EBV proteins could hijack the normal functioning of ApoE3 and, therefore, could result in the accumulation of unbound A β ₄₂. This free-floating A β ₄₂ in the cell cytoplasm could give rise to proteinaceous plaques, developing AD-related pathology.

To test our hypothesis, we evaluated the binding efficiency of various EBV proteins with ApoE3 at two positions, namely the receptor-binding region at N-terminal domain (NTD) and the lipid-binding region at C-terminal domain (CTD). We screened two of the EBV protein: EBNA-1 and BZLF1, as potential interactors of ApoE3 based on preliminary results of site-specific docking of various EBV proteins at the NTD and CTD regions of the ApoE3. Further, the molecular dynamic simulation performed to validate the interaction corroborated the binding. The analysis of root mean square deviations (RMSD), root mean square fluctuations (RMSF), the radius of gyration (Rg), solvent accessible surface area (SASA), and hydrogen bond analysis of the complexes formed between the proteins supported our hypothesis. Our study demonstrated the possibility that EBV proteins (EBNA-1 and BZLF1) are stably binding at the CTD of ApoE3. The investigation might provide a new outlook on EBV-mediated AD pathology.

Nevertheless, addressing the non-availability of treatment for EBV infection-mediated pathologies is of utmost importance. Multitrophic viruses such as EBV could lead to various manifestations like cancer or neurodegeneration. Viral mediation of fatal and life-altering pathologies such as neurological ailments should be considered while planning the treatment. Surprisingly, viral infections as a possible cause of degenerative changes associated with AD in the brain have been overlooked for so long. Therefore, we attempted to target the EBV infection in the cerebral microenvironment using phytochemicals in Chapter 4. In an attempt to hinder the virus's normal functioning, we analysed the binding efficiency of various phytochemicals with neuroprotective, anti-inflammatory, and anti-viral properties to an essential EBV protein, the *dUTPase* (deoxyuridine-triphosphatase). The viral *dUTPase* protein is essential for the maintenance of nucleotide balance and thus, plays a vital role in the viral replication cycle. Additionally, the protein has recently been shown to induce neuromodulatory/neuroinflammatory effects. We hypothesized that the stable binding of a phytochemical at the protein's active site would act competitively to inhibit the binding of natural ligand dUTP, thus hindering the virus's nucleotide metabolism and thereby viral replication and propagation.

We performed site-specific docking of ~45 phytochemicals with the properties mentioned above against the active site of EBV-*dUTPase*. Further, we

performed molecular dynamic (MD) simulations of four protein-ligand complexes bound with the highest efficiency along with the complex of protein bound to natural ligand, i.e., dUTP, as a comparative standard. The data obtained were analysed for RMSD, RMSF, Rg, and SASA to corroborate the binding efficiency of the ligands. Our investigations showed that Dehydroevodiamine (DHED), a phytochemical primarily found in the traditional Chinese medicinal herb *Tetradium ruticarpum*, could be a potent drug development candidate against EBV-*dUTPase*. It was noteworthy to recount the neuroprotective properties of the phytochemical DHED. The additive effects of neuroprotective and anti-viral properties of DHED make it an ideal candidate for drug development against EBV-mediated neuropathologies. However, further *in-vitro* evaluations are required to establish the validity of the predicted anti-EBV *dUTPase* activity of DHED.

In summary, we aimed to address various aspects of EBV infection in the neural microenvironment during this work, which could culminate in AD. We tried to address the effects of direct EBV infection in neurons and concluded that EBV proteins could give rise to amyloidogenic peptides, potentially initiating the aggregation cascade. Further, we evaluated the effects of EBV infection in glial cells that could incur indirect insult to neurons, ultimately resulting in neurodegeneration. We observed that EBV primarily modulates the cholesterol biochemistry in the microglial cells. After that, we attempted to evaluate the interaction between various EBV proteins and Apolipoprotein E, a risk factor in AD prominently associated with cholesterol metabolism and lipid transport. We recorded a probable interaction between EBV proteins (EBNA-1 and BZLF1) and the CTD lipid-binding site of ApoE3. Later, in our investigation, we aimed to target the EBV replication cycle to obstruct the viral reactivation and further spread, which might result in severe neurological manifestations. In the pursuit, we targeted an EBV protein *dUTPase* that is crucial for maintaining the nucleotide balance and thus replication. We found a phytochemical DHED, which has anti-viral, anti-inflammatory, and neuroprotective properties as a potential candidate capable of binding efficiently with EBV-*dUTPase*. Our investigations have tried to peek into the underexplored role of EBV in mediating AD pathology and have produced some exciting results that opened up new avenues for further exploration.

1.4. References

- [1] L. Zhou, M. Miranda-Saksena, and N. K. Saksena, “Viruses and neurodegeneration,” *Viol J*, vol. 10, no. 1, p. 172, Dec. 2013, doi: 10.1186/1743-422X-10-172.
- [2] H. C. Jha *et al.*, “Gammaherpesvirus Infection of Human Neuronal Cells,” *mBio*, vol. 6, no. 6, Dec. 2015, doi: 10.1128/mBio.01844-15.
- [3] D. Tiwari, S. Jakhmola, D. K. Pathak, R. Kumar, and H. C. Jha, “Temporal *In Vitro* Raman Spectroscopy for Monitoring Replication Kinetics of Epstein–Barr Virus Infection in Glial Cells,” *ACS Omega*, vol. 5, no. 45, pp. 29547–29560, Nov. 2020, doi: 10.1021/acsomega.0c04525.
- [4] H. C. Jha, Y. Pei, and E. S. Robertson, “Epstein–Barr Virus: Diseases Linked to Infection and Transformation,” *Front. Microbiol.*, vol. 7, Oct. 2016, doi: 10.3389/fmicb.2016.01602.
- [5] N. Zhang, Y. Zuo, L. Jiang, Y. Peng, X. Huang, and L. Zuo, “Epstein-Barr Virus and Neurological Diseases,” *Front. Mol. Biosci.*, vol. 8, p. 816098, Jan. 2022, doi: 10.3389/fmolb.2021.816098.
- [6] I. Carbone *et al.*, “Herpes virus in Alzheimer’s disease: relation to progression of the disease,” *Neurobiology of Aging*, vol. 35, no. 1, pp. 122–129, Jan. 2014, doi: 10.1016/j.neurobiolaging.2013.06.024.
- [7] S.-M. Shim, H.-S. Cheon, C. Jo, Y. H. Koh, J. Song, and J.-P. Jeon, “Elevated Epstein-Barr Virus Antibody Level is Associated with Cognitive Decline in the Korean Elderly,” *JAD*, vol. 55, no. 1, pp. 293–301, Nov. 2016, doi: 10.3233/JAD-160563.
- [8] S. Jakhmola and H. C. Jha, “Glial cell response to Epstein-Barr Virus infection: A plausible contribution to virus-associated inflammatory reactions in the brain,” *Virology*, vol. 559, pp. 182–195, Jul. 2021, doi: 10.1016/j.virol.2021.04.005.
- [9] O. Indari, R. Chandramohanadas, and H. C. Jha, “Epstein–Barr virus infection modulates blood–brain barrier cells and its co-infection with *Plasmodium falciparum* induces RBC adhesion,” *Pathogens and Disease*, vol. 79, no. 1, p. ftaa080, Jan. 2021, doi: 10.1093/femspd/ftaa080.
- [10] J. M. Bennett, R. Glaser, W. B. Malarkey, D. Q. Beversdorf, J. Peng, and J. K. Kiecolt-Glaser, “Inflammation and reactivation of latent herpesviruses in

older adults,” *Brain, Behavior, and Immunity*, vol. 26, no. 5, pp. 739–746, Jul. 2012, doi: 10.1016/j.bbi.2011.11.007.

[11] M. Kleines, J. Schiefer, A. Stienen, M. Blaum, K. Ritter, and M. Häusler, “Expanding the spectrum of neurological disease associated with Epstein-Barr virus activity,” *Eur J Clin Microbiol Infect Dis*, vol. 30, no. 12, pp. 1561–1569, Dec. 2011, doi: 10.1007/s10096-011-1261-7.

[12] A. Alzheimer, R. A. Stelzmann, H. N. Schnitzlein, and F. R. Murtagh, “An English translation of Alzheimer’s 1907 paper, ‘Über eine eigenartige Erkrankung der Hirnrinde,’” *Clin Anat*, vol. 8, no. 6, pp. 429–431, 1995, doi: 10.1002/ca.980080612.

[13] M. A. DeTure and D. W. Dickson, “The neuropathological diagnosis of Alzheimer’s disease,” *Mol Neurodegeneration*, vol. 14, no. 1, p. 32, Dec. 2019, doi: 10.1186/s13024-019-0333-5.

[14] S. X. Naughton, U. Raval, and G. M. Pasinetti, “The Viral Hypothesis in Alzheimer’s Disease: Novel Insights and Pathogen-Based Biomarkers,” *JPM*, vol. 10, no. 3, p. 74, Jul. 2020, doi: 10.3390/jpm10030074.

[15] W. A. Eimer *et al.*, “Alzheimer’s Disease-Associated β -Amyloid Is Rapidly Seeded by Herpesviridae to Protect against Brain Infection,” *Neuron*, vol. 99, no. 1, pp. 56–63.e3, Jul. 2018, doi: 10.1016/j.neuron.2018.06.030.

[16] B. Readhead *et al.*, “Multiscale Analysis of Independent Alzheimer’s Cohorts Finds Disruption of Molecular, Genetic, and Clinical Networks by Human Herpesvirus,” *Neuron*, vol. 99, no. 1, pp. 64–82.e7, Jul. 2018, doi: 10.1016/j.neuron.2018.05.023.

[17] K. Bourgade, G. Dupuis, E. H. Frost, and T. Fülöp, “Anti-Viral Properties of Amyloid- β Peptides,” *J Alzheimers Dis*, vol. 54, no. 3, pp. 859–878, Oct. 2016, doi: 10.3233/JAD-160517.

[18] V. K. Singh, S. Kumar, and S. Tapryal, “Aggregation Propensities of Herpes Simplex Virus-1 Proteins and Derived Peptides: An *In Silico* and *In Vitro* Analysis,” *ACS Omega*, vol. 5, no. 22, pp. 12964–12973, Jun. 2020, doi: 10.1021/acsomega.0c00730.

[19] D. Tiwari *et al.*, “Indication of Neurodegenerative Cascade Initiation by Amyloid-like Aggregate-Forming EBV Proteins and Peptide in Alzheimer’s Disease,” *ACS Chem. Neurosci.*, vol. 12, no. 20, pp. 3957–3967, Oct. 2021, doi: 10.1021/acchemneuro.1c00584.

- [20] G. L. Nicolson, “Chronic Bacterial and Viral Infections in Neurodegenerative and Neurobehavioral Diseases,” *Laboratory Medicine*, vol. 39, no. 5, pp. 291–299, May 2008, doi: 10.1309/96M3BWYP42L11BFU.
- [21] M. A. Husain, B. Laurent, and M. Plourde, “APOE and Alzheimer’s Disease: From Lipid Transport to Physiopathology and Therapeutics,” *Front. Neurosci.*, vol. 15, p. 630502, Feb. 2021, doi: 10.3389/fnins.2021.630502.
- [22] E. Porcellini, I. Carbone, M. Ianni, and F. Licastro, “Alzheimer’s disease gene signature says: beware of brain viral infections,” *Immun Ageing*, vol. 7, no. 1, p. 16, Dec. 2010, doi: 10.1186/1742-4933-7-16.
- [23] M. A. Wozniak *et al.*, “Does apolipoprotein E determine outcome of infection by varicella zoster virus and by Epstein-Barr virus?,” *Eur J Hum Genet*, vol. 15, no. 6, pp. 672–678, Jun. 2007, doi: 10.1038/sj.ejhg.5201812.
- [24] D. J. Bonda *et al.*, “Review: Cell cycle aberrations and neurodegeneration,” *Neuropathology and Applied Neurobiology*, vol. 36, no. 2, pp. 157–163, Apr. 2010, doi: 10.1111/j.1365-2990.2010.01064.x.
- [25] A. McShea *et al.*, “Neuronal cell cycle re-entry mediates Alzheimer disease-type changes,” *Biochimica et Biophysica Acta (BBA) - Molecular Basis of Disease*, vol. 1772, no. 4, pp. 467–472, Apr. 2007, doi: 10.1016/j.bbadis.2006.09.010.
- [26] T. Barrett, K. A. Stangis, T. Saito, T. Saido, and K. H. J. Park, “Neuronal Cell Cycle Re-Entry Enhances Neuropathological Features in AppNLF Knock-In Mice,” *JAD*, vol. 82, no. 4, pp. 1683–1702, Aug. 2021, doi: 10.3233/JAD-210091.
- [27] A. McShea, P. L. Harris, K. R. Webster, A. F. Wahl, and M. A. Smith, “Abnormal expression of the cell cycle regulators P16 and CDK4 in Alzheimer’s disease,” *Am J Pathol*, vol. 150, no. 6, pp. 1933–1939, Jun. 1997.
- [28] Z. Nagy, M. M. Esiri, and A. D. Smith, “Expression of cell division markers in the hippocampus in Alzheimer’s disease and other neurodegenerative conditions,” *Acta Neuropathol*, vol. 93, no. 3, pp. 294–300, Mar. 1997, doi: 10.1007/s004010050617.
- [29] I. Vincent, G. Jicha, M. Rosado, and D. W. Dickson, “Aberrant expression of mitotic cdc2/cyclin B1 kinase in degenerating neurons of Alzheimer’s disease brain,” *J Neurosci*, vol. 17, no. 10, pp. 3588–3598, May 1997.

- [30] M. G. Davenport and J. S. Pagano, "Expression of EBNA-1 mRNA Is Regulated by Cell Cycle during Epstein-Barr Virus Type I Latency," *J. Virol.*, vol. 73, no. 4, pp. 3154–3161, Apr. 1999, doi: 10.1128/JVI.73.4.3154-3161.1999.
- [31] A. Saha and E. S. Robertson, "Impact of EBV essential nuclear protein EBNA-3C on B-cell proliferation and apoptosis," *Future Microbiology*, vol. 8, no. 3, pp. 323–352, Mar. 2013, doi: 10.2217/fmb.12.147.
- [32] T. Faqing *et al.*, "EPSTEIN —BARR VIRUS LMP1 INITIATES CELL PROLIFERATION AND APOPTOSIS INHIBITION VIA REGULATING EXPRESSION OF SURVIVIN IN NASOPHARYNGEAL CARCINOMA," *Experimental Oncology*, p. 6, 2005.
- [33] N. Ohtani *et al.*, "Epstein-Barr virus LMP1 blocks p16INK4a–RB pathway by promoting nuclear export of E2F4/5," *Journal of Cell Biology*, vol. 162, no. 2, pp. 173–183, Jul. 2003, doi: 10.1083/jcb.200302085.
- [34] Y. Xu *et al.*, "Epstein-Barr Virus encoded LMP1 regulates cyclin D1 promoter activity by nuclear EGFR and STAT3 in CNE1 cells," *J Exp Clin Cancer Res*, vol. 32, no. 1, p. 90, 2013, doi: 10.1186/1756-9966-32-90.
- [35] X. Yang, Z. He, B. Xin, and L. Cao, "LMP1 of Epstein–Barr virus suppresses cellular senescence associated with the inhibition of p16INK4a expression," *Oncogene*, vol. 19, no. 16, pp. 2002–2013, Apr. 2000, doi: 10.1038/sj.onc.1203515.
- [36] A. Mauser, E. Holley-Guthrie, D. Simpson, W. Kaufmann, and S. Kenney, "The Epstein-Barr Virus Immediate-Early Protein BZLF1 Induces both a G₂ and a Mitotic Block," *J Virol*, vol. 76, no. 19, pp. 10030–10037, Oct. 2002, doi: 10.1128/JVI.76.19.10030-10037.2002.

LIST OF PUBLICATIONS

A. Publications arising out of the PhD Thesis

Tiwari, D.; Singh, V. K.; Baral, B.; Pathak, D. K.; Jayabalan, J.; Kumar, R.; Tapryal, S.; Jha, H*. C. “Indication of Neurodegenerative Cascade Initiation by Amyloid-like Aggregate-Forming EBV Proteins and Peptide in Alzheimer’s Disease”. ACS Chem. Neurosci. 2021, 12 (20), 3957–3967. <https://doi.org/10.1021/acchemneuro.1c00584>

Tiwari, D.¹; Jakhmola, S¹.; Pathak, D. K.; Kumar, R*.; Jha, H. C*. “Temporal In Vitro Raman Spectroscopy for Monitoring Replication Kinetics of Epstein–Barr Virus Infection in Glial Cells.” ACS Omega 2020, 5 (45), 29547–29560. <https://doi.org/10.1021/acsomega.0c04525>

Tiwari, D.; Jha, H. C*. “Detection and Analysis of Human Brain Disorders.” In Machine Intelligence and Signal Analysis; Tanveer, M., Pachori, R. B., Eds.; Advances in Intelligent Systems and Computing; Springer Singapore: Singapore, 2019; Vol. 748, pp 717–726. https://doi.org/10.1007/978-981-13-0923-6_61

Tiwari, D.¹; Murmu S¹; Indari, O.; Kumar, S.*; Jha, H.C.* “Targeting Epstein-Barr virus *dUTPase*, an immunomodulatory protein using anti-viral, anti-inflammatory and neuroprotective phytochemicals.” Chemistry & Biodiversity 2022, *cbdv.202200527*. <https://doi.org/10.1002/cbdv.202200527>

Tiwari, D.; Mittal N.; Jha H.C*, “Unravelling the mysterious links between neurodegeneration and Epstein-Barr virus mediated cell cycle dysregulation”. Current Research in Neurobiology 2022, 3, 100046. <https://doi.org/10.1016/j.crneur.2022.100046>

Tiwari, D.; Indari, O.; Shrivastava, G.; Tripathi, V.; Siddqui, M.; Jha, H.C.* “An *in-silico* insight into the predictive interaction of Apolipoprotein-E with Epstein-Barr virus proteins and their probable role in mediating Alzheimer’s diseases”. (Accpeted in Journal of Biomolecular Structure and Dynamics; <https://doi.org/10.1080/07391102.2022.2138978>)

B. Publications apart from PhD Thesis

1. Kashyap, D.; Jakhmola, S.; **Tiwari, D.**; Kumar, R.; Moorthy, N. S. H. N.; Elangovan, M.; Brás, N. F.; Jha, H. C. Plant Derived Active Compounds as Potential Anti SARS-CoV-2 Agents: An in-Silico Study. *Journal of Biomolecular Structure and Dynamics* 2021, 1–22. (<https://doi.org/10.1080/07391102.2021.1947384>)
2. **Tiwari, D.**¹; Rani, A¹; Jha, H. C*. “Homocysteine and Folic acid metabolism.” In *Homocysteine Metabolism: Implications in Nutrition and Health*; Springer (https://doi.org/10.1007/978-981-16-6867-8_1)
3. Varshney, N.; Rani, A.; Kashyap, D.; **Tiwari, D.**; Jha, H. C*. “Aurora kinase: An emerging potential target in therapeutics.” In *Protein Kinase Inhibitors: From Discovery to Therapeutics*; Md. Imtaiyaz Hassan, Saba Noor In Elsevier; Vol 1. (<https://doi.org/10.1016/B978-0-323-91287-7.00028-4>)
4. Indari, O.; **Tiwari, D.**; Tanwar, M; Kumar, R., & Jha H.C.*. Early biomolecular changes in brain microvascular endothelial cells under Epstein-Barr Virus influence: a Raman microspectroscopic investigation. *Integrative Biology* 2022, *14* (4), 89–97. (<https://doi.org/10.1093/intbio/zyac009>)
5. Indari, O.¹; Singh, A. K.¹; **Tiwari, D.** Jha, H. C.*, & Jha A. N.* Repurposing antimalarial compounds to target viral pathogens associated with malaria. (Communicated)

TABLE OF CONTENTS

ACKNOWLEDGEMENTS	1
SYNOPSIS	i
1.1. Introduction	i
1.1.1. Epstein-Barr virus (EBV) and associated spectrum of diseases.....	i
1.1.2. The viral hypothesis in Alzheimer’s disease.....	ii
1.2. Scope and Objectives of the Research	iii
1.2.1. Scope.....	iii
1.2.2. Objectives.....	iv
1.2.3. Chapters	iv
1.3. Summary of the Results and Conclusions	v
1.4. References	ix
LIST OF PUBLICATIONS	i
A. Publications arising out of the PhD Thesis	i
B. Publications apart from PhD Thesis	ii
TABLE OF CONTENTS	iii
LIST OF FIGURES	vii
LIST OF TABLES	vii
NOMENCLATURE	xi
ACRONYMS	1
Chapter 1	6
Literature review	6
1.1. Introduction: Epstein-Barr Virus (EBV) and associated spectrum of diseases	6
1.1.1 Neurological complications associated with EBV infection	8
1.2 Introduction: Alzheimer’s Disease.....	9
1.2.1 Implication of EBV in Alzheimer’s Disease	10
1.3References	11
Chapter 2	18
Scope and Objective of the Research	18
Chapter 3	20
Indication of Neurodegenerative Cascade Initiation by amyloid-like Aggregate- Forming EBV Proteins and Peptide in Alzheimer’s Disease	20
3.1 Graphical abstract	20
3.2 Abstract	21
3.3 Introduction	21
3.4 Results and Discussion	24
3.4.1 In-silico screening of aggregation-prone EBV proteins:	26

3.4.2 20S Proteasome cleavage site prediction and identification of aggregation-prone peptides:	29
3.4.3 <i>In vitro</i> aggregation analysis of the EBV peptide:	31
3.4.4 Secondary structure in peptide aggregates:	35
3.4.5 Cytotoxic properties of EBV gM ₁₄₆₋₁₅₇ peptide:	37
3.5 Conclusions	38
3.6 Materials and Methods	39
3.6.1 Sequence Retrieval of EBV Proteins	39
3.6.2 <i>In Silico</i> Aggregation Proclivity Prediction Tools	39
3.6.3 Prediction of 20s Proteasome Cleavage Sites on Full-Length Proteins	40
3.6.4 Preparation of Aggregation Sample.....	40
3.6.5 <i>In Vitro</i> Aggregation Analysis by Congo Red Absorption Assay	40
3.6.6 In Vitro Aggregation Kinetics Analysis by Thioflavin-S (ThioS) Fluorescence Assay	41
3.6.7 Atomic Force Microscopy (AFM)	41
3.6.8 Raman Spectroscopy	41
3.6.9 Cell Cytotoxicity Assay	42
3.7 References	42
Chapter 4.....	48
<i>In vitro</i> Raman spectroscopy of Epstein-Barr virus-infected glial cells to analyze temporal replication kinetics	48
4.1 Graphical abstract	48
4.2 Abstract.....	48
4.3 Introduction	49
4.4 Results.....	52
4.4.1 Raman Spectra	52
4.4.2 Biomolecules' peak identification in the glial cells	53
4.4.3 Varying biomolecular expression at nucleus and periphery of glial cells with continuing EBV infection	62
4.4.4 Pathway Analysis of selected biomolecules	63
4.5 Discussion	65
4.6 Materials and Methods.....	69
4.6.1 Cell culture	69
4.6.2 Virus isolation and purification.....	69
4.6.3 EBV infection in glial cells	70
4.6.4 Raman Spectroscopy	70
4.6.5 Data Analysis	70
4.6.5.1. Graphical analysis.....	70
4.6.5.2. Statistical analysis.....	71

4.6.6 Interactome study	71
4.7 References.....	71
Chapter 5.....	83
An <i>in-silico</i> insight into the predictive interaction of Apolipoprotein-E with Epstein-Barr virus proteins and their probable role in mediating Alzheimer’s disease.....	83
5.1 Graphical abstract	83
5.2 Abstract.....	83
5.3 Introduction	84
5.4 Results and Discussion	88
5.4.1 Structure modelling & Docking.....	88
5.4.2 Trajectory Analysis of Molecular Dynamic (MD) Simulations	91
5.4.3 Binding Free Energy	94
5.4.4 Hydrogen Bond Analysis	95
5.5 Conclusions	96
5.6 Materials and methods	97
5.6.1 3D structure retrieval and preparation of host and viral proteins	97
5.6.2 Molecular Docking.....	97
5.6.3 Molecular Dynamic (MD) Simulations	98
5.7 References.....	98
Chapter 6.....	104
Targeting Epstein-Barr virus <i>dUTPase</i> , an immunomodulatory protein using anti-viral, anti-inflammatory and neuroprotective phytochemicals.....	104
6.1 Graphical abstract	104
6.2 Abstract.....	104
6.3 Introduction	105
6.4 Results.....	109
6.4.1 Molecular Docking of EBV- <i>dUTPase</i> with dUTP and other phytochemicals..	109
6.4.2 Molecular Dynamic (MD) Simulations Analysis.....	112
6.4.3 Root-Mean-Square Deviation	112
6.4.4 Root-Mean-Square Fluctuation.....	112
6.4.5 Radius of Gyration (Rg) and Solvent Accessible Surface Area (SASA) Analysis	114
6.4.6 Hydrogen Bond Analysis	115
6.4.7 Binding Free Energy Estimation	116
6.4.8. ADMET Analysis	120
6.5 Discussion.....	122
6.6 Methodology	124
6.6.1 Retrieval of protein-ligand structure and preparation for molecular docking	124

6.6.2 Active site validation and Molecular docking studies	124
6.6.3 Molecular Dynamic (MD) Simulations	125
6.6.4 Trajectory Analysis	125
6.6.5 Binding Free Energy Calculations.....	126
6.6.6 ADMET/Drug Likeliness Properties	126
6.7 References	127
Chapter 7.....	134
Conclusion and future perspective	134
APPENDIX A	138
Supplementary Figures	138
Supplementary Tables	141

LIST OF FIGURES

ACKNOWLEDGEMENTS	1
SYNOPSIS	i
LIST OF PUBLICATIONS	i
TABLE OF CONTENTS	iii
LIST OF FIGURES	vii
LIST OF TABLES	vii
NOMENCLATURE	xi
ACRONYMS	1
Chapter 1	6
Figure 1.1 The structural arrangement of the Human Herpesvirus-4 (HHV4), also known as Epstein-Barr virus (EBV). The EBV genome is a double-stranded DNA enclosed within an icosahedral nucleocapsid. The core is surrounded by a viral tegument entrapped inside an outer envelope.....	6
Chapter 2	18
Chapter 3	20
Figure 3.1 Average aggregation scores of EBV proteins. (a) Average aggregation score of various EBV proteins compared to the positive control ($A\beta_{42}$) and negative control FMRP-1 as calculated by TANGO and AGGRESCAN. The EBV peptides showed comparable aggregation scores with $A\beta_{42}$ (b) Aggregation score of EBV-gM plotted along the entire protein length compared to the positive and negative control as calculated by TANGO. (c) as calculated by AGGRESCAN. Both the plots show that the aggregation score of EBV-gM along the entire protein length is higher than the positive control.	28
Figure 3.2 Various properties of EBV-gM peptide depicting its aggregation capability. (a) Average aggregation score of EBV-gM ₁₄₆₋₁₅₇ per residue as compared to the positive ($A\beta_{1-42}$) and negative control (FMRP-1). EBV-gM ₁₄₆₋₁₅₇ showed a higher per residue aggregation score than the $A\beta_{42}$ as calculated by TANGO and AGGRESCAN. (b) The hydrophobicity index of the EBV-gM ₁₄₆₋₁₅₇ peptide is higher than the negative control and comparable to the positive control. (c) The average aggregation score per residue of the EBV-gM is much higher than the positive control $A\beta_{42}$	30
Figure 3.3 Congo-Red absorption assay. The Congo-red absorption spectrum of the EBV-gM ₁₄₆₋₁₅₇ aggregates showing the characteristic bathochromic shift (of ~20 nm) from 480 nm to 500 nm. The shift indicates the presence of amyloid-like aggregates in the aggregate solution of concentrations 125, 250, and 500 μ M.	32
Figure 3.4 Thioflavin-S fluorescence emission by EBV-gM₁₄₆₋₁₅₇ peptide after incubation. The fluorescence spectra were obtained after (a) 12 hours and (b) 24 hours incubation in the range of 400-600 nm. The quantification of normalized fluorescence intensity at maxima plotted with increasing dosage of aggregates, i.e., 31.25, 62.5, 125, 250, and 500 μ M, at (c) 12 hours and (d) 24 hours post-incubation at 37°C. The highly significant ($p < 0.001$) increase in fluorescence intensity at higher concentrations (125, 250, and 500 μ M) at 12 hours demonstrated the formation of more aggregates at higher concentrations. (d) Comparative analysis of fluorescence intensity at 12- and 24-hours post-incubation for different concentrations revealed significant changes in the aggregation tendency of peptides over time.	33

Figure 3.5 Thioflavin-S fluorescence intensity of 125µM with time. (a) The fluorescence intensity spectrum of 125µM EBV-gM ₁₄₆₋₁₅₇ peptide was recorded between 400-600 nm. The spectrum shows maximum fluorescence emission at 2 hours. (b) Quantification of fluorescence at maxima revealed a gradual increase until 2 hours, followed by a decrease depicting a temporal pattern in aggregate formation.	34
Figure 3.6 Raman spectroscopy of EBV-gM₁₄₆₋₁₅₇ peptide. a) Raman spectrum of EBV peptide obtained between 400-2000 cm ⁻¹ shows the secondary structural conformations present in the aggregation solution of 125µM. The Raman band at 1224, 1321, and 1610 cm ⁻¹ depicts the vibrations generated from Amide III, II, and I, respectively. Amide III reflects the formation of amyloid-like beta structures. The plot shows the presence of maximum beta-sheet structures at 2 hours post-incubation. (b) Comparative analysis of the Raman intensity of (i) Amide III at 1224cm ⁻¹ , (ii) Amide II at 1321cm ⁻¹ and (iii) Amide I at 1610cm ⁻¹ with time till 12 hours showed a gradual decrease in the stability of beta-sheet and alpha-helix conformation after initial 2 hours, (iv) the maximum change in secondary structure conformation is observed at 2hours post-incubation of the peptide at 37°C.	36
Figure 3.7 Cytotoxicity analysis of EBV-gM₁₄₆₋₁₅₇ peptide using MTT assay. The MTT assay showed that the TD ₅₀ for EBV-gM ₁₄₆₋₁₅₇ lies at ~37 µM post 72 hours of incubation with the aggregates. It indicates that aggregates formed at 125 µM post 2 hours of incubation at 37°C, are cytotoxic for neuroblastoma cells even at a much lower concentration of 37 µM.....	38
Chapter 4.....	48
Figure 4.1 Raman spectra were acquired from (A) the nucleus of HMC-3 [(I) and (II)] and (B) the periphery of HMC-3 [(I) and (II)]. The Raman spectra were acquired in the range of 400 to 4000 cm ⁻¹ . 633 nm laser excitation source was used to record the data.	53
Figure 4.2 Expression of various biomolecules at different time points post EBV infection in HMC-3 cells. The intensity levels of each biomolecule group upon EBV infection are plotted separately in comparison to that of uninfected cells. The data was recorded at the time intervals of 2, 4, 6, 12, 24, 36 hpi for HMC-3 cells. Changes in the Raman intensity related to nucleic acid, amino acids, lipids, and carbohydrates were observed in microglial cell line.	55
Figure 4.3. Representative view of changes in biomolecular activity upon continuous infection progression. Briefly, the biomolecules represented by their corresponding wavenumber values are plotted against the time interval of their occurrence. The recorded data was plotted for consequent time intervals of 0-2, 2-4, 4-6, 6-12, 12-24, and 24-36 for HMC-3 at both cellular locations (nucleus and periphery) separately. Maximum molecular activity was recorded (A) at the nucleus of HMC-3 cells during 0-2, 6-12, and 24-36 hpi, (B) at the periphery of HMC-3 cells during 0-2, 4-6, and 24-36 hpi.	63
Figure 4.4. Connectome representing the interlinks of biomolecules observed to be modulated on EBV infection in HMC-3 (Microglia). The network depicts the molecules implicated in various neurodegenerative pathologies (according to the IPA knowledge database. Molecular metabolism related to (A) cholesterol, lipids, lactic acid metabolism, and PIP signaling cascade were recorded to be modulated in HMC-3 cells.	65
Chapter 5.....	83
Figure 5.1 a) Structure of human Apolipoprotein E. The N-terminal region (red), ranging from the 1-167th amino acid, consists of four helices arranged in anti-parallel bindles and contains the receptor-binding domain (134-150 residue; yellow). The C-terminal	

region (blue), ranging from the 206-299th residue, contains a ligand-binding domain (244-272 residue; cyan). The two regions are connected by a hinge (168-205). b) Polymorphism in human ApoE. The three isoforms of human ApoE differ at 112th and 154th residue with ApoE3, the healthy isoform having a Cys at 112nd and an Arg residue at 154th position. The disease-associated isoforms ApoE2 and ApoE4, respectively, contain Cys and Arg at both positions.	86
Figure 5.2 . Root mean square deviations (RMSD) in the bound complexes throughout MD simulation (100ns). a) RMSD of the entire bound complexes, b) RMSD of the ApoE (NTD/CTD) in the bound complex, and c) RMSD of the EBV proteins (EBNA1/BZLF1) in the bound complex.	92
Figure 5.3 Root mean square fluctuations (RMSF) plots of respective chains in the bound complexes. a) RMSF of various residues of a) NTD in complex with EBNA1 and BZLF1, b) CTD in complex with EBNA1 and BZLF1, c) EBNA1 in complex with NTD and CTD, d) BZLF1 in complex with NTD and CTD of ApoE3.	93
Figure 5.4 a) Radius of gyration (Rg), b) Solvent accessible surface area (SASA) plots.	94
Figure 5.5 Hydrogen Bond Analysis of the respective complexes. The average number of H-bonds in complex a) EBNA1 + NTD were 8, b) BZLF1 + NTD were 2, c) EBNA1 + CTD were 14, and d) BZLF1 + CTD were 21 throughout the duration of MD simulation.	96
Chapter 6.....	104
Figure 6.1 Structural details of the EBV-dUTPase. a) Location and orientation of the domains I (1-116), II (117-219), and III (220-278) forming the secondary structure of EBV-dUTPase is shown in red, blue, and green color, respectively. b) The conserved motifs I (magenta), II (orange), III (red), and IV (blue) constitute the active site of the EBV-dUTPase. Due to its flexibility and disordered structure, motif V is generally invisible. c) The sequence alignment of the human dUTPase with that of EBV. The location of each of the motifs I, II, III, IV, and V is highlighted respectively in magenta, yellow, cyan, green, and grey. d) The active site of EBV-dUTPase is depicted in blue residues; inset: The residues involved in the active site formation are shown in red.	107
Figure 6.2. Structural representation of the phytochemicals: (a) Deoxyuridine triphosphate (dUTP), (b) Mangiferin, (c) Sarsasapogenin, (d) Dehydroevodiamine, and (d) Kaempferol-3-O-Rutinoside.	110
Figure 6.3. a) Root-mean-square deviations (RMSDs) of the EBV-dUTPase backbone atoms during MD simulation, b) RMSF analysis of Cα during MD simulation, c) Solvent accessible surface area (SASA) analysis, and d) Rg plot of EBV-dUTPase bound and unbound with phytochemicals.	113
Figure 6.4. Hydrogen bond analysis of the docked complexes.	115
Figure 6.5. 2D visualization of ligand-bound protein before and after MD simulation. Various types of interactions taking part in the protein-ligand binding are listed below, with the key. Throughout the simulation, the ligands remain bound to the protein EBV-dUTPase, establishing a stable connection towards the end of 100 ns.	120
Chapter 7.....	134
APPENDIX A.....	138
Figure S3.1 Atomic Force Microscopic (AFM) image of EBV-gM₁₄₆₋₁₅₇ aggregates formed at 250μM concentration. The AFM image of the aggregates showing spheroid oligomers formed at 1 μ m scale bar. The inset at lower left corner shows magnified image of the spheroid oligomers.	138

Figure S3.2 Cytotoxicity of EBV-gM₁₄₆₋₁₅₇ against neuroblastoma cells IMR-32 after 48 hours of incubation. The cytotoxicity analysis using MTT dye revealed TD₅₀ of EBV-gM₁₄₆₋₁₅₇ to be ~58μM upon 48 hours of incubation..... 139

Figure S5.1 Ramachandran plot of EBNA1 (EBV nuclear antigen-1) modeled using iTASSER. The graph shows almost 99% of the residues lying in the favoured region, implying the acceptability of the modeled structure..... 140

LIST OF TABLES

ACKNOWLEDGEMENTS	1
SYNOPSIS.....	i
LIST OF PUBLICATIONS	i
TABLE OF CONTENTS	iii
LIST OF FIGURES.....	vii
LIST OF TABLES	vii
NOMENCLATURE	xi
ACRONYMS.....	1
Chapter 1.....	6
Chapter 2.....	18
Chapter 3.....	20
Chapter 4.....	48
Table 4.1 The Raman signature of the biomolecules that are known to be altered on infection with different viruses and how the virus utilizes them. Error! Bookmark not defined.	
Chapter 5.....	83
Table 5.1 The binding energy of various EBV proteins with NTD and CTD of ApoE3 based on docking by HADDOCK and HDOCK.....	90
Table 5.2. Binding free energy decomposition.....	94
Chapter 6.....	104
Table 6.1. A detailed description of the natural ligand of dUTPase (dUTP) and the top 5 phytochemicals possessing anti-viral and neuroprotective properties with the highest binding affinities towards EBV-dUTPase based on a molecular docking study; Dehydrouridine triphosphate (dUTP), Kaempferol-3-rutinoside (K3R), Mangiferin (MANG), Sarsasapogenin (SARA), Dehydroevodiamine (DHED).....	111
Table 6.2. MM-PBSA analysis of the bound complexes	116
Table 6.3 Pharmacokinetic properties and toxicity prediction of phytocompounds through the pkCSM and SwissADMET server.....	120
Chapter 7.....	134
APPENDIX A.....	138
Table S3.1 Average aggregation score of EBV protein sequences, positive and negative control as calculated by TANGO and AGGRESCAN.....	141
Table S3. 2 Distribution of predicted cleavage sites	144
Table S3. 3 Analysis of aggregation prone consensus sequences as predicted by Amylpred2 in A β ₄₂ and EBV-gM ₁₄₆₋₁₅₇	145
Table S6. 1 Detailed description of the phytochemicals with anti-viral and neuroprotective properties with binding affinities towards EBV-dUTPase based on molecular docking study.....	146

NOMENCLATURE

ml	millilitre
mM	millimolar
ng	nanogram
nM	nanomolar
nS	nanosecond
μ L	microlitre
μ M	micro-molar
$^{\circ}$ C	Degree centigrade

ACRONYMS

α -Syn α -synuclein

ABCA-1 ATP binding cassette subfamily A member 1

ACH Amyloid cascade hypothesis

ACh Acetylcholine

AChE Acetylcholine cholinesterases

AD Alzheimer's Disease

ADME Absorption, Distribution, Metabolism, and Excretion

AFM Atomic Force Microscopy

Agg_{AV} Average aggregation score

ALS Amyotrophic lateral sclerosis

APCs Antigen-presenting cells

Apo Apolipoprotein

APP Amyloid precursor protein

A β amyloid- β

BACE-1 Beta site APP cleaving enzyme-1

BBB Blood-brain barrier

BChE Butyrylcholine cholinesterases

BL Burkitt's lymphoma

BZLF-1 BamHI Z fragment leftward open reading frame-1

CASTp Computed Atlas of Surface Tomography of Protein

CFS Chronic fatigue syndrome

CNS Central nervous system

CSF Cerebrospinal fluid

CTD C-terminal domain

CTLs Cytotoxic T lymphocytes

DCs Dendritic cells

DENV Dengue virus

DHED Dehydroevodiamine

DMSO Dimethyl sulfoxide

dUDP Deoxyuridine diphosphate

dUTP Deoxyuridine triphosphate

dUTPase Deoxyuridine-triphosphatase

EBNAs EBV nuclear antigens

EBV Epstein-Barr virus

EBERs EBV encoded small noncoding RNAs

ER Endoplasmic reticulum

FMRP-1 Fragile X mental retardation-1

GBD Global Burden of Disease

GBS Guillain-Barre syndrome

gM glycoprotein-M

gp350 glycoprotein-350

HBV Hepatitis-B virus

HCMV Human cytomegalovirus

HCV Hepatitis-C virus

HDL High-density lipoprotein

HHVs Human Herpesviruses

HIV Human Immunodeficiency Virus

HL Hairy leukoplakia

HPI hours post-infection

HPV Human papillomavirus

HSV Herpes simplex virus

IBD Inflammatory bowel disease

IE Immediate-early

IM Infectious mononucleosis

IPA Ingenuity Pathway Analysis

IPKB Ingenuity pathway knowledge base

K3R Kaempferol-3-rutinoside

KSHV Kaposi's sarcoma-associated herpesvirus

LBD Ligand Binding Domain

LMPs latent membrane proteins

LOAD Late-onset AD

MANG Mangiferin

MAP-2 Matrix associated protein-2

MBP Myelin basic protein

MCI Mild cognitive impairment

MD Molecular dynamics

MHC major histocompatibility complex

MHV-68 Murine gammaherpesvirus-68

MM-PBSA Molecular mechanics Poisson-Boltzmann surface area

MS Multiple sclerosis

NDD Neurodegenerative disorders

NFT Neurofibrillary tangle

NF- κ B Nuclear factor kappa-light-chain-enhancer of activated B cells

NPC Nasopharyngeal carcinoma

NTD N-terminal domain

OR Odds Ratio

PBLs Peripheral blood lymphocytes

PBS Phosphate Buffered Saline

PCA Principal component analysis

PD Parkinson's Disease

PFA Paraformaldehyde

PHK Primary human keratinocytes

PI-3K Phosphoinositide 3-kinase

PIP Phospho-inositol-pyruvate

PLP-1 Proteolipid protein-1

PPI Protein-Protein interactions

PSEN Presenilin

RBD Receptor Binding Domain

Rg Radius of gyration

RMSD Root mean square deviations

RMSF Root mean square fluctuations

ROS Reactive oxygen species

RS Raman spectroscopy

SARA Sarsasapogenin

SARS-CoV-2 Severe acute respiratory syndrome causing Corona virus-2

SASA Solvent accessible surface area

SDF Structure data files

SGPL-1 Sphingosine-1-phosphate lyase-1

SNCA Synuclein alpha

SNpc Substantia nigra pars compacta

SOAT-1 Sterol-O-Acyltransferase-1

SVM Support vector machine

TAP Transporter associated with antigen processing

TD₅₀ Mean toxic dose

T_{EMRA} T effector memory CD45RA⁺

THH Tau hyperphosphorylation hypothesis

ThioS Thioflavin-S

TLR2 Toll-like receptor 2

UI Uninfected

VZV Varicella-Zoster virus

WHO World health Organization

Chapter 1

Literature review

1.1. Introduction: Epstein-Barr Virus (EBV) and associated spectrum of diseases

Human Herpesvirus-4 (HHV-4), also called Epstein-Barr virus (EBV) after its discoverers Anthony Epstein, Yvonne Barr, and Burt Achong [1]. It is a double-stranded DNA virus with a ~122-180 nm diameter. Structurally, EBV contains ~184kb genome encoding for ~85 genes entrapped inside the nucleocapsid, followed by the tegument layer enclosed in an outer envelope [2].

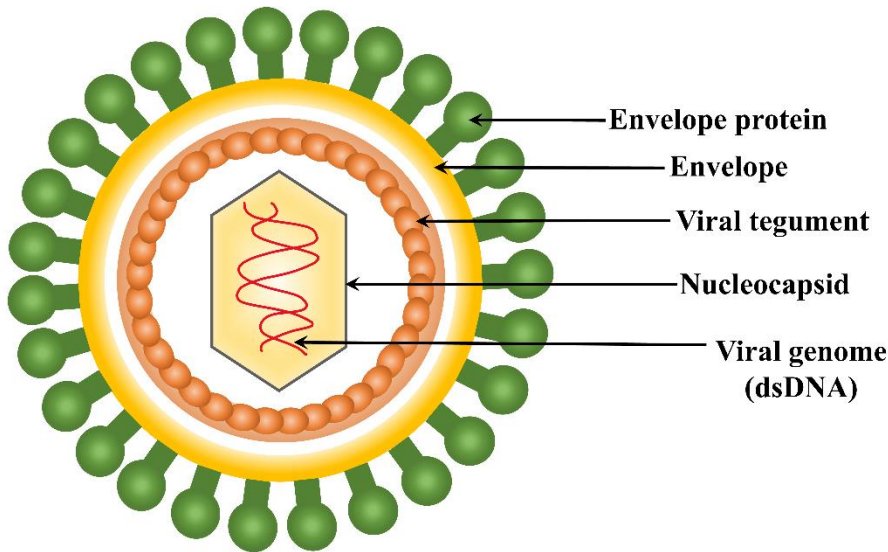


Figure 1.1 The structural arrangement of the Human Herpesvirus-4 (HHV4), also known as Epstein-Barr virus (EBV). The EBV genome is a double-stranded DNA enclosed within an icosahedral nucleocapsid. The core is surrounded by a viral tegument entrapped inside an outer envelope.

The virus is transmitted by exchanging bodily fluids such as saliva, blood, and genital secretions; and infects about ~95% of the global population [3]. Primary infection in childhood often remains asymptomatic; however, exposure in young adulthood could result in a condition called infectious mononucleosis, also known as mono or glandular fever [4]. Upon initial exposure, the virus establishes latent infection in the B-lymphocytes with limited gene expression to evade the host immune system [5]. Although, for viral progeny dissemination,

the virus switches to the lytic replication cycle and gets reactivated from these latently infected cells from time to time.

B-lymphocytes act as the primary reservoir of the virus, which can also infect epithelial cells [6]. Besides, recent studies have suggested that EBV does possess the property of multi-tropism, i.e., it can infect a variety of cells, including neurons [7], glial cells [8], [9], brain microvascular endothelial cells [10], etc. The virus utilizes envelope glycoproteins (gp350/220, gp42, gHgL, and gB) to interact and attach with the host cell surface receptors, including CD21, HLA-DR, Integrin, Ephrin, and so on [6]. Post-infection the virus could either establish latency or enter the lytic phase of its life cycle to produce progeny virions for further propagation of infection. EBV could exist in different latency programs from latency III, II, I, and 0. During latency III, most of the viral genes, including EBV nuclear antigens (EBNA-I, II, and III), latent membrane proteins (LMP-I and II), and EBV encoded small noncoding RNAs (EBERs), are expressed. Latency II is characterized by a lack of expression of EBNA-II and III. Latency I show expression of only EBNA-I and EBERs. At the same time, at the latency 0 stage, EBV is supposed to express only EBERs. The switch between these latency programs and the lytic cycle helps the virus regulate the transmission and perseverance in the host cell.

To maintain life-long persistence inside the host, EBV maintains a delicate balance between the latent and lytic cycle. However, external factors, including immunological stress due to co-infection by other pathogens, immunosuppression, and pharmacological stimulation, could disturb this balance and cause viral reactivation [11], [12]. The viral reactivation is prevalently linked with severe consequences like various lymphatic or epithelial malignancies such as Hodgkin's and Burkitt's (Non-Hodgkin's) lymphoma or nasopharyngeal carcinoma. EBV infection is also linked to non-neoplastic diseases like infectious mononucleosis (IM) and lymphoproliferative disorders [13]. EBV is also reported to aggravate gastric cancer [14]. A study intriguingly reported that EBV infection could get laterally transferred from its natural host cells of B-cell lineage to the cells of epithelial origin [15].

1.1.1) Neurological complications associated with EBV infection

Although, the neurovirulent and neuroinvasive capability of the virus is still debated. Recent reports from various groups have suggested EBV's involvement in neurological manifestations such as multiple sclerosis, cerebellar ataxia, meningoencephalitis, cranial nerve palsies, and other neurodegenerative disorders, including Guillain-Barrè syndrome (GBS), Alzheimer's (AD) and Parkinson's disease (PD) [16]–[20]. Interestingly, the genetic material of EBV and antiviral antibodies against the virus has been prevalently found in the cerebrospinal fluid (CSF) samples of patients suffering from Neurodegenerative diseases (NDDs) [19], [21].

It is proposed that >25% of EBV-positive individuals have CSF disorders that can manifest as various neuropathologies such as meningitis, nerve neuropathies, encephalitis, etc. [22], [23]. The most common among these is viral meningitis which can be validated by the presence of EBV DNA in the CSF samples of the subjects. Further, IM patients are often reported to present neurological symptoms like ataxia, diffuse encephalopathy, and coma post-onset of the disease. However, primary infection of EBV may show up as encephalitis [23], with clinical symptoms overlapping with Herpes simplex encephalitis [24]. Additionally, cranial neuropathies like that of cranial nerves I, II, III, IV, V, VI, VIII, and IX alone or in combination are commonplace complications associated with IM [24]. EBV infection is also linked with peripheral nerve neuropathy as described by a case study on a patient who presented with sensory loss, areflexia, and pseudoarthrosis [25]. Moreover, ~2-10% GBS patients are reported to be EBV positive [26]. The virus is also associated with primary CNS lymphomas [27]. Notably, the neurological complications associated with EBV are mostly a consequence of direct or indirect stimulation of neuro-inflammatory response by the virus. An earlier study by Jha et al. has also established the neurotropic potential of EBV in primary neurons, Ntera2, and SH-Sy5y cell lines [7].

Additionally, our recent study has shown that EBV can infect and modulate the glial cells [28], [29] in the brain, corroborating a previous finding by Menet et al. [30]. Also, we have observed that EBV can infect and alter the endothelial cells of the blood-brain barrier (BBB) [31]. These clues indicate the possibility

of EBV being capable of establishing successful infection in neural cells: namely glial cells and neurons.

1.2 Introduction: Alzheimer's Disease

Alzheimer's disease is named after its discoverer Dr. Alois Alzheimer, who first characterized the disease based on the study of a patient named Auguste Deter. He described the illness as progressive and irreparable damage inflicted on the neurons, leading to cognitive impairment [32]. The presence of proteinaceous plaques in the brain formed from A β fragments, tau proteins (neurofibrillary tangles), and α -Synuclein (Lewy bodies) are now established pathological hallmarks of the disease. These signs are accompanied by a gradual decline of cognitive abilities, including memory and sense of self, at later stages of the disease [33], [34]. According to the World Health Organization (WHO) reports, it is the predominant cause of senile dementia globally, contributing 60-70% of the total cases [19]. Between 2001-2040, incidents of dementia associated with AD are speculated to increase by more than 300% in South-East Asian countries, including India [35], [36].

Though the disease pathology has been well characterized, its pathogenesis is still under investigation. Various hypotheses were proposed to address the ambiguity surrounding the causation and progression of the disease. The most prevalent ones include the Amyloid cascade hypothesis (ACH) [37] and the Tau hyperphosphorylation hypothesis (THH) [38], apart from the genetic predisposition hypothesis [39]–[41]. However, an emerging theory that has divided the scientific community implicates pathogen infection as an instigator of AD pathology. The newly proposed theory suggests that amyloid plaques are seeded as a protective mechanical barrier to trap the pathogen and further stop infection spread [42]. Various neuroinvasive pathogenic microorganisms, including bacteria (*Chlamydia pneumonia* [43], *Borrelia burgdorferi* [44], *Helicobacter pylori* [45], and *Porphyromonas gingivalis* [46], etc.), and viruses (Herpesviruses including HSV-1, HHV-4, 6 [47], etc.) are believed to be involved in the process. It is proposed that long-standing ACH, THH, and

genetic predisposition along with viral infection could lead to multipathology convergence to chronic neuronal stress and lead towards neurodegeneration.

1.2.1) The implication of EBV in Alzheimer's Disease

Interestingly, one of the omnipresent yet overlooked viral pathogens hypothesized to be involved in AD pathology is the EBV. Its seropositivity has been demonstrated consistently over the decades in patients suffering from AD. However, the role of EBV in the disease remained debatable and underexplored. Several recent studies have provided convincing proof implicating EBV in the etiology of AD. A recent study was done by Gate et al., in which they showed that adaptive immune changes mediated by EBV were involved in AD pathogenesis [48]. They reported the presence of CD8⁺ T effector memory CD45RA⁺ (T_{EMRA}) cells specific for EBV as a part of adaptive immunity in AD patients. Previously, it has also been observed by Eimer et al. that members of the Herpesviridae family, like EBV, are capable of stimulating the A β fibrillation, a protective measure against brain infection [49]. Furthermore, contemporary research has suggested that cell-cycle dysregulation in neurons is integral to AD [50]. Terminally differentiated neurons in the adult human brain are supposed to be resting in the G₀ phase of the cell cycle. However, reports have shown that if somehow triggered to re-enter the cell cycle, they die instead of duplicating due to the abortive cell cycle [51]. Multiple *in-vitro* and *in-vivo* studies on AD models have demonstrated the presence of markers indicating the ongoing cell cycle in the adult neuron [52]–[55]. Furthermore, being an oncogenic virus, EBV has an indisputable capability to manipulate the host cell cycle. Various EBV proteins such as EBV nuclear antigens (EBNA-1, 2, 3) [56], [57], latent membrane proteins (LMP-1, 2a, 2b) [58]–[61], and several other viral transcripts (EBER, BZLF-1, etc.) [62] are implicated in modulating the host cell cycle at different stages. Latest experimental evidence of EBV's capability to infect neuronal cells can be extrapolated to imply a probable link between EBV-mediated cell cycle dysregulation in neurons and AD. Altogether, these facts indicate that the neurodegenerative pathology in AD might result from immune modulation mediated by EBV.

1.3 References

- [1] M. A. Epstein, B. G. Achong, and Y. M. Barr, "VIRUS PARTICLES IN CULTURED LYMPHOBLASTS FROM BURKITT'S LYMPHOMA," *The Lancet*, vol. 283, no. 7335, pp. 702–703, Mar. 1964, doi: 10.1016/S0140-6736(64)91524-7.
- [2] L. S. Young, "Epstein–Barr Virus: General Features," in *Encyclopedia of Virology*, Elsevier, 2008, pp. 148–157. doi: 10.1016/B978-012374410-4.00391-5.
- [3] S. Tzellos and P. J. Farrell, "Epstein-barr virus sequence variation-biology and disease," *Pathog. Basel Switz.*, vol. 1, no. 2, pp. 156–174, Nov. 2012, doi: 10.3390/pathogens1020156.
- [4] S. K. Dunmire, K. A. Hogquist, and H. H. Balfour, "Infectious Mononucleosis," *Curr. Top. Microbiol. Immunol.*, vol. 390, no. Pt 1, pp. 211–240, 2015, doi: 10.1007/978-3-319-22822-8_9.
- [5] M. E. Rensing, M. van Gent, A. M. Gram, M. J. G. Hooykaas, S. J. Piersma, and E. J. H. J. Wiertz, "Immune Evasion by Epstein-Barr Virus," in *Epstein-Barr Virus Volume 2*, vol. 391, C. Münz, Ed. Cham: Springer International Publishing, 2015, pp. 355–381. doi: 10.1007/978-3-319-22834-1_12.
- [6] A. Rani, S. Jakhmola, S. Karnati, H. S. Parmar, and H. Chandra Jha, "Potential entry receptors for human γ -herpesvirus into epithelial cells: A plausible therapeutic target for viral infections," *Tumour Virus Res.*, vol. 12, p. 200227, Dec. 2021, doi: 10.1016/j.tvr.2021.200227.
- [7] H. C. Jha *et al.*, "Gammaherpesvirus Infection of Human Neuronal Cells," *mBio*, vol. 6, no. 6, Dec. 2015, doi: 10.1128/mBio.01844-15.
- [8] D. Tiwari, S. Jakhmola, D. K. Pathak, R. Kumar, and H. C. Jha, "Temporal *In Vitro* Raman Spectroscopy for Monitoring Replication Kinetics of Epstein–Barr Virus Infection in Glial Cells," *ACS Omega*, vol. 5, no. 45, pp. 29547–29560, Nov. 2020, doi: 10.1021/acsomega.0c04525.
- [9] S. Jakhmola and H. C. Jha, "Glial cell response to Epstein-Barr Virus infection: A plausible contribution to virus-associated inflammatory reactions in the brain," *Virology*, vol. 559, pp. 182–195, Jul. 2021, doi: 10.1016/j.virol.2021.04.005.

- [10] O. Indari, R. Chandramohanadas, and H. C. Jha, "Epstein–Barr virus infection modulates blood–brain barrier cells and its co-infection with *Plasmodium falciparum* induces RBC adhesion," *Pathog. Dis.*, vol. 79, no. 1, p. ftaa080, Jan. 2021, doi: 10.1093/femspd/ftaa080.
- [11] A. Blazquez-Navarro *et al.*, "Risk factors for Epstein–Barr virus reactivation after renal transplantation: Results of a large, multi-centre study," *Transpl. Int.*, vol. 34, no. 9, pp. 1680–1688, Sep. 2021, doi: 10.1111/tri.13982.
- [12] Y. Chen *et al.*, "Environmental Factors for Epstein-Barr Virus Reactivation in a High-Risk Area of Nasopharyngeal Carcinoma: A Population-Based Study," *Open Forum Infect. Dis.*, vol. 9, no. 5, p. ofac128, May 2022, doi: 10.1093/ofid/ofac128.
- [13] G. Niedobitek, N. Meru, and H. J. Delecluse, "Epstein-Barr virus infection and human malignancies," *Int. J. Exp. Pathol.*, vol. 82, no. 3, pp. 149–170, Jun. 2001, doi: 10.1046/j.1365-2613.2001.iep0082-0149-x.
- [14] C. Sonkar, T. Verma, D. Chatterji, A. K. Jain, and H. C. Jha, "Status of kinases in Epstein-Barr virus and *Helicobacter pylori* Coinfection in gastric Cancer cells," *BMC Cancer*, vol. 20, no. 1, p. 925, Dec. 2020, doi: 10.1186/s12885-020-07377-0.
- [15] C. Shannon-Lowe and M. Rowe, "Epstein-Barr virus entry; kissing and conjugation," *Curr. Opin. Virol.*, vol. 4, pp. 78–84, Feb. 2014, doi: 10.1016/j.coviro.2013.12.001.
- [16] M. Biström *et al.*, "Epstein–Barr virus infection after adolescence and human herpesvirus 6A as risk factors for multiple sclerosis," *Eur. J. Neurol.*, vol. 28, no. 2, pp. 579–586, Feb. 2021, doi: 10.1111/ene.14597.
- [17] K. Ali and C. Lawthom, "Epstein-Barr virus-associated cerebellar ataxia," *Case Rep.*, vol. 2013, no. apr22 1, pp. bcr2013009171–bcr2013009171, Apr. 2013, doi: 10.1136/bcr-2013-009171.
- [18] B. C. Jacobs *et al.*, "The spectrum of antecedent infections in Guillain-Barré syndrome: A case-control study," *Neurology*, vol. 51, no. 4, pp. 1110–1115, Oct. 1998, doi: 10.1212/WNL.51.4.1110.
- [19] I. Carbone *et al.*, "Herpes virus in Alzheimer's disease: relation to progression of the disease," *Neurobiol. Aging*, vol. 35, no. 1, pp. 122–129, Jan. 2014, doi: 10.1016/j.neurobiolaging.2013.06.024.

- [20] X.-L. Bu *et al.*, “The association between infectious burden and Parkinson’s disease: A case-control study,” *Parkinsonism Relat. Disord.*, vol. 21, no. 8, pp. 877–881, Aug. 2015, doi: 10.1016/j.parkreldis.2015.05.015.
- [21] D. Gate *et al.*, “Clonally expanded CD8 T cells patrol the cerebrospinal fluid in Alzheimer’s disease,” *Nature*, vol. 577, no. 7790, pp. 399–404, Jan. 2020, doi: 10.1038/s41586-019-1895-7.
- [22] E. P. Corssmit, M. A. Leverstein-Van Hall, P. Portegies, and P. Bakker, “Case Report Severe neurological complications in association with Epstein-Barr virus infection,” *J. Neurovirol.*, vol. 3, no. 6, pp. 460–464, Jan. 1997, doi: 10.3109/13550289709031193.
- [23] K. P. Connelly and L. D. DeWitt, “Neurologic complications of infectious mononucleosis,” *Pediatr. Neurol.*, vol. 10, no. 3, pp. 181–184, May 1994, doi: 10.1016/0887-8994(94)90021-3.
- [24] P. Portegies and N. Corssmit, “Epstein-Barr virus and the nervous system:,” *Curr. Opin. Neurol.*, vol. 13, no. 3, pp. 301–304, Jun. 2000, doi: 10.1097/00019052-200006000-00012.
- [25] D. I. Rubin and J. R. Daube, “Subacute sensory neuropathy associated with Epstein-Barr virus,” *Muscle Nerve*, vol. 22, no. 11, pp. 1607–1610, Nov. 1999, doi: 10.1002/(sici)1097-4598(199911)22:11<1607::aid-mus21>3.0.co;2-j.
- [26] A. F. Hahn, “Guillain-Barré syndrome,” *The Lancet*, vol. 352, no. 9128, pp. 635–641, Aug. 1998, doi: 10.1016/S0140-6736(97)12308-X.
- [27] P. Cinque *et al.*, “Epstein-Barr virus DNA in cerebrospinal fluid from patients with AIDS-related primary lymphoma of the central nervous system,” *The Lancet*, vol. 342, no. 8868, pp. 398–401, Aug. 1993, doi: 10.1016/0140-6736(93)92814-A.
- [28] D. Tiwari, S. Jakhmola, D. K. Pathak, R. Kumar, and H. C. Jha, “Temporal *In Vitro* Raman Spectroscopy for Monitoring Replication Kinetics of Epstein–Barr Virus Infection in Glial Cells,” *ACS Omega*, vol. 5, no. 45, pp. 29547–29560, Nov. 2020, doi: 10.1021/acsomega.0c04525.
- [29] S. Jakhmola and H. C. Jha, “Glial cell response to Epstein-Barr Virus infection: A plausible contribution to virus-associated inflammatory reactions in the brain,” *Virology*, vol. 559, pp. 182–195, Jul. 2021, doi: 10.1016/j.virol.2021.04.005.

- [30] A. Menet *et al.*, “Epstein-Barr Virus Infection of Human Astrocyte Cell Lines,” *J. Virol.*, vol. 73, no. 9, pp. 7722–7733, Sep. 1999, doi: 10.1128/JVI.73.9.7722-7733.1999.
- [31] O. Indari, R. Chandramohanadas, and H. C. Jha, “Epstein–Barr virus infection modulates blood–brain barrier cells and its co-infection with *Plasmodium falciparum* induces RBC adhesion,” *Pathog. Dis.*, vol. 79, no. 1, p. ftaa080, Jan. 2021, doi: 10.1093/femspd/ftaa080.
- [32] A. Alzheimer, R. A. Stelzmann, H. N. Schnitzlein, and F. R. Murtagh, “An English translation of Alzheimer’s 1907 paper, ‘Über eine eigenartige Erkrankung der Hirnrinde,’” *Clin. Anat. N. Y. N.*, vol. 8, no. 6, pp. 429–431, 1995, doi: 10.1002/ca.980080612.
- [33] A. W. R. Jones and J. S. Richardson, “Alzheimer’s Disease: Clinical and Pathological Characteristics,” *Int. J. Neurosci.*, vol. 50, no. 3–4, pp. 147–168, Jan. 1990, doi: 10.3109/00207459008987168.
- [34] D. J. Selkoe, “The molecular pathology of Alzheimer’s disease,” *Neuron*, vol. 6, no. 4, pp. 487–498, Apr. 1991, doi: 10.1016/0896-6273(91)90052-2.
- [35] R. Sathianathan and S. Kantipudi, “The dementia epidemic: Impact, prevention, and challenges for India,” *Indian J. Psychiatry*, vol. 60, no. 2, p. 165, 2018, doi: 10.4103/psychiatry.IndianJPsychiatry_261_18.
- [36] “2020 Alzheimer’s disease facts and figures,” *Alzheimers Dement.*, vol. 16, no. 3, pp. 391–460, Mar. 2020, doi: 10.1002/alz.12068.
- [37] J. A. Hardy and G. A. Higgins, “Alzheimer’s Disease: The Amyloid Cascade Hypothesis,” *Science*, vol. 256, no. 5054, pp. 184–185, Apr. 1992, doi: 10.1126/science.1566067.
- [38] C. M. Wischik, M. Novak, P. C. Edwards, A. Klug, W. Tichelaar, and R. A. Crowther, “Structural characterization of the core of the paired helical filament of Alzheimer disease.,” *Proc. Natl. Acad. Sci.*, vol. 85, no. 13, pp. 4884–4888, Jul. 1988, doi: 10.1073/pnas.85.13.4884.
- [39] D. J. Selkoe, “Alzheimer’s Disease: Genes, Proteins, and Therapy,” *Physiol. Rev.*, vol. 81, no. 2, pp. 741–766, Apr. 2001, doi: 10.1152/physrev.2001.81.2.741.
- [40] C. K. Chai, “The Genetics of Alzheimer’s Disease,” *Am. J. Alzheimers Dis. Dementiasr*, vol. 22, no. 1, pp. 37–41, Feb. 2007, doi: 10.1177/1533317506295655.

- [41] G. D. Schellenberg, “Genetic dissection of Alzheimer disease, a heterogeneous disorder,” *Proc. Natl. Acad. Sci.*, vol. 92, no. 19, pp. 8552–8559, Sep. 1995, doi: 10.1073/pnas.92.19.8552.
- [42] M. L. Gosztyla, H. M. Brothers, and S. R. Robinson, “Alzheimer’s Amyloid- β is an Antimicrobial Peptide: A Review of the Evidence,” *J. Alzheimers Dis.*, vol. 62, no. 4, pp. 1495–1506, Mar. 2018, doi: 10.3233/JAD-171133.
- [43] K. Shima, G. Kuhlenbäumer, and J. Rupp, “Chlamydia pneumoniae infection and Alzheimer’s disease: a connection to remember?,” *Med. Microbiol. Immunol. (Berl.)*, vol. 199, no. 4, pp. 283–289, Nov. 2010, doi: 10.1007/s00430-010-0162-1.
- [44] A. G. Senejani *et al.*, “Borrelia burgdorferi Co-Localizing with Amyloid Markers in Alzheimer’s Disease Brain Tissues,” *J. Alzheimers Dis.*, vol. 85, no. 2, pp. 889–903, Jan. 2022, doi: 10.3233/JAD-215398.
- [45] G. Albaret *et al.*, “Alzheimer’s Disease and Helicobacter pylori Infection: Inflammation from Stomach to Brain?,” *J. Alzheimers Dis.*, vol. 73, no. 2, pp. 801–809, Jan. 2020, doi: 10.3233/JAD-190496.
- [46] S. Kanagasingam, S. S. Chukkapalli, R. Welbury, and S. K. Singhrao, “Porphyromonas gingivalis is a Strong Risk Factor for Alzheimer’s Disease,” *J. Alzheimers Dis. Rep.*, vol. 4, no. 1, pp. 501–511, Dec. 2020, doi: 10.3233/ADR-200250.
- [47] R. Rizzo, “Controversial role of herpesviruses in Alzheimer’s disease,” *PLOS Pathog.*, vol. 16, no. 6, p. e1008575, Jun. 2020, doi: 10.1371/journal.ppat.1008575.
- [48] J.-S. Kang and P.-P. Liu, “Human herpesvirus 4 and adaptive immunity in Alzheimer’s disease,” *Signal Transduct. Target. Ther.*, vol. 5, no. 1, p. 48, Dec. 2020, doi: 10.1038/s41392-020-0125-y.
- [49] W. A. Eimer *et al.*, “Alzheimer’s Disease-Associated β -Amyloid Is Rapidly Seeded by Herpesviridae to Protect against Brain Infection,” *Neuron*, vol. 99, no. 1, pp. 56-63.e3, Jul. 2018, doi: 10.1016/j.neuron.2018.06.030.
- [50] D. J. Bonda *et al.*, “Review: Cell cycle aberrations and neurodegeneration,” *Neuropathol. Appl. Neurobiol.*, vol. 36, no. 2, pp. 157–163, Apr. 2010, doi: 10.1111/j.1365-2990.2010.01064.x.

- [51] A. McShea *et al.*, “Neuronal cell cycle re-entry mediates Alzheimer disease-type changes,” *Biochim. Biophys. Acta BBA - Mol. Basis Dis.*, vol. 1772, no. 4, pp. 467–472, Apr. 2007, doi: 10.1016/j.bbadis.2006.09.010.
- [52] T. Barrett, K. A. Stangis, T. Saito, T. Saido, and K. H. J. Park, “Neuronal Cell Cycle Re-Entry Enhances Neuropathological Features in AppNLF Knock-In Mice,” *J. Alzheimers Dis.*, vol. 82, no. 4, pp. 1683–1702, Aug. 2021, doi: 10.3233/JAD-210091.
- [53] A. McShea, P. L. Harris, K. R. Webster, A. F. Wahl, and M. A. Smith, “Abnormal expression of the cell cycle regulators P16 and CDK4 in Alzheimer’s disease,” *Am. J. Pathol.*, vol. 150, no. 6, pp. 1933–1939, Jun. 1997.
- [54] Z. Nagy, M. M. Esiri, and A. D. Smith, “Expression of cell division markers in the hippocampus in Alzheimer’s disease and other neurodegenerative conditions,” *Acta Neuropathol. (Berl.)*, vol. 93, no. 3, pp. 294–300, Mar. 1997, doi: 10.1007/s004010050617.
- [55] I. Vincent, G. Jicha, M. Rosado, and D. W. Dickson, “Aberrant expression of mitotic cdc2/cyclin B1 kinase in degenerating neurons of Alzheimer’s disease brain,” *J. Neurosci. Off. J. Soc. Neurosci.*, vol. 17, no. 10, pp. 3588–3598, May 1997.
- [56] M. G. Davenport and J. S. Pagano, “Expression of EBNA-1 mRNA Is Regulated by Cell Cycle during Epstein-Barr Virus Type I Latency,” *J. Virol.*, vol. 73, no. 4, pp. 3154–3161, Apr. 1999, doi: 10.1128/JVI.73.4.3154-3161.1999.
- [57] A. Saha and E. S. Robertson, “Impact of EBV essential nuclear protein EBNA-3C on B-cell proliferation and apoptosis,” *Future Microbiol.*, vol. 8, no. 3, pp. 323–352, Mar. 2013, doi: 10.2217/fmb.12.147.
- [58] T. Faqing *et al.*, “EPSTEIN —BARR VIRUS LMP1 INITIATES CELL PROLIFERATION AND APOPTOSIS INHIBITION VIA REGULATING EXPRESSION OF SURVIVIN IN NASOPHARYNGEAL CARCINOMA,” *Exp. Oncol.*, p. 6, 2005.
- [59] N. Ohtani *et al.*, “Epstein-Barr virus LMP1 blocks p16INK4a–RB pathway by promoting nuclear export of E2F4/5,” *J. Cell Biol.*, vol. 162, no. 2, pp. 173–183, Jul. 2003, doi: 10.1083/jcb.200302085.

- [60] Y. Xu *et al.*, “Epstein-Barr Virus encoded LMP1 regulates cyclin D1 promoter activity by nuclear EGFR and STAT3 in CNE1 cells,” *J. Exp. Clin. Cancer Res.*, vol. 32, no. 1, p. 90, 2013, doi: 10.1186/1756-9966-32-90.
- [61] X. Yang, Z. He, B. Xin, and L. Cao, “LMP1 of Epstein–Barr virus suppresses cellular senescence associated with the inhibition of p16INK4a expression,” *Oncogene*, vol. 19, no. 16, pp. 2002–2013, Apr. 2000, doi: 10.1038/sj.onc.1203515.
- [62] A. Mauser, E. Holley-Guthrie, D. Simpson, W. Kaufmann, and S. Kenney, “The Epstein-Barr Virus Immediate-Early Protein BZLF1 Induces both a G₂ and a Mitotic Block,” *J. Virol.*, vol. 76, no. 19, pp. 10030–10037, Oct. 2002, doi: 10.1128/JVI.76.19.10030-10037.2002.

Chapter 2

Scope and Objective of the Research

Scope

EBV infection in the CNS could lead to varied outcomes, including encephalitis, meningitis, neuropathies, or well-known neurodegenerative disorders like AD, PD, MS, etc. The virus can enter the CNS either by penetrating through the BBB by infecting the endothelial lining of BBB or could transverse as a “trojan-horse” hidden inside the patrolling B-lymphocytes. Once inside the CNS, it could either infect the neuronal or glial cells directly; or induce an indirect inflammatory response in these cells. It is hypothesized that upon directly infecting the neurons, as an oncogenic virus, EBV could drive them towards abortive replication resulting in neuronal death. At the same time, infection in glial cells could activate the neuroinflammatory response and incur indirect damage to neurons. However, precise mechanistic nuances of the process are still not known. Therefore, it is imperative to elucidate the response of various components of the CNS upon EBV infection. The investigation would help understand the sequential events that might occur during EBV infection in the neural milieu and how they might lead to neurodegenerative pathologies such as AD. The objectives of the current work are formulated to address the conundrum mentioned above of EBV’s potential role in mediating AD neuropathology. The objectives are as follows:

Objectives

➤ **Understanding the involvement of EBV in aggregate formation: a characteristic pathology of AD**

The first step in an attempt to evaluate the involvement of EBV in AD-associated neurodegeneration would be to check if it can give rise to AD hallmark pathology. Therefore, it is essential to understand if EBV by some means can contribute to amyloid pathogenesis and what its effects are on the neurons.

➤ **Investigating the biochemical effect of EBV infection in glial cells, which may mediate indirect insult to the neurons causing degeneration**

Apart from studying the direct effect of EBV and related molecules on neurons, it is also crucial to understand the indirect effect mounted via glial cell infection. The alterations in the biochemical profile of the host cell are inevitable and can be used to monitor the sequential progression of infection.

➤ **Employing an *in-silico* approach to study probable interaction between viral and host proteins conspiring to create a deleterious microenvironment in neuronal milieu culminating in AD**

It is of utmost importance to study the interaction of the virus with the host factors well known to be associated with AD neurodegeneration. The role of apolipoprotein variants is well established in predisposing an individual to AD. However, concurrent research has also suggested its role in susceptibility to viral infection. Therefore, in pursuit of the same, apolipoproteins make the first exploration target to evaluate the possibility of interaction with various EBV proteins.

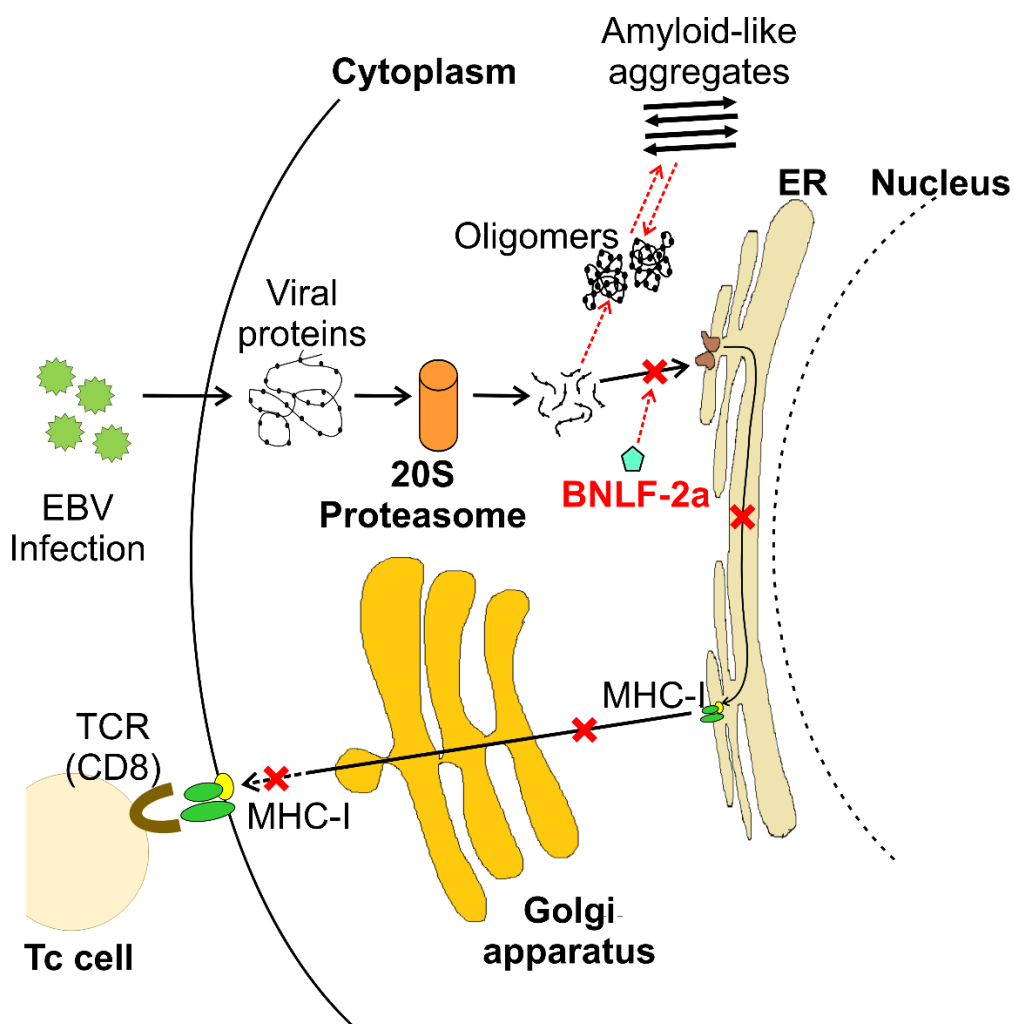
➤ **Attempting to target various aspects of EBV infection in the neural milieu to hinder the progression of neurodegeneration using computational tools**

Only attempting to understand the mechanistic details of EBV infection and progression in the neuronal milieu is not enough to fight off the severe virus-associated outcomes. It is the need of the hour to investigate the probable drug targets in viral assembly and the use of drugs against them. With the development of naturopathy and its advocated benefits, it is worth exploring the vast plethora of phytochemicals for their efficacy against viruses.

Chapter 3

Indication of Neurodegenerative Cascade Initiation by amyloid-like Aggregate-Forming EBV Proteins and Peptide in Alzheimer's Disease

3.1 Graphical abstract



3.2 Abstract

The neurotropic potential of the EBV was demonstrated quite recently; however, the mechanistic details are yet to be explored. Therefore, the effects of EBV infection in the neural milieu remain underexplored. Previous reports have suggested the potential role of virus-derived peptides in seeding the A β aggregation cascade, which lies at the center of AD pathophysiology. However, no such study has been undertaken to explore the role of EBV peptides in AD. In our research, ~100 EBV proteins were analyzed for their aggregation proclivity *in-silico* using bioinformatic tools, followed by the prediction of 20S proteasomal cleavage activity generating short antigenic peptides of viral origin. Our study reports a high aggregate-forming tendency of an 11-amino-acid long (₁₄₆SYKHVFLSAFVY₁₅₇) peptide derived from EBV glycoprotein-M (EBV-gM). The *in-vitro* analysis of the aggregate formation, done using Congo red and Thioflavin-S (ThioS) assays, demonstrated dose- and time-dependent kinetics. Thereafter, Raman spectroscopy (RS) was used to validate the formation of secondary structures (α helix, β sheets) in the aggregates. Additionally, a cytotoxicity assay revealed that even a low concentration of these aggregates has a lethal effect on the neuroblastoma cells. The findings of this study provide insights into the mechanistic role of EBV in AD and open up new avenues to explore in the future.

Keywords: Epstein-Barr virus, amyloid-like aggregates, viral peptides, EBV glycoprotein M (EBV-gM), Alzheimer's disease (AD), neurodegeneration

3.3 Introduction

Amongst all the neurodegenerative disorders, AD is the most common and contributes to around 60-70% of dementia cases. According to the latest WHO report, people suffering from AD are projected to reach 82 million by 2030 [1]. Therefore, it accounts for significant health concerns in the contemporary world. It is pathologically characterized by the presence of A β plaques and neurofibrillary tangles in the brain [2]. However, the origination of proteinaceous plaque formation is still a subject of research [3], [4]. The plaque build-up results in multiple pathophysiological effects like neuronal

excitotoxicity, synaptic dysfunctioning, excitotoxicity, mitochondrial alterations, oxidative stress, disturbed calcium homeostasis, etc. [5]. As a result of pathological effects upon disease advancement, the patient suffers from progressive loss of memory, spatial sense, and ultimately loss of motor functions in the severe stage of the disease [6]. Although numerous hypotheses have been proposed as a cause of the disease, none have been proven to be the sole reason for disease development. AD is now believed to be caused by the interplay of multiple factors that govern the course of disease development. These elements could be lifestyle factors, nearby environment, genetic makeup, infection of certain pathogenic organisms, and epigenetics [7]. Among all these, infectious agents are considered a prominent risk factor in developing late-onset AD (LOAD), which accounts for 95% of total AD cases [8]. Various infectious agents such as viruses, bacteria, fungi, and some parasites are associated with disease pathogenesis [9], [10]. Although the notion of pathogen infection as an initiator of neurodegenerative pathology is a decade old, still very few studies explore their role in AD [11].

Among various viruses, members of *Herpesviridae* are most prominently reported to be involved in the pathogenesis of AD. In particular, herpes simplex virus-1, 2 (HSV-1, 2), human cytomegalovirus (HCMV), Epstein-Barr virus (EBV), human herpesvirus-6A, and 6B (HHV-6A, HHV-6B) are primarily known to be involved in AD pathogenesis [12]. However, thus far, no study has established the role of EBV as a causative agent of neurodegeneration. EBV, which is taxonomically known as Human herpesvirus-4 (HHV-4), infects the adult population ubiquitously [13]. Following infection, EBV, like most herpesviruses, can enter a latent phase and become reactivated when the host immunity is compromised [14]–[16]. Furthermore, serological studies have frequently reported the presence of herpesviruses (particularly HSV-1, EBV, and HCMV) in the peripheral blood lymphocytes (PBL) of AD patients [17]. EBV and its transcripts have also been recorded in AD patients' CSF and post-mortem brain tissue [18]. Therefore, EBV is considered a veiled and menacing threat to human health, coupled with its capability to reactivate. Thus far, the research has established the association of EBV infection with the development of AD pathophysiology; the mechanistic understanding of the event is still elusive.

Additionally, a few clinical findings have also controversially linked EBV with macular and primary cutaneous amyloidosis [19], [20]. Interestingly, our recent *in-vitro* study showed that EBV could infect various cells from the neuronal microenvironment, namely, astrocytes, microglia, and endothelial cells from the BBB [21], [22].

Although, the implication could not only be limited to AD alone, given the ubiquitous nature of EBV infection in the human body and its tropism. In this study, we have tried to explore the mechanistic role of EBV in AD progression. Interestingly, the interaction between various aggregation-prone proteins and peptides of either cellular or pathogenic origin has long been supposed to promote an aberrant aggregation cascade giving rise to plaques [23]–[25]. Therefore, as one possibility, we have supposed EBV proteins derived peptides could form amyloid-like aggregates and seed aggregate deposition leading to the development of neurodegenerative pathology. Such tendency of herpesviral peptides to form aggregate has previously been demonstrated by glycoprotein-K of HSV-1 [26]. In general, the host-mediated 20S proteasomal cleavage of the viral antigens gives rise to peptide fragments, which are then presented on the surface of T-cells in general and help in mounting immune response to the infection [27], [28]. However, EBV proteins have not been subjected to any such analysis of their aggregation potential to date. Our study demonstrated the aggregate forming tendency of these peptides *in-silico* and *in-vitro*. Using online servers TANGO and AGGRESCAN, we evaluated the aggregation tendency of the sequence of EBV proteins retrieved from online databanks. Thereafter, we predicted the 20S proteasomal cleavage sites *in-silico*, present within the aggregation-prone regions of selected proteins, using an online server based on the support vector machine (SVM). The hydrophobicity of the entire protein sequence was then analyzed. Based on these parameters, 11 amino acids long (₁₄₆SYKHVFLSAFVY₁₅₇) peptide derived from EBV glycoprotein-M (EBV-gM) showed aggregation score and hydrophobicity values comparable to A β ₁₋₄₂ was identified. Subsequent *in-vitro* studies with synthetic EBV-gM₁₄₆₋₁₅₇ peptide using Congo-red and Thio-S based aggregation analysis showed positive results. Further, to validate the formation of secondary structure in the aggregates RS was utilized [29]. All these analyses suggested the formation of amyloid-like

aggregates from EBV-gM₁₄₆₋₁₅₇ peptide. The cytotoxicity examination of the peptide using MTT assay against neuroblastoma cell line showed dose dependent increase in toxicity. This study may open up a new avenue for exploration of probable mechanisms of EBV mediated neurodegeneration.

3.4 Results and Discussion

EBV is predominantly known as an oncogenic virus. However, it was recently discovered to be capable of successfully infecting cells from neural backgrounds, namely, glia and neuronal cells. It is commonly known to cause IM in adults. Although primary infection in childhood usually remains asymptomatic, reactivation of EBV later in life as an adult is associated with various pathologies such as lymphomas, IM-like disease, hemophagocytic syndrome, and chronic active EBV infection [30]. The recurrent reactivation of EBV may also allow it to enter the CNS and result in neurodegenerative conditions [31].

A recent study published by Gate et al. unambiguously demonstrated the role of EBV-initiated immune response via its antigens EBNA3A and BZLF1 in AD pathogenesis [32]. The study demonstrated the role of EBV instigated adaptive immune response mediated by T_{EMRA} cells in AD pathogenesis. They found that the cognition in mild cognitive impairment (MCI) or AD patients is negatively related to the population of T_{EMRA} cells. Interestingly, they also observed the co-localization of T_{EMRA} cells with A β plaques in the hippocampus and CSF of the AD patients. Further, they showed the cytotoxic effects of clonal T_{EMRA} cells in the CSF of AD patients. These CD8⁺ T cells help the cell keep the viral infection under check by recognizing the antigen displayed on the cell surface of antigen-presenting cells (APCs) with the help of major histocompatibility complex-I (MHC-I) molecules. In the human brain, MHC-I molecules are predominantly present on the surface of endothelium and microglia in the hippocampus area and neurons of the substantia nigra pars compacta (SNpc) and locus coeruleus.

Furthermore, the potential role of neuroinflammation is well studied in the case of neurodegenerative conditions such as AD, PD, and MS. Previous studies have also demonstrated the anti-viral potential of A β plaques toward various

herpesviruses [33]. Scientists have therefore extrapolated the possibility of herpesviruses being capable of initiating the A β mediated defense cascade [34]. However, the mechanism of instigation is poorly understood.

The periodic reactivation of EBV under the immunocompromised state of a patient suggests that EBV is very well capable of eluding the host immune system response, at least during the initial stages of infection. Identification of viral antigenic peptides conjugated with MHC-I by APCs initiates the death of infected cells by various pathways. Therefore, the generation of viral peptides by 20S proteasomal activity of the infected cells and their presentation is crucial to successfully fight off the infection by mounting an immune response against the virus [35]. However, blocking antigen presentation to cytotoxic T lymphocytes (CTLs) helps the virus evade the host immune response and stay hidden. In general, the infected cells present peptides derived from viral proteins along with those from intracellular proteins. After the 20S proteasomal cleavage, further processing of these peptides happens in the cytoplasmic and endoplasmic reticulum (ER), where they get trimmed for MHC-I presentation. The thus generated viral antigenic peptides are then transported through ER via a transporter associated with antigen processing (TAP). Further cleavage of these peptides at ER gives rise to much shorter fragments that are then loaded onto MHC-I molecules and presented on the cell surface. Under physiological conditions, this event generates an immune response, especially by activation of CTLs following recognition of virus-infected cells.

In 2016, Jainmin Zuo *et al.* suggested that the EBV gene BDLF3 mediated ubiquitination and downregulation of MHC-I and II in circumventing the host immunity [36]. Another group led by Andrew D. Hislop in 2009 demonstrated stage-specific inhibition of MHC-I presentation by EBV via protein BNLF2a [37]. The study showed that EBV encoded BNLF2a could act as a TAP blocker [38]. Such previous studies, along with our findings, led us to hypothesize that upon infection, events such as obstruction of TAP by EBV-encoded BNLF2 and downregulation of MHC-I and II via BDLF3 in a cell could lead to the accumulation of cellular as well as viral peptides in its milieu. This pool could consist of various viral peptides, including EBV-gM₁₄₆₋₁₅₇, apart from cellular peptides. Even if not during every reactivation, eventually, upon repeated

reactivation event, it may contribute to the intracellular aggregate pool as depicted in the schematic diagram.

Additionally, the reactivation of EBV infection could also be linked to another pathophysiology of AD, i.e., accumulation of α -synuclein (α -syn) protein. Various studies have demonstrated that monoclonal antibodies against EBV encoded LMP1 exhibit cross-reactivity with α -syn protein [39]. Although α -syn has been extensively linked with the pathology of parkinsonian disorders, recent evidence points toward its involvement in AD [40]. The study conducted by Crews, Leslie *et al.* suggested that α -syn may directly or indirectly interact with $A\beta_{42}$ and other aggregate forming proteins and fuel the process of oligomerization, exerting toxic effects on the cell. Therefore, during active EBV infection in the neuronal microenvironment, the expression of EBV encoded BNLF2a could obstruct TAP-mediated transport of peptides leading to peptide accumulation in the ER lumen. At the same time, LMP1 mimicking the cellular protein α -syn could trigger oligomerization of peptides leading to aggregate formation. Numerous previous reports have shown that $A\beta$ is seeded in response to viral infection as a neuroprotective measure [41]. A study on HSV-1 done by Bourgade *et al.* claimed that “the anti-viral activity of $A\beta$ is associated with its capability to interact with viral coat proteins” [42]. It is now well known that interactions between the various cellular peptide and $A\beta$ monomers could kick-start the amyloid cascade and cause the deposition of proteinaceous aggregates leading to the pathophysiological abnormalities observed in AD neurodegeneration [43]. We hypothesize that virus-derived peptides may also act similarly to initiate an aggregation cascade leading to neurodegeneration. Therefore, we first evaluated various EBV proteins for their overall aggregation potential *in-silico*.

3.4.1 In-silico screening of aggregation-prone EBV proteins:

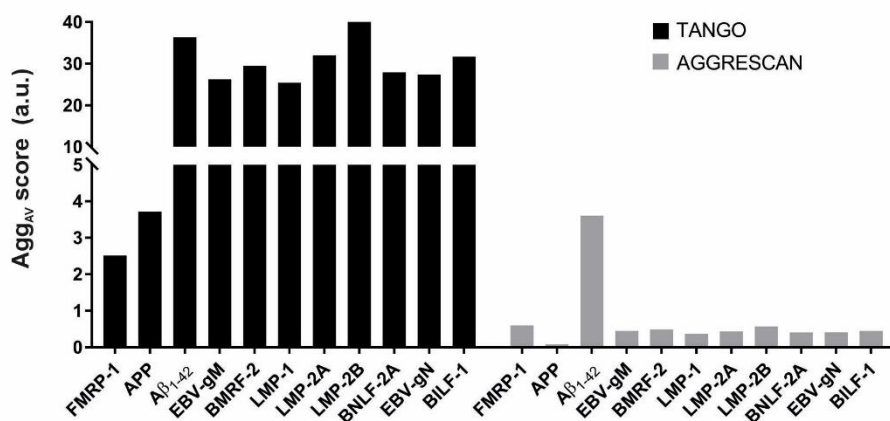
Freely available online servers TANGO and AGGRESCAN were used to determine the average aggregation score (Agg_{AV}) of ~100 EBV proteins [Table S3.1] along with $A\beta_{1-42}$ and FMRP-1 (Fragile X mental retardation-1) proteins. FMRP-1 was chosen as a negative control due to its abundance in the neurons,

role in synaptic plasticity, and mental retardation while having no aggregation tendency. Whereas, A β ₁₋₄₂, chosen as the positive control, is a well-established aggregate forming protein fragment predominantly known to be involved in neurodegeneration. Therefore, protein/ peptide fragments having an Agg_{AV} score closer to that of A β ₁₋₄₂ have a high probability of forming aggregates. The Agg_{AV} score was calculated for each protein by dividing the total aggregation score (additive aggregation score of each residue) by the number of residues in the protein. The Agg_{AV} score of all proteins calculated by TANGO/AGGRESCAN was then compared with the Agg_{AV} of positive control, A β ₁₋₄₂ (36.6/3.61), and the negative control FMRP-1 (2.52/0.6). Based on the Agg_{AV} calculation by TANGO, nine EBV proteins were identified to have an aggregation score comparable to the positive control A β ₁₋₄₂ [Figure 3.1(a)]. However, five proteins were excluded from further analysis on account of being membrane proteins. The Agg_{AV} of the other four proteins was comparable with A β ₁₋₄₂, i.e., 26.24 of EBV-gM, 29.46 of BMRF2, 27.88 of BNLF1, and 27.36 of EBV-gN. Hence, for further analysis, only these proteins were selected. Notably, the shorter length of A β ₁₋₄₂ could influence its aggregation score values. Therefore, the aggregation score per residue across the entire protein length was considered to avoid this prejudice while comparing the aggregation scores. As shown in [Figure 3.1 (b, c)], the selected proteins displayed several intermittent segments having Agg_{AV} scores comparable to A β ₁₋₄₂.

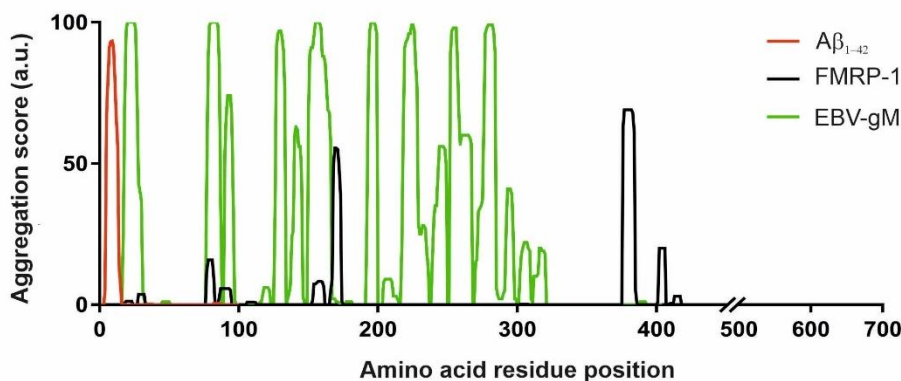
In contrast, FMRP-1 expressed the least number of such regions. This analysis corroborates the high aggregation proclivity of the selected proteins. Further, to evaluate the sectional aggregation potential of fragments probably generated after the 20S proteasomal cleavage of the whole protein, we predicted the cleavage sites on these proteins and calculated their individual Agg_{AV} scores.

Figure 3.1

a) Agg_{AV} of EBV proteins



b) TANGO- Agg_{AV} per residue



c) AGGRESCAN- Agg_{AV} per residue

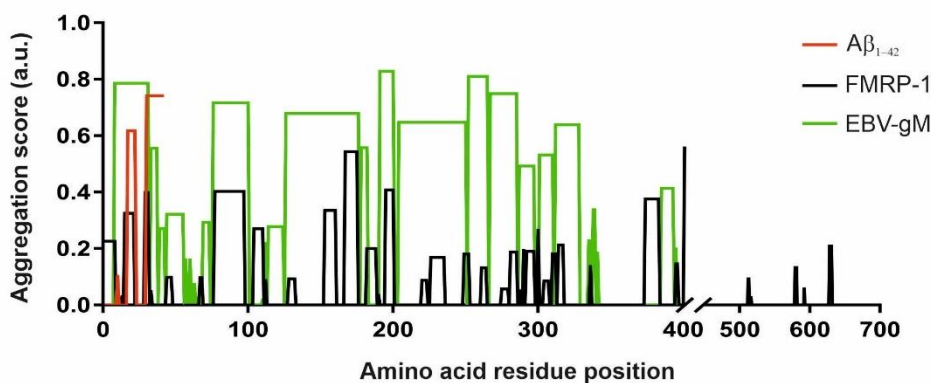


Figure 3.1 Average aggregation scores of EBV proteins. (a) Average aggregation score of various EBV proteins compared to the positive control (Aβ₄₂) and negative control FMRP-1 as calculated by TANGO and AGGRESCAN. The EBV peptides showed comparable aggregation scores with Aβ₄₂ (b) Aggregation score of EBV-gM plotted along the entire protein length compared to the positive and negative control as calculated by TANGO. (c) as calculated by AGGRESCAN. Both the plots show that the aggregation score of EBV-gM along the entire protein length is higher than the positive control.

3.4.2 20S Proteasome cleavage site prediction and identification of aggregation-prone peptides:

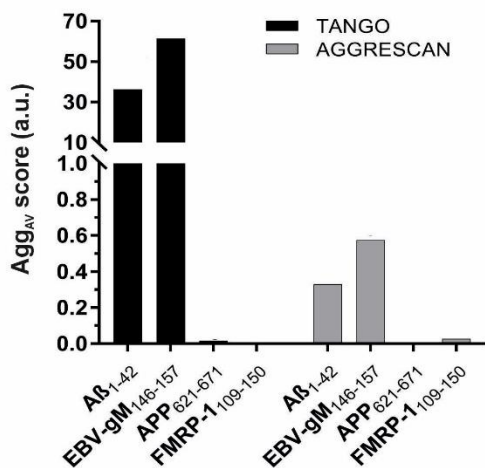
The online servers- Pcleavage and NetChop ver3.0 were used for *in-silico* determination of the 20S proteasomal cleavage sites on the selected proteins. The data thus obtained suggested that the predicted 20S cleavage sites on the protein overlapped with its aggregation-prone regions. The aggregation-prone segments in the selected proteins (identified using TANGO) located between two adjacent 20S cleavage sites were considered for further analysis. Across the entire length of proteins, eight segments for EBV-gM, nine for BMRF2, and one each for BNLF2A and EBV-gN were identified. Aggregation analysis of all the aggregation-prone regions of EBV-gM and BMRF2 revealed five segments of each EBV-gM and BMRF2 having high aggregation propensity compared to the positive control A β ₁₋₄₂ (as shown in [Table S3. 2]). Thereafter, we compared the hydrophobicity and Agg_{AV} score for each peptide fragment that was calculated using the peptide analyzing tool (Thermo Fisher) and TANGO/ AGGRESCAN, respectively. For EBV-gM₁₄₆₋₁₅₇, the Agg_{AV} value was 61.5 [Figure 3.2 (a)], and the hydrophobicity value was found to be 41.89 [Figure 3.2 (b)], which is comparable with that of A β ₁₋₄₂, i.e., 36.48 and 54.77, respectively. The TANGO aggregation score of the EBV-gM₁₄₆₋₁₅₇ peptide (61.5) was found to be almost double that of the A β ₁₋₄₂ peptide (36.48). Although the Agg_{AV} scores calculated using AGGRESCAN also show a higher value for the EBV-gM₁₄₆₋₁₅₇ peptide (0.58), the multifold increase was not observed as compared to the A β ₁₋₄₂ peptide (0.33). The comparison of Agg_{AV} per residue along the entire length of the EBV-gM₁₄₆₋₁₅₇ peptide also revealed its higher tendency to form aggregates than the A β ₁₋₄₂ [Figure 3.2 (a)]. Both the peptides were also analyzed for the presence of consensus amyloidogenic features using AMYLPRED2 (a web-based tool that analyzes the unanimity of amyloidogenic sequences present in a protein predicted by different methods compared to the positive control A β ₁₋₄₂ peptide. It provides an idea about the amyloidogenic aggregate forming potential of the test peptide. These *in-silico* analyses of the EBV-gM₁₄₆₋₁₅₇ advocate its amyloidogenic properties, and hence it was selected for further *in-vitro* studies.

We recorded that the aggregation scores of EBV-gM₁₄₆₋₁₅₇ were higher than A β ₄₂, though the peptide's size was relatively small compared to the latter. In

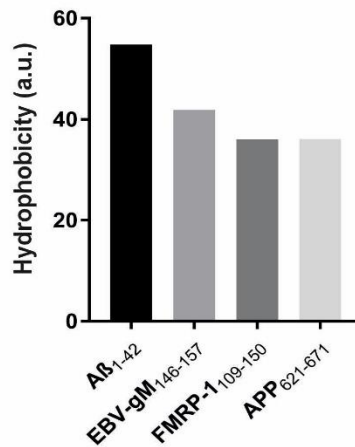
addition to the aggregation scores, the EBV-gM₁₄₆₋₁₅₇ peptide showed a comparable hydrophobicity score with A β ₄₂, which makes it more prone to instant aggregation. We observed similar peptide behavior upon *in-vitro* solubilization done for analyzing the aggregation kinetics as previously mentioned reports.

Figure 3.2

a) Agg_{AV} score of peptides



b) Hydrophobic index



c) Agg_{AV} score per residue

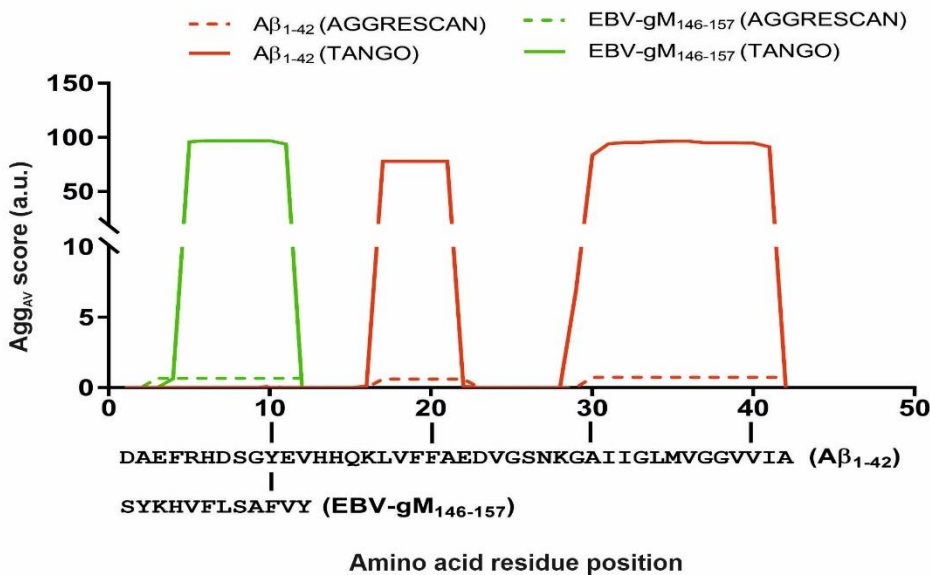


Figure 3.2 Various properties of EBV-gM peptide depicting its aggregation capability. (a) Average aggregation score of EBV-gM₁₄₆₋₁₅₇ per residue as compared to the positive (A β ₁₋₄₂) and negative control (FMRP-1). EBV-gM₁₄₆₋₁₅₇ showed a higher per residue aggregation score than the A β ₄₂ as calculated by TANGO and AGGRESCAN. (b) The hydrophobicity index of the EBV-gM₁₄₆₋₁₅₇ peptide is higher than the negative control and comparable to the positive control. (c) The average aggregation score per residue of the EBV-gM is much higher than the positive control A β ₄₂.

After the *in-silico* analysis of various EBV proteins revealed a potential candidate, i.e., EBV-gM₁₄₆₋₁₅₇ peptide having comparable Agg_{AV} score with A β ₄₂, we proceeded to evaluate the *in-vitro* likelihood of the peptide forming amyloid-like aggregates.

3.4.3 *In vitro* aggregation analysis of the EBV peptide:

For *in-vitro* experiments, the DMSO solubilized EBV peptide (EBV-gM₁₄₆₋₁₅₇) was further dissolved in the buffer and left to form aggregates under specified conditions as required. As described previously in the Materials and Methods section, aggregation samples were prepared at concentrations of 31.25, 62.5, 125, 250, and 500 μ M in 1XPBS. Turbidity was observed in the solutions upon incubation at 37°C at higher concentrations, suggesting a stronger tendency of the EBV-gM₁₄₆₋₁₅₇ peptide to form aggregates. Thereafter, the samples prepared at 125, 250, and 500 μ M peptide concentration were subjected to Congo red absorption assay to analyze the presence of amyloid-like aggregates in them. As shown in [Figure 3.3], upon conjugation with the aggregation samples, a characteristic bathochromic shift from 480 nm to 500 nm was observed in the absorption maxima of Congo red. This 20 nm shift in the absorption maxima of Congo red implied the probability of the presence of amyloid-like aggregates. To further validate the presence of amyloid-like aggregates in the samples, an amyloid-specific ThioS fluorescence assay was then performed.

Figure 3.3

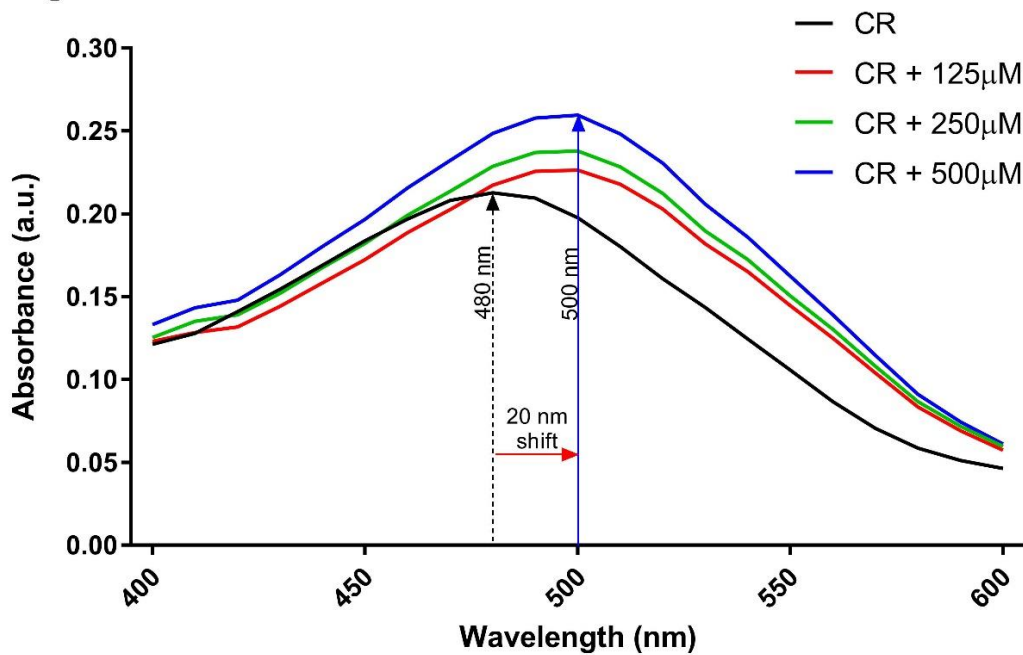


Figure 3.3 Congo-Red absorption assay. The Congo-red absorption spectrum of the EBV-gM₁₄₆₋₁₅₇ aggregates showing the characteristic bathochromic shift (of ~20 nm) from 480 nm to 500 nm. The shift indicates the presence of amyloid-like aggregates in the aggregate solution of concentrations 125, 250, and 500 μM.

As explained in the Materials and Methods sections, the peptide samples prepared at the concentrations of 31.25, 62.5, 125, 250, and 500 μM were mixed with the ThioS dye. The resultant samples were excited at 391 nm, and the emission spectra were recorded in the range of 400-600, with the peak lying between 440-450. As shown in [Figure 3.4 (a, b)], a concentration-dependent increase in fluorescence signals was observed. After 12-hour incubation at 37°C while on stir, the fluorescence intensity increased significantly for the peptide concentrations of 125, 250, and 500 μM [Figure 3.4 (c)]. Whereas, upon 24-hour incubation significant increase in the fluorescence was observed for all the concentrations [Figure 3.4 (d)]. Also, on comparing the fluorescence intensity from 12 to 24 hours, we observed a significant change at the concentrations of 125, 250, and 500 μM [Figure 3.4 (e)]. The Congo-red absorbance assay corroborated the claim.

Figure 3.4 Thioflavin-S Fluorescence after incubation

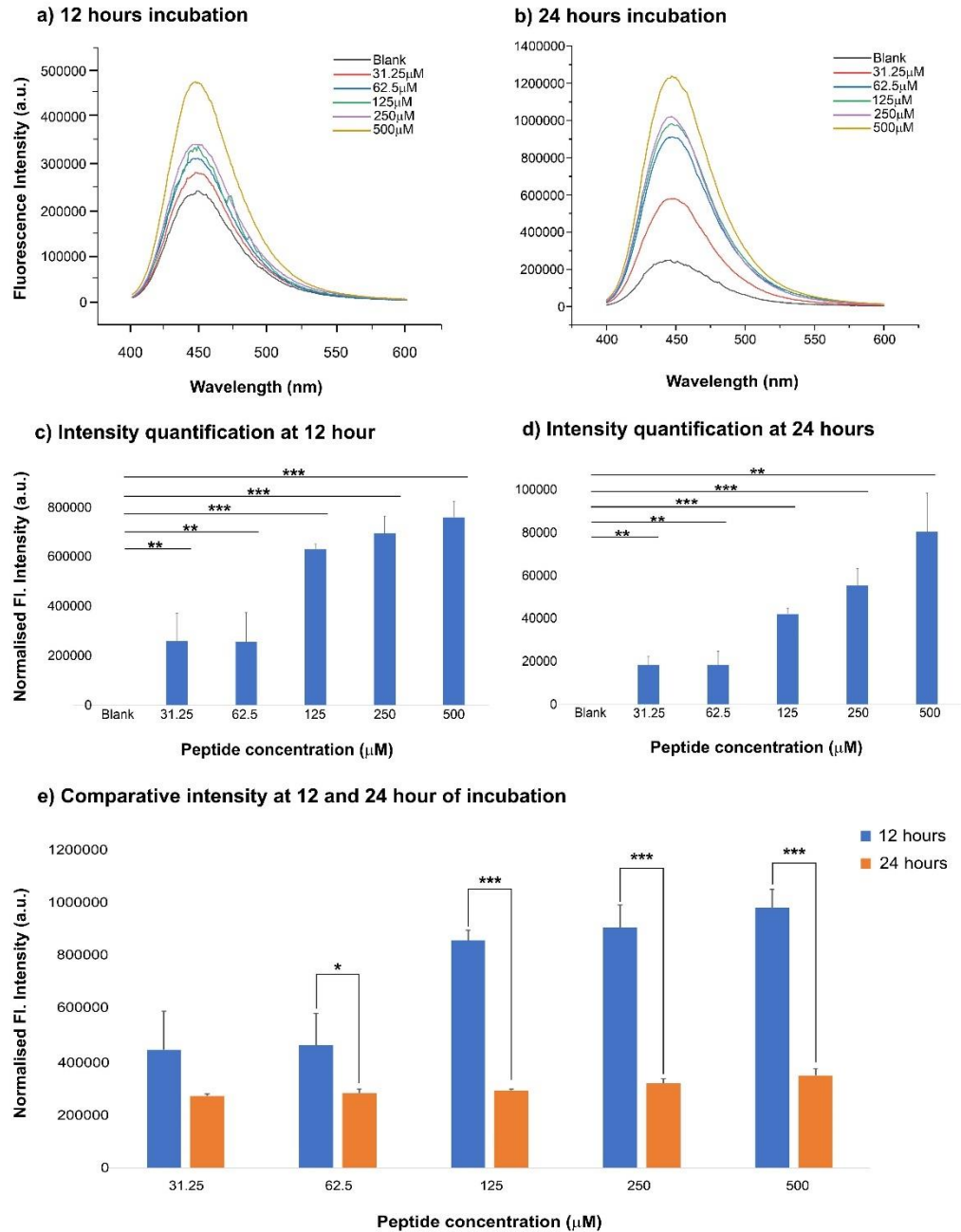


Figure 3.4 Thioflavin-S fluorescence emission by EBV-gM₁₄₆₋₁₅₇ peptide after incubation. The fluorescence spectra were obtained after (a) 12 hours and (b) 24 hours incubation in the range of 400-600 nm. The quantification of normalized fluorescence intensity at maxima plotted with increasing dosage of aggregates, i.e., 31.25, 62.5, 125, 250, and 500 μ M, at (c) 12 hours and (d) 24 hours post-incubation at 37°C. The highly significant ($p < 0.001$) increase in fluorescence intensity at higher concentrations (125, 250, and 500 μ M) at 12 hours demonstrated the formation of more aggregates at higher concentrations. (d) Comparative analysis of fluorescence intensity at 12- and 24-hours post-incubation for different concentrations revealed significant changes in the aggregation tendency of peptides over time. To ascertain the statistical significance of the data T-test was performed

and, *P*-values of <0.01, <0.001, and <0.001 are considered significant and are represented with *, **, and *** respectively.

Further, the ThioS fluorescence assay demonstrated maximum aggregation occurring at 2-hour post-incubation at 37°C while stirring. The fluorescence emission recorded for 48 hours showed a decrease in intensity with passing time. The temporal and concentration-dependent study of aggregation kinetics of EBV-gM₁₄₆₋₁₅₇ peptide clearly demonstrated that its presence in free form is improbable. These observations indicate the time-dependence of aggregate formation in solution. Therefore, to analyze the temporal kinetics of aggregation, the minimum concentration forming aggregate at 12 hours, i.e., 125 μM, was studied over 12 hours. After setting up the aggregation reaction, the samples were withdrawn at 0.5, 1, 2, 4, 8, and 12 hours. The diluted samples were then mixed with ThioS dye, and an emission spectrum was recorded as described earlier. A gradual increase was observed till maximum fluorescence was reached at 2 hours, and thereafter a decrease was noted [Figure 3.5 (a, b)].

Figure 3.5 Thioflavin-S fluorescence intensity of 125μM with time

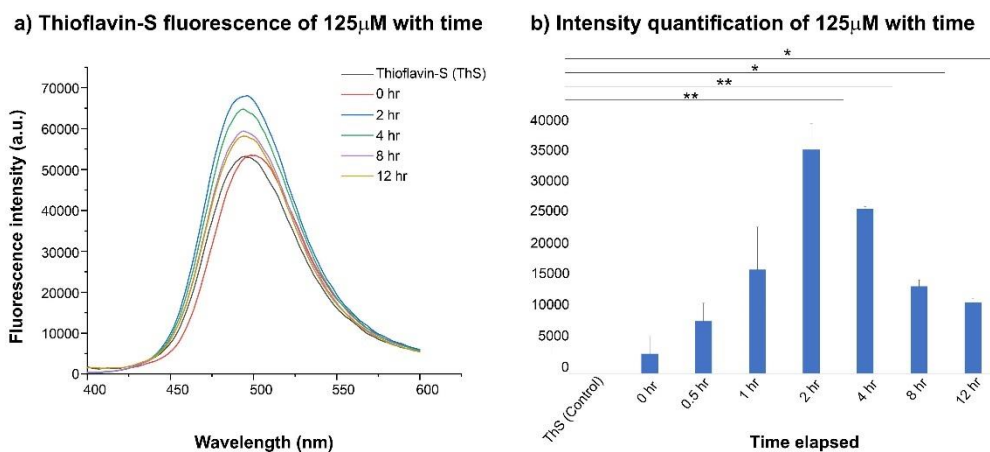


Figure 3.5 Thioflavin-S fluorescence intensity of 125μM with time. (a) The fluorescence intensity spectrum of 125μM EBV-gM₁₄₆₋₁₅₇ peptide was recorded between 400-600 nm. The spectrum shows maximum fluorescence emission at 2 hours. (b) Quantification of fluorescence at maxima revealed a gradual increase until 2 hours, followed by a decrease depicting a temporal pattern in aggregate formation. To ascertain the statistical significance of the data T-test was performed and, *P*-values of <0.01, <0.001, and <0.001 are considered significant and are represented with *, **, and *** respectively.

Furthermore, the aggregation samples prepared at 62.5, 125, and 250 μM, as mentioned in the Materials and Methods section, were subjected to Atomic Force

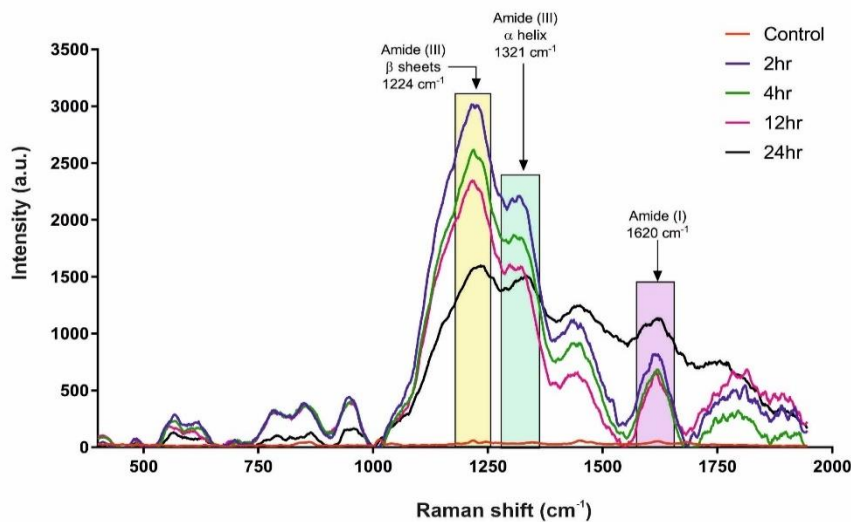
Microscopy (AFM) further to analyze the structural features of the peptide aggregates. Although no classical amyloid fibrils were observed, the peptide aggregates formed at 250 μM showed spheroid oligomeric formations under 5X5 μm scans, as depicted in the images [Figure S3. 1]. The AFM analysis of the peptide aggregates further corroborates the formation of spheroid aggregates in the samples.

3.4.4 Secondary structure in peptide aggregates:

The aggregates were subjected to RS to verify the secondary structure formation in the peptide aggregates. The analysis of Raman spectra of the entity would allow the prediction of the protein secondary structure content [44]. The Raman spectrum of a protein often displays different peaks generated due to vibrational contributions from the amino acid side chains and protein backbone. The peak generated by C=O stretching in the peptide is designated as amide I ($\sim 1620\text{-}1670\text{ cm}^{-1}$), and the N-H banding pattern is denoted as amide II ($\sim 1550\text{ cm}^{-1}$), and C-N stretching is denoted as amide III ($1200\text{-}1300\text{ cm}^{-1}$). The Raman peak pertaining to amide III helps predict the secondary structure (beta sheets and alpha helixes) of the protein/ peptide [Figure 3.6 (a)]. The Raman spectra of the aggregates display sharp bands at 1208 cm^{-1} and 1295 cm^{-1} , indicating the presence of high β -sheet content, further indicating the presence of amyloid-like aggregates. Comparing the intensities of the Amide III band obtained around 1224 cm^{-1} at different time points of incubation, an abrupt increase at 2 hours has been observed, followed by a gradual decline of the band intensity until 24 hours [Figure 3.6 (b-i)]. The intensity of the Amide III band at 1321 cm^{-1} follows a similar pattern, indicating the formation of the secondary structures- β -sheet and α -helixes are maximum at 2-hour post-incubation [Figure 3.6 (b-ii)]. However, the stability of these structures decreases over 24 hours duration, and the pattern of band intensity variation of Amide I does not follow any trend [Figure 3.6 (b-iii)]. The comparison between Raman intensities of all the amide III bands revealed a significant increase in the first 2 hours post-incubation [Figure 3.6 (b-iv)]. Thereafter, to check the cytotoxic effect of the peptide on neuroblastoma cell lines, aggregates of EBV-gM₁₄₆₋₁₅₇ peptide were generated at $125\mu\text{M}$ concentration, followed by the addition of diluted samples to the IMR-32 cells.

Figure 3.6

a). Secondary structure determination in EBV-gM₁₄₆₋₁₅₇ by Raman spectroscopy



b) Raman intensity quantification of secondary structure bands

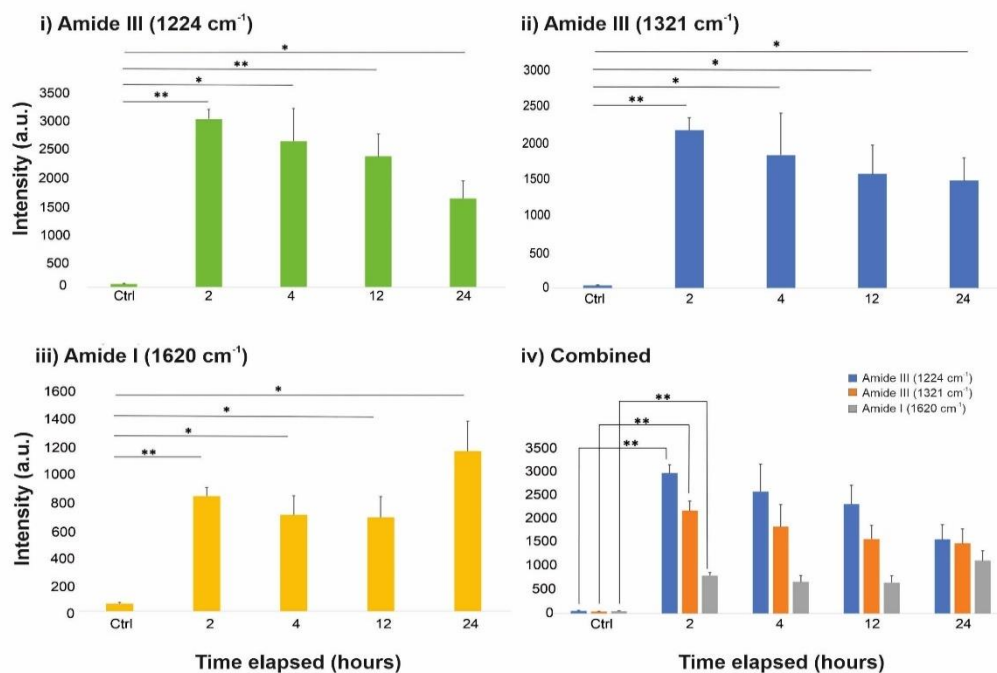


Figure 3.6 Raman spectroscopy of EBV-gM₁₄₆₋₁₅₇ peptide. a) Raman spectrum of EBV peptide obtained between 400-2000 cm⁻¹ shows the secondary structural conformations present in the aggregation solution of 125μM. The Raman band at 1224, 1321, and 1610 cm⁻¹ depicts the vibrations generated from Amide III, II, and I, respectively. Amide III reflects the formation of amyloid-like beta structures. The plot shows the presence of maximum beta-sheet structures at 2 hours post-incubation. (b) Comparative analysis of the Raman intensity of (i) Amide III at 1224cm⁻¹, (ii) Amide II at 1321cm⁻¹ and (iii) Amide I at 1610cm⁻¹ with time till 12 hours showed a gradual decrease in the stability of beta-sheet and alpha-helix conformation after initial 2 hours, (iv) the maximum change in secondary structure conformation is observed at 2hours post-incubation of the peptide at 37°C. To ascertain the statistical significance of the data T-test was performed and, P-values

*of <0.01, <0.001, and <0.001 are considered significant and are represented with *, **, and *** respectively.*

3.4.5 Cytotoxic properties of EBV gM₁₄₆₋₁₅₇ peptide:

The most prominent pathological hallmark of AD is the formation of plaques containing A β ₁₋₄₂ peptides. The neurotoxic effects of A β ₁₋₄₂ peptide aggregates have long been established in-vitro. The MTT assay was performed upon a neuroblastoma cell line IMR-32 to determine if the amyloid-like aggregates produced by EBV-gM₁₄₆₋₁₅₇ were cytotoxic. The cells were treated with different concentrations (0.31, 0.62, 1.25, 2.5, 5, 10, 20, 50, and 100 μ M) of aggregates formed at 125 μ M for 48 and 72 hours in separate sets as described in the Material and Methods section. A dose-dependent increase in the cytotoxicity was observed at both the time points (48- and 72-hours treatment). The untreated cells appeared to be healthy after the passage of the above-mentioned time interval. However, extensive cell death was observed in treated cells with $\geq 20\%$ and $\geq 30\%$ cytotoxicity of 2.5 μ M at 48- and 72-hours of treatment, respectively. The mean toxic dose (TD₅₀) was recorded to be ~ 58 μ M at 48-hours of treatment [Figure S3. 2], whereas with 72-hour treatment, the TD₅₀ was reduced to 37 μ M [Figure 3.7]. This observation indicates that the toxic effect of EBV peptides on neuroblastoma cells is enhanced over time. As per our findings, the EBV encoded peptide EBV-gM₁₄₆₋₁₅₇ showed potential self-aggregation, and the generated aggregates were cytotoxic for neuroblastoma cells.

The aggregate showed concentration-dependent cytotoxicity. The TD₅₀ of aggregates for IMR-32 cells was 58 μ M post 48 hours and 37 μ M post 72 hours of incubation. Albeit the precise mechanism of cytotoxic action of these aggregates is yet to be explored, it is noteworthy that they are lethal for a cell even at low concentrations ($\sim 37\mu$ M). Interestingly, the concentration of 37 μ M peptide is equivalent to 0.05 mg/mL, which is much lower than the total cytoplasmic protein and macromolecular content of a mammalian cell estimated to be ~ 200 -300 mg/mL [45] and ~ 400 mg/mL [46], respectively. However, due to the crowded cytoplasmic microenvironment, the effective concentration of the freshly generated peptide could remain high inside the ER lumen due to its increased transport. The occurrence of such events is increased during EBV infection and may enhance the probability of aggregate formation. As observed

in this study, once the aggregates are formed, they start exerting cytotoxic effects even at very low concentrations.

Figure 3.7 Cytotoxicity of EBV-gM at 72 hours

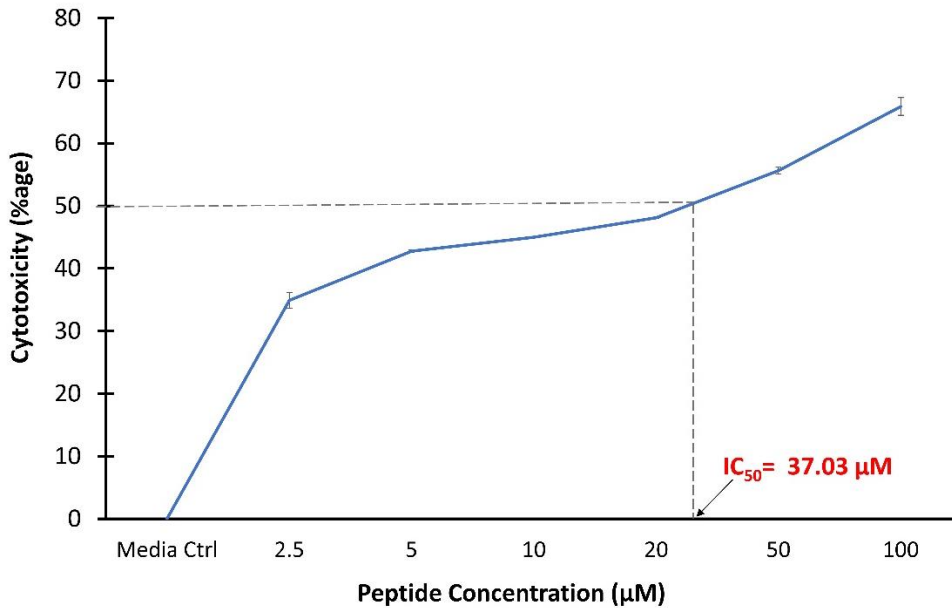


Figure 3.7 Cytotoxicity analysis of EBV-gM₁₄₆₋₁₅₇ peptide using MTT assay. The MTT assay showed that the TD₅₀ for EBV-gM₁₄₆₋₁₅₇ lies at ~37 µM post 72 hours of incubation with the aggregates. It indicates that aggregates formed at 125 µM post 2 hours of incubation at 37°C, are cytotoxic for neuroblastoma cells even at a much lower concentration of 37 µM.

Although the AFM analysis of the peptide EBV-gM₁₄₆₋₁₅₇ did not reveal the characteristic amyloid fibril formation, it established the presence of peptide oligomers. The oligomeric structural characteristics of the aggregates formed provided more substantial evidence to corroborate our postulation. The study revealed that the peptide EBV-gM₁₄₆₋₁₅₇ has a high tendency to form toxic amyloid-like spheroid oligomeric aggregate and may play a role in initiating aggregation cascade.

3.5 Conclusions

In summary, the possibility of EBV infection playing a crucial role in developing AD pathophysiology via the viral peptides generated through cellular proteasomal activity in amalgamation with other infection-induced events has been explored. In silico analysis of viral proteins identified multiple candidates having aggregate formation tendency. Furthermore, *in-vitro* experiments performed on a screened 11-amino-acid-long peptide generated from

proteasomal processing of EBV-gM corroborated the hypothesis. A correlation between aggregate formation and viral infection, depicted by concentration and time-dependent evolution of fluorescence, Raman signals, and cytotoxicity data analysis, strongly suggests the aforementioned possibility. Based on these results, a mechanism for viral protein processing inside the host cell leading to the formation of proteinaceous aggregates has been proposed and explained. This operational insight provides a novel outlook on how the infection of EBV could lead to the characteristic neurodegenerative pathology of AD. However, the conjecture needs to be explored further with more *in-vitro* and *in-vivo* studies.

3.6 Materials and Methods

3.6.1 Sequence Retrieval of EBV Proteins

Amino acid sequences of 183 EBV proteins were retrieved from UniProt (<https://www.uniprot.org/>) and NCBI protein database (<https://www.ncbi.nlm.nih.gov/protein/>) using keywords like Epstein-Barr virus, Human herpesvirus 4, EBNA1, LMP1, or respective protein names. Additionally, the sequence of A β ₁₋₄₂, a well-known amyloidogenic protein, was used as a positive control. However, Fragile-X-Mental Retardation-1 Protein (FMRP-1), a protein abundantly expressed in the neurons of a healthy brain not known for having any amyloidogenic properties was used as a negative control for *in-silico* aggregation predictions.

3.6.2 *In Silico* Aggregation Proclivity Prediction Tools

Freely available online software tools such as TANGO (<http://tango.crg.es/>), AGGRESCAN (<http://bioinf.uab.es/aggrescan/>), and AMYLPRED (<http://aias.biol.uoa.gr/AMYLPRED2/input.php>) were used to predict the aggregation-prone regions in unfolded peptide chains. Using these softwares, aggregation scores of respective proteins were obtained at default settings, i.e., pH 7.4 and temperature 310 K. The algorithms of these tools are designed to predict cross- β aggregation and utilize the data obtained from *in-vitro* experiments on the aggregation propensity scale for natural amino acids. They are broadly based on the assumption that short stretches of specific amino acid sequence modulate a protein's aggregation tendency.

3.6.3 Prediction of 20s Proteasome Cleavage Sites on Full-Length Proteins

To predict the proteasomal cleavage sites on the proteins, Pcleavage (<http://crdd.osdd.net/raghava/pcleavage/>) and NetChop 3.1 (<https://services.healthtech.dtu.dk/service.php?NetChop-3.1>) were used. Pcleavage is an SVM-based method for predicting proteasomal cleavage sites in antigenic sequences. In contrast, the prediction algorithm of NetChop 3.1 is based on the neural network for cleavage sites of the human proteasome. The threshold values of 0.5 and 0.9 were set for Pcleavage and NetChop 3.1, respectively.

3.6.4 Preparation of Aggregation Sample.

An 11-amino-acid-long peptide fragment (${}_{146}\text{SYKHFVLSAFVY}_{157}$) of EBV gM was synthesized chemically and obtained in the lyophilized form at >95% purity ("S" BioChem, India). Dimethyl sulfoxide (DMSO, 125 μL) was added to a vial containing 5 mg of the lyophilized peptide and stored at $-80\text{ }^\circ\text{C}$ till future use. For further experiments, 25 μL of peptide dissolved in DMSO was diluted with autoclaved double distilled water to prepare a stock solution of 1 mg/mL such that the final concentration of DMSO remained <3%. Aggregation samples of desired concentrations, i.e., 31.25, 62.5, 125, 250, and 500 μM , were prepared in $1\times$ PBS. Furthermore, the resultant solutions were incubated at $37\text{ }^\circ\text{C}$ while stirring at 350 rpm for the respective time intervals (i.e., 0.5, 1, 2, 4, 8, 12, and 24 h). Thereafter, the samples were subjected to analysis by Congo red absorption and ThioS fluorescence assays.

3.6.5 *In Vitro* Aggregation Analysis by Congo Red Absorption Assay

Congo red dye is known to show bathochromic shift upon binding with peptide aggregates [47]. Therefore, to ascertain the presence of aggregates in the peptide samples, Congo red dye was added, and the absorption spectrum was recorded in the range of 400-600 nm using an ELISA plate reader. A stock solution of (0.1%) 1435 μM Congo red was used to prepare the working solution of 20 μM . The aggregation samples (31.25, 62.5, 125, 250, and 500 μM) were then mixed

with Congo red stock solution. The resultant mixture of solution (300 μL) contained 20 μM of peptide aggregate and 20 μM Congo red in 1 X PBS.

3.6.6 In Vitro Aggregation Kinetics Analysis by ThioS Fluorescence Assay

On binding with mature aggregates, ThioS (dissolved in 50% methanol) emits fluorescence in the range of 440-450 nm [48], [49]. For analyzing the dose dependence of aggregate formation, different aggregation samples (31.25, 62.5, 125, 250, and 500 μM) were prepared as described previously and incubated at 37°C for 12 and 24 hours in separate sets. After completing the respective incubation period, 0.05% ThioS (from 0.01% stock) is mixed with 20 μM of each aggregation sample in 1XPBS. The resultant solutions were excited at 391 nm, and the fluorescence emission was recorded in the range of 400-600 nm. The slit width (both excitation and emission) for dose-dependent experiments was kept at 2.5 nm. This experiment aided in selecting optimum concentration showing aggregate formation for further analysis in a time-dependent manner. The aggregation sample of the selected concentration, i.e., 125 μM , was prepared and incubated for various time intervals (0.5, 1, 2, 4, 8, and 12 hours). ThioS fluorescence assay was then performed as described earlier. The slit width for time-dependent analysis was kept at 1 nm.

3.6.7 Atomic Force Microscopy (AFM)

A custom cut silicon wafer of 10 X 10 mm dimension and 2 mm thickness was used to coat the prepared peptide aggregates. As mentioned earlier, the aggregate samples were prepared while incubating the sample for 2 hours at 37°C on stir. A drop of the prepared peptide aggregate was coated onto the silicon wafer and allowed to air dry for 24 hours in a dust-free environment. The AFM scan was then done to obtain the images.

3.6.8 Raman Spectroscopy

To determine the temporal kinetics of secondary structure formation, Raman spectroscopy of the sample was performed [50]. The peptide sample showing maximum aggregate formation, i.e., 125 μM , was incubated at 37°C while stirring for various time intervals (i.e., 2, 4, 12, and 24 hours). The resultant solutions were drop-cast onto a 1.35 mm thick glass slide, leaving a drop of

aggregates suspended in water to be air-dried overnight. The Raman spectra of the sample were then recorded in the range of 400-2000 cm^{-1} . The freshly prepared aggregation sample (at the final concentration of 1mg/mL) was used as a control for the experiment.

3.6.9 Cell Cytotoxicity Assay

The MTT assay was performed to determine the cytotoxic activity of the aggregates towards neuroblastoma cell lines IMR-32. The cells were counted using the trypan blue method and seeded in a 96-well plate at a 2×10^3 cells/well density. The cells were cultured in 200uL of growth medium containing DMEM and 10% fetal bovine serum supplied with 0.5% antibiotics solution (Pen-Strep). After 12 hours of culture, cells were treated with different dilutions of 125 μM aggregation samples, i.e., 50, 20, 10, 5, 2.5, 1.25, 0.62, 0.31 μM , and incubated for 48 and 72 hours in separate sets. After the completion of the respective incubation period, MTT dye was added to the cells and kept at 37°C for 3 hours in a CO_2 incubator. Thereafter, the solution was removed, and to dissolve the formazan crystals formed, 100uL of DMSO/well was added and shaken for 2 hours on the rocker. The optical density was then recorded on the ELISA plate reader at 590 nm.

3.7 References

- [1] “2020 Alzheimer’s disease facts and figures,” *Alzheimers Dement.*, vol. 16, no. 3, pp. 391–460, Mar. 2020, doi: 10.1002/alz.12068.
- [2] T. Tripathi and P. Kalita, “Synergistic Effect of Amyloid- β and Tau Disrupts Neural Circuits,” *ACS Chem. Neurosci.*, vol. 10, no. 3, pp. 1129–1130, Mar. 2019, doi: 10.1021/acscchemneuro.9b00037.
- [3] S. D. Moran and M. T. Zanni, “How to Get Insight into Amyloid Structure and Formation from Infrared Spectroscopy,” *J. Phys. Chem. Lett.*, vol. 5, no. 11, pp. 1984–1993, Jun. 2014, doi: 10.1021/jz500794d.
- [4] G.-N. Gomes and Z. A. Levine, “Defining the Neuropathological Aggresome across *in Silico*, *in Vitro*, and *ex Vivo* Experiments,” *J. Phys. Chem. B*, vol. 125, no. 8, pp. 1974–1996, Mar. 2021, doi: 10.1021/acs.jpccb.0c09193.
- [5] H. Hillen, “The Beta Amyloid Dysfunction (BAD) Hypothesis for Alzheimer’s Disease,” *Front. Neurosci.*, vol. 13, p. 1154, Nov. 2019, doi: 10.3389/fnins.2019.01154.

- [6] A. Atri, “The Alzheimer’s Disease Clinical Spectrum,” *Med. Clin. North Am.*, vol. 103, no. 2, pp. 263–293, Mar. 2019, doi: 10.1016/j.mcna.2018.10.009.
- [7] R. A. Armstrong, “Review article What causes alzheimer’s disease?,” *Folia Neuropathol.*, vol. 3, pp. 169–188, 2013, doi: 10.5114/fn.2013.37702.
- [8] C. Reitz, E. Rogaeva, and G. W. Beecham, “Late-onset vs nonmendelian early-onset Alzheimer disease: A distinction without a difference?,” *Neurol. Genet.*, vol. 6, no. 5, p. e512, Oct. 2020, doi: 10.1212/NXG.0000000000000512.
- [9] M. Sochocka, K. Zwolińska, and J. Leszek, “The Infectious Etiology of Alzheimer’s Disease,” *Curr. Neuropharmacol.*, vol. 15, no. 7, Aug. 2017, doi: 10.2174/1570159X15666170313122937.
- [10] A. Douros *et al.*, “Infectious Disease Burden and the Risk of Alzheimer’s Disease: A Population-Based Study,” *J. Alzheimers Dis.*, pp. 1–10, Mar. 2021, doi: 10.3233/JAD-201534.
- [11] A. Sait, C. Angeli, A. J. Doig, and P. J. R. Day, “Viral Involvement in Alzheimer’s Disease,” *ACS Chem. Neurosci.*, vol. 12, no. 7, pp. 1049–1060, Apr. 2021, doi: 10.1021/acchemneuro.0c00719.
- [12] D. Vidasova, M. Nemergut, B. Liskova, and J. Damborsky, “Multi-pathogen infections and Alzheimer’s disease,” *Microb. Cell Factories*, vol. 20, no. 1, p. 25, Dec. 2021, doi: 10.1186/s12934-021-01520-7.
- [13] D. A. Thorley-Lawson, J. B. Hawkins, S. I. Tracy, and M. Shapiro, “The pathogenesis of Epstein–Barr virus persistent infection,” *Curr. Opin. Virol.*, vol. 3, no. 3, pp. 227–232, Jun. 2013, doi: 10.1016/j.coviro.2013.04.005.
- [14] H. Lövheim *et al.*, “Interaction between Cytomegalovirus and Herpes Simplex Virus Type 1 Associated with the Risk of Alzheimer’s Disease Development,” *J. Alzheimers Dis.*, vol. 61, no. 3, pp. 939–945, Jan. 2018, doi: 10.3233/JAD-161305.
- [15] R. P. Stowe, M. K. Peek, M. P. Cutchin, and J. S. Goodwin, “Reactivation of herpes simplex virus type 1 is associated with cytomegalovirus and age,” *J. Med. Virol.*, vol. 84, no. 11, pp. 1797–1802, Nov. 2012, doi: 10.1002/jmv.23397.
- [16] K. D. Tarter, A. M. Simanek, J. B. Dowd, and A. E. Aiello, “Persistent Viral Pathogens and Cognitive Impairment Across the Life Course in the Third National Health and Nutrition Examination Survey,” *J. Infect. Dis.*, vol. 209, no. 6, pp. 837–844, Mar. 2014, doi: 10.1093/infdis/jit616.
- [17] J. Wouk, D. Z. Rechenchoski, B. C. D. Rodrigues, E. V. Ribelato, and L. C. Faccin-Galhardi, “Viral infections and their relationship to neurological

disorders,” *Arch. Virol.*, vol. 166, no. 3, pp. 733–753, Mar. 2021, doi: 10.1007/s00705-021-04959-6.

[18] I. Carbone *et al.*, “Herpes virus in Alzheimer’s disease: relation to progression of the disease,” *Neurobiol. Aging*, vol. 35, no. 1, pp. 122–129, Jan. 2014, doi: 10.1016/j.neurobiolaging.2013.06.024.

[19] Y. Nahidi, N. Tayyebi Meibodi, Z. Meshkat, and N. Nazeri, “Macular Amyloidosis and Epstein-Barr Virus,” *Dermatol. Res. Pract.*, vol. 2016, pp. 1–5, 2016, doi: 10.1155/2016/6089102.

[20] F. Drago, E. Ranieri, A. Pastorino, S. Casazza, F. Crovato, and A. Rebora, “Epstein-Barr virus-related primary cutaneous amyloidosis. Successful treatment with acyclovir and interferon-alpha,” *Br. J. Dermatol.*, vol. 134, no. 1, pp. 170–174, Jan. 1996, doi: 10.1046/j.1365-2133.1996.d01-754.x.

[21] D. Tiwari, S. Jakhmola, D. K. Pathak, R. Kumar, and H. C. Jha, “Temporal *In Vitro* Raman Spectroscopy for Monitoring Replication Kinetics of Epstein–Barr Virus Infection in Glial Cells,” *ACS Omega*, vol. 5, no. 45, pp. 29547–29560, Nov. 2020, doi: 10.1021/acsomega.0c04525.

[22] O. Indari, R. Chandramohanadas, and H. C. Jha, “Epstein–Barr virus infection modulates blood–brain barrier cells and its co-infection with *Plasmodium falciparum* induces RBC adhesion,” *Pathog. Dis.*, vol. 79, no. 1, p. ftaa080, Jan. 2021, doi: 10.1093/femspd/ftaa080.

[23] K. V. Biza, K. C. Nastou, P. L. Tsiolaki, C. V. Mastrokalou, S. J. Hamodrakas, and V. A. Iconomidou, “The amyloid interactome: Exploring protein aggregation,” *PLOS ONE*, vol. 12, no. 3, p. e0173163, Mar. 2017, doi: 10.1371/journal.pone.0173163.

[24] T. D. Do, N. J. Economou, A. Chamas, S. K. Buratto, J.-E. Shea, and M. T. Bowers, “Interactions between Amyloid- β and Tau Fragments Promote Aberrant Aggregates: Implications for Amyloid Toxicity,” *J. Phys. Chem. B*, vol. 118, no. 38, pp. 11220–11230, Sep. 2014, doi: 10.1021/jp506258g.

[25] K. Ezzat *et al.*, “The viral protein corona directs viral pathogenesis and amyloid aggregation,” *Nat. Commun.*, vol. 10, no. 1, p. 2331, Dec. 2019, doi: 10.1038/s41467-019-10192-2.

[26] V. K. Singh, S. Kumar, and S. Tapryal, “Aggregation Propensities of Herpes Simplex Virus-1 Proteins and Derived Peptides: An *In Silico* and *In Vitro* Analysis,” *ACS Omega*, vol. 5, no. 22, pp. 12964–12973, Jun. 2020, doi: 10.1021/acsomega.0c00730.

[27] A. J. Rivett and A. R. Hearn, “Proteasome Function in Antigen Presentation: Immunoproteasome Complexes, Peptide Production, and

Interactions with Viral Proteins,” *Curr. Protein Pept. Sci.*, vol. 5, no. 3, pp. 153–161, Jun. 2004, doi: 10.2174/1389203043379774.

[28] X. Zhao and J. Yang, “Amyloid- β Peptide Is a Substrate of the Human 20S Proteasome,” *ACS Chem. Neurosci.*, vol. 1, no. 10, pp. 655–660, Oct. 2010, doi: 10.1021/cn100067e.

[29] C. C. VandenAkker *et al.*, “Multimodal Spectroscopic Study of Amyloid Fibril Polymorphism,” *J. Phys. Chem. B*, vol. 120, no. 34, pp. 8809–8817, Sep. 2016, doi: 10.1021/acs.jpcc.6b05339.

[30] L. C. F. Gequelin, I. N. Riediger, S. M. Nakatani, A. W. Biondo, and C. M. Bonfim, “Epstein-Barr virus: general factors, virus-related diseases and measurement of viral load after transplant,” *Rev. Bras. Hematol. E Hemoter.*, vol. 33, no. 5, pp. 383–388, 2011, doi: 10.5581/1516-8484.20110103.

[31] M. Kleines, J. Schiefer, A. Stienen, M. Blaum, K. Ritter, and M. Häusler, “Expanding the spectrum of neurological disease associated with Epstein-Barr virus activity,” *Eur. J. Clin. Microbiol. Infect. Dis.*, vol. 30, no. 12, pp. 1561–1569, Dec. 2011, doi: 10.1007/s10096-011-1261-7.

[32] D. Gate *et al.*, “Clonally expanded CD8 T cells patrol the cerebrospinal fluid in Alzheimer’s disease,” *Nature*, vol. 577, no. 7790, pp. 399–404, Jan. 2020, doi: 10.1038/s41586-019-1895-7.

[33] K. Bourgade, G. Dupuis, E. H. Frost, and T. Fülöp, “Anti-Viral Properties of Amyloid- β Peptides,” *J. Alzheimers Dis. JAD*, vol. 54, no. 3, pp. 859–878, Oct. 2016, doi: 10.3233/JAD-160517.

[34] F. Li, M. Hearn, and L. E. Bennett, “The role of microbial infection in the pathogenesis of Alzheimer’s disease and the opportunity for protection by anti-microbial peptides,” *Crit. Rev. Microbiol.*, vol. 47, no. 2, pp. 240–253, Mar. 2021, doi: 10.1080/1040841X.2021.1876630.

[35] H. Luo, “Interplay between the virus and the ubiquitin–proteasome system: molecular mechanism of viral pathogenesis,” *Curr. Opin. Virol.*, vol. 17, pp. 1–10, Apr. 2016, doi: 10.1016/j.coviro.2015.09.005.

[36] L. L. Quinn, L. R. Williams, C. White, C. Forrest, J. Zuo, and M. Rowe, “The Missing Link in Epstein-Barr Virus Immune Evasion: the BDLF3 Gene Induces Ubiquitination and Downregulation of Major Histocompatibility Complex Class I (MHC-I) and MHC-II,” *J. Virol.*, vol. 90, no. 1, pp. 356–367, Jan. 2016, doi: 10.1128/JVI.02183-15.

[37] N. P. Croft *et al.*, “Stage-specific inhibition of MHC class I presentation by the Epstein-Barr virus BNLF2a protein during virus lytic cycle,” *PLoS*

Pathog., vol. 5, no. 6, p. e1000490, Jun. 2009, doi: 10.1371/journal.ppat.1000490.

[38] A. D. Hislop *et al.*, “A CD8+ T cell immune evasion protein specific to Epstein-Barr virus and its close relatives in Old World primates,” *J. Exp. Med.*, vol. 204, no. 8, pp. 1863–1873, Aug. 2007, doi: 10.1084/jem.20070256.

[39] J. Woulfe, H. Hoogendoorn, M. Tarnopolsky, and D. G. Munoz, “Monoclonal antibodies against Epstein-Barr virus cross-react with α -synuclein in human brain,” *Neurology*, vol. 55, no. 9, pp. 1398–1401, Nov. 2000, doi: 10.1212/WNL.55.9.1398.

[40] D. Twohig and H. M. Nielsen, “ α -synuclein in the pathophysiology of Alzheimer’s disease,” *Mol. Neurodegener.*, vol. 14, no. 1, p. 23, Jun. 2019, doi: 10.1186/s13024-019-0320-x.

[41] W. A. Eimer *et al.*, “Alzheimer’s Disease-Associated β -Amyloid Is Rapidly Seeded by Herpesviridae to Protect against Brain Infection,” *Neuron*, vol. 99, no. 1, pp. 56–63.e3, Jul. 2018, doi: 10.1016/j.neuron.2018.06.030.

[42] K. Bourgade *et al.*, “ β -Amyloid peptides display protective activity against the human Alzheimer’s disease-associated herpes simplex virus-1,” *Biogerontology*, vol. 16, no. 1, pp. 85–98, Feb. 2015, doi: 10.1007/s10522-014-9538-8.

[43] J. Luo *et al.*, “Cellular Polyamines Promote Amyloid-Beta ($A\beta$) Peptide Fibrillation and Modulate the Aggregation Pathways,” *ACS Chem. Neurosci.*, vol. 4, no. 3, pp. 454–462, Mar. 2013, doi: 10.1021/cn300170x.

[44] T. Weymuth and M. Reiher, “Characteristic Raman Optical Activity Signatures of Protein β -Sheets,” *J. Phys. Chem. B*, vol. 117, no. 40, pp. 11943–11953, Oct. 2013, doi: 10.1021/jp405981h.

[45] K. Luby-Phelps, “Cytoarchitecture and physical properties of cytoplasm: volume, viscosity, diffusion, intracellular surface area,” *Int. Rev. Cytol.*, vol. 192, pp. 189–221, 2000, doi: 10.1016/s0074-7696(08)60527-6.

[46] G. Guigas, C. Kalla, and M. Weiss, “Probing the nanoscale viscoelasticity of intracellular fluids in living cells,” *Biophys. J.*, vol. 93, no. 1, pp. 316–323, Jul. 2007, doi: 10.1529/biophysj.106.099267.

[47] A. Espargaró, S. Llabrés, S. J. Saupe, C. Curutchet, F. J. Luque, and R. Sabaté, “On the Binding of Congo Red to Amyloid Fibrils,” *Angew. Chem.*, vol. 132, no. 21, pp. 8181–8184, May 2020, doi: 10.1002/ange.201916630.

[48] A. Espargaró, R. Sabate, and S. Ventura, “Thioflavin-S staining coupled to flow cytometry. A screening tool to detect *in-vivo* protein aggregation,” *Mol. Biosyst.*, vol. 8, no. 11, p. 2839, 2012, doi: 10.1039/c2mb25214g.

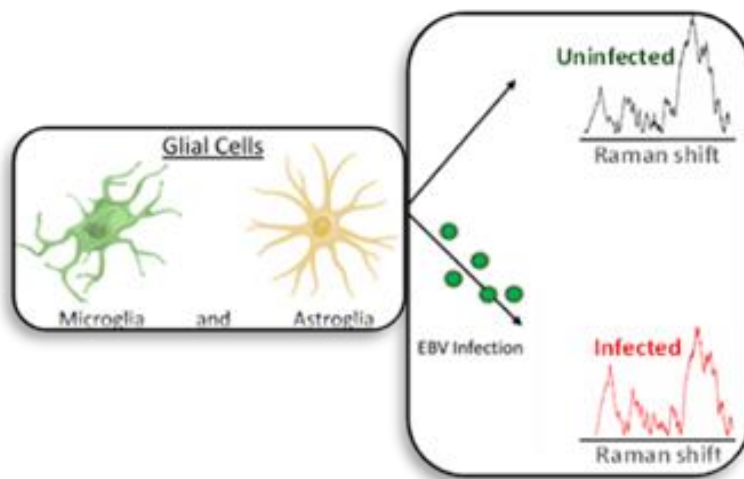
[49] J. Shin, S. Park, H. Lee, and Y. Kim, “Thioflavin-positive tau aggregates complicating quantification of amyloid plaques in the brain of 5XFAD transgenic mouse model,” *Sci. Rep.*, vol. 11, no. 1, p. 1617, Dec. 2021, doi: 10.1038/s41598-021-81304-6.

[50] G. Devitt, W. Rice, A. Crisford, I. Nandhakumar, A. Mudher, and S. Mahajan, “Conformational Evolution of Molecular Signatures during Amyloidogenic Protein Aggregation,” *ACS Chem. Neurosci.*, vol. 10, no. 11, pp. 4593–4611, Nov. 2019, doi: 10.1021/acchemneuro.9b00451.

Chapter 4

***In vitro* Raman spectroscopy of Epstein-Barr virus-infected glial cells to analyze temporal replication kinetics**

4.1 Graphical abstract



4.2 Abstract

RS is an effective tool for studying biochemical changes. RS can be utilized to elucidate the biochemical homeostasis modulations occurring inside a cell upon viral infection. Thus far, the entire picture of EBV entry and infection establishment has remained ambiguous. Our study discerned biochemical alteration in human microglial cells (HMC-3) upon EBV infection. We used RS to detect the biochemical alterations in microglial cells post-EBV infection at two cellular locations (nucleus and periphery) through elapsed time at various instances. Two phenomena, the first one probably associated with the cell's response to 'viral attachment and invasion' and another involved in 'viral replication' followed by an escape from the host cell, were examined. These changes occurring inside the microglia cells upon EBV infection coincide with the signature Raman spectra of specific biomolecules, depicting virus-mediated alterations in their biochemistry. Interestingly, the biochemical modulations vary

based on the cellular location and infection time elapsed, indicating disparate molecules and signaling processes involved. We observed differential Raman signals originating from cholesterol, glucose, phenylalanine, phosphoinositide, etc. These molecules are associated with maintaining biochemical homeostasis, and thus, their alteration at distinct infection times reflects their periodic involvement, depending on the stage of virus infection. Therefore, our study proposes RS as a tool to explore the viral infection progression in cells at biomolecular levels.

Keywords: Raman Spectroscopy; EBV; Glial cells; Biomolecules; astrocytes; microglia.

4.3 Introduction

Various techniques can elucidate biochemical changes occurring in a cell, and RS is one of the latest techniques to be used for this purpose. RS is a state-of-the-art technology that captures the signature bond vibrations of a molecule and uses them to identify it. This feature of RS can be utilized to determine the minute biochemical changes happening in complex biological systems like cells, tissues, and various body fluids [1]. Unarguably, disruption of biochemical homeostasis manifests either as the diseased state of an individual or as an aftermath of the illness [2]. For example, alterations in carbohydrate metabolism could result in pathologies like galactosemia, diabetes, diabetic ketoacidosis, hyperglycemia, hereditary fructose intolerance, and glycogen storage disorders [3]. Disordered protein homeostasis in the body could cause phenylketonuria, tyrosinemia, maple syrup urine syndrome, etc. [4]. Likewise, altered lipid metabolism is associated with various disordered metabolic conditions such as familial hypercholesterolemia, hypertriglyceridemia, and low HDL (high-density lipoprotein) [5].

Furthermore, RS was utilized to detect various aforementioned metabolic disorders in human serum samples by analyzing the biochemical profile of glucose, cholesterol, lipids, phenylalanine, etc. [6]. Hitherto RS has been successfully used as a diabetes management tool to monitor the subcutaneous blood glucose levels [7] and screen phenylketonuria in newborns [8]. These applications suggest that the technique has immense potential for development

as a disease diagnostic tool. In addition, RS is widely applied to figure out the intricacies of cancer, infection, and inflammation in the human body [1]. RS as a diagnostic technique is reported to differentiate between invasive and non-invasive breast cancer in studies conducted by multiple groups [9], [10]. Furthermore, RS has been employed to detect inflammation in the colon of patients suffering from inflammatory bowel disease (IBD) [11], in *in-vitro* TNF- α (a pro-inflammatory cytokine) treated endothelial cells [12], or in *in-vivo* experiments on the tympanic membrane of a murine model [13]. In the study, signature Raman spectra of lipids, collagen, or DNA content of the respective samples, were used to identify the disease-associated alterations.

Besides, RS can be successfully used to differentiate between viral infections presenting with similar clinical symptoms, such as dengue and malaria, based on the differentially regulated metabolites in both conditions [14]. RS also found its usage in studying attributes of virus infections such as that of Kaposi's sarcoma-associated herpesvirus (KSHV) in various cells of lymphoid lineage (BCBL-1, BC-1, and BJAB) [15]; Human papillomavirus (HPV) in primary human keratinocytes (PHK), and CaSki cells [16]; and *in-vitro* detection of Rotavirus [17]. Alarmingly in the last few decades, the prevalence of omnipresent Herpesviruses has accounted for a majority of disease burden globally [18]. The Human Herpesvirus – 4 (HHV-4), also known as Epstein – Barr virus (EBV), is a notably infamous member of the *Herpesviridae* family that infects around ~90% of the world population [19]. Although primary infection of EBV in children largely remains asymptomatic, infection in young adults could cause infectious mononucleosis (IM), also called glandular fever [20]. After initial exposure, the virus is known to reside latently in the cells of lymphoid and epithelial origin in an individual [21]. However, the virus may reactivate at later stages of life, resulting in severe consequences such as IM-like disease, hemophagocytic syndrome, chronic active EBV infection, and lymphomas [22]. Furthermore, as a well-known oncogenic virus, EBV has been implicated in the development of various neoplasms associated with lymphocytes, such as B-cell lymphoma (Burkitt's and Hodgkin's lymphoma) or lymphoproliferative disorders. At the same time, EBV infection in the cells of epithelial lineage could result in nasopharyngeal carcinoma or EBV-associated gastric cancer [23]. Interestingly, recent reports of EBV transcripts and DNA found in CSF of

patients suffering from NDDs like AD [24], PD [25], MS [26], [27], etc., suggest the possibility of EBV infecting the brain cells (neurons and glial cells).

Typically, to infect a host cell, a virus must first attach itself to its surface, followed by penetration of the outer cell membrane to allow the insertion of genetic material inside the host cell. Essentially, the viral entry inside a cell is governed by the interaction between viral surface proteins and host cell surface receptors. As a consequence of this interaction, viral infectivity is limited to the cells possessing compatible surface receptors and thus defines the virus's tropism [28]. Nevertheless, some viruses like SARS-CoV-2 and Zika virus possess the property of multi-tropism, i.e., they can infect cells of multiple origins [29], [30]. Likewise, contemporary research demonstrated that EBV also shows the property of multi-tropism by infecting B-cells and epithelial cells with the plausibility of infecting neural cells [31]–[34]. A glycoprotein (gp350) present on the surface of EBV aid it in interacting with the CD-21 surface marker on the host B-cells [35]. However, EBV interacts with epithelial cells in CD-21 independent manner. The predicted cell receptors to aid the entry of EBV in epithelial cells include integrins and ephrin molecules, among others, by interacting with gHgL: a viral glycoprotein) [34].

Interestingly, Jha et al. performed a first-ever *in-vitro* study to characterize and demonstrate EBV infection in a neuroblastoma cell line (ShSy-5y), teratocarcinoma neurons (Ntera2), and primary human foetal neurons [36]. Following the pursuit, our study establishes successful infection of EBV in glial cells, namely, HMC-1 (microglia) and U-87 MG (glioblastoma) cell lines. However, the entry path of EBV in the neural cell is still under exploration. It is believed that the virus exploits diverse pathways to enter cells of different origins and carry out its life cycle [37]. The type of viral genetic material (DNA or RNA) governs further processing inside the host cell, which involves replication, transcription, and translation of the viral genome. The viral processing inside the host cell dramatically influences the host's biochemistry. The biomolecular pathways adopted by viruses to hijack the host differ from cell to cell depending on their origin, thus greatly affecting the infection kinetics differently in each cell [38]. It could affect the duration of time elapsed from attachment to gain entry and further progress of the replication cycle [39]. For instance, EBV infection in B-cells produces transcriptional alterations only after the first 24

hours, which precedes metabolic and phenotypic changes. EBV mediates transcriptional reprogramming of B-cells at three stages; RNA synthesis, manipulating metabolic pathways, and cell division that occurs sequentially on the 2nd, 3rd, and 4th day post-infection (dpi), respectively [40]. Contrastingly, *de novo* (cell-in-cell) EBV infection in epithelial cells can initiate as early as 4 hours post-infection (hpi). Whereas in neuronal cell lines such as ShSy-5y and Ntera2, it may take only up to 1 hpi for EBV to establish infection, and signs of lytic replication can be observed by 9 hpi [36]. Thereby, it is evident that the same virus may take various time intervals to establish successful infection in cells of different origins.

Therefore, in the current study, we sought to investigate the changes in the biomolecular profile of glial cells upon EBV infection over time using RS. We intended to identify the signature Raman signals generated upon viral invasion and infection in the glial cells. Additionally, we recorded differential regional regulations of various biomolecules in the cell, i.e., at the nucleus and cell body (periphery). These biomolecular alterations are also reflected in the regulation of various biochemical signaling pathways in the cell. The temporal (infection progression over time) and spatial (with respect to different locations inside the cell) analysis of the Raman spectrum of a cell upon infection provide a profound insight into the dynamics of the viral infection.

4.4 Results

4.4.1 Raman Spectra

We observed different peaks for HMC-3, pre- and post-infection, by plotting the raw data points (wavenumber vs. intensity) of Raman spectra using Origin-2018b software at various time duration (2, 4, 6, 12, 24, and 36 H). For HMC-3, five major Raman peaks were observed in the wavenumber range of 547-560 cm^{-1} , 1097-1109 cm^{-1} , 2047-2054 cm^{-1} , 2669-2676 cm^{-1} , and 3825-3840 cm^{-1} in the nucleus [Figure 4.1-A (I and II)]. Whereas, at periphery five peaks were documented in the range of 548-554 cm^{-1} , 1097-1125 cm^{-1} , 2043-2051 cm^{-1} , 2673-2679 cm^{-1} , and 3828-3843 cm^{-1} [Figure 4.1-B (I and II)]. For ease of further processing and validating the number of major peaks, the dimensionality of the

raw data was reduced using principal component analysis (PCA). We obtained probable solutions, i.e., the principal components in our data range from 3 to 8, thus, validating the number of peaks observed in the graph.

Figure 4.1 Raman spectrum of HMC-3 (Microglia)

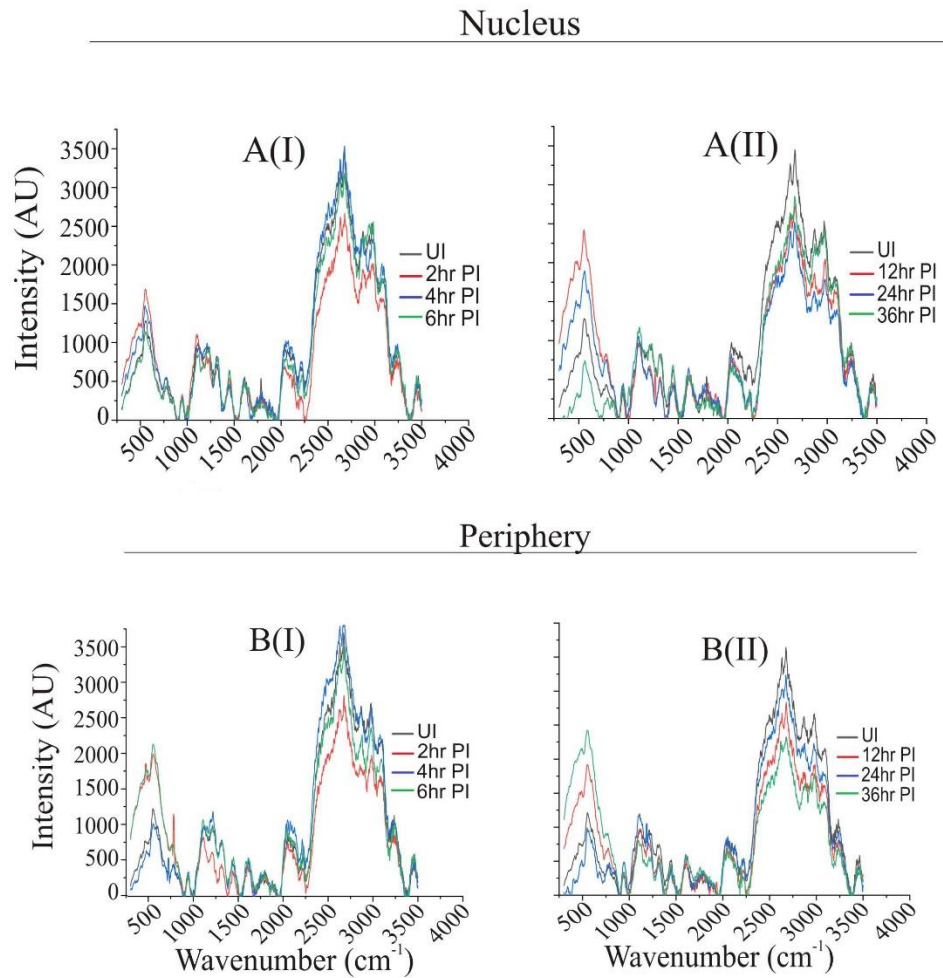


Figure 4.1 Raman spectra were acquired from (A) the nucleus of HMC-3 [(I) and (II)] and (B) the periphery of HMC-3 [(I) and (II)]. The Raman spectra were acquired in the range of 400 to 4000 cm^{-1} . 633 nm laser excitation source was used to record the data.

4.4.2 Biomolecules' peak identification in the glial cells

The distinct peaks we obtained from the graph correspond to the signature spectrum of unique biomolecules [Table 1]. In comparing the Raman signals of these molecules in the infected samples with the uninfected ones, we observed variations in vibrational intensity at different time points. The positive variation, i.e., upregulation of intensity above the basal level of uninfected cells,

represented an increase in the amount of the molecules probably due to its enhanced anabolic activity. Also, decline of signal intensity of the molecule below the basal levels depicted a decrease in amount due to its consumption/catabolism.

Specifically, upon EBV infection in the microglial cells, we observed the highest activity of DNA and glycogen ($481-495\text{ cm}^{-1}$) [41] molecules at 2 and 12 hpi in the nucleus [Figure 4.2- A1(I)], while no signals are obtained from the periphery [Figure 4.2- A1(II)]. The intensities have been used with respect to the control (uninfected) samples with negative values means the decrease in intensity with respect to the control sample. The signals associated with cholesterol and cholesterol esters ($548-560\text{ cm}^{-1}$) [42], [43] were elevated at 2 and 12 hpi in the nucleus depicting their maximum anabolic activity at these time points [Figure 4.2-A2(I)]. Whereas on the periphery their activity appeared to be highest at 2, 6 and 36 hpi [Figure 4.2-A2(II)]. Similarly, the maximum amount of PIP, uracil and phosphodiester group ($740-790\text{ cm}^{-1}$) [42], [44], [45] was noted on 2, 4 and 12 hpi in the nucleus [Figure 4.2-A3(I)] and at 2, 6 and 36 hpi on the periphery [Figure 4.2-A3(II)]. The Raman signals depicted the highest amount of polysaccharide, proline and valine molecules ($939-952\text{ cm}^{-1}$) [46], [47] in the nucleus at 24 hpi. Additionally, we observed maximum consumption of these molecules in the nucleus at 6 hpi denoted by reduced signals [Figure 4.2-A4(I)]. While their maximum expression levels on the periphery appear at 4, and 24 hpi [Figure 4.2-A4(II)]. Consumption of purines and amide III ($1300-1320\text{ cm}^{-1}$) [48], [49] was observed to be maximum at both the locations in cell at 2, and 24 hpi [Figure 4.2-A5(I) and (II)]. Fatty acids and triglycerides ($1439-1448\text{ cm}^{-1}$) [50], [51] from the nucleus showed their highest assimilation in the nucleus at 4, and 24 hpi [Figure 4.2-A6(I)]. However, at the peripheral site fatty acid and triglyceride molecules were getting used up earlier starting at 2 and 12 hpi [Figure 4.2-A6(II)]. In the nucleus of HMC-3, phenylalanine, tyrosine and tryptophan molecule ($1600-1628\text{ cm}^{-1}$) [52], [53] reserves were consumed maximally at 6 hpi, followed by replenishment with highest anabolic activity at 24 hpi [Figure 4.2-A7(I)]. Although at the periphery the consumption of these amino acid molecules started as early as 2 hpi and got replenished at 6 and 36 hpi [Figure 4.2-A7(II)]. The Raman signals originating from OH-NH-CH

stretching vibrations ($2300\text{-}3800\text{ cm}^{-1}$) [54] in the nucleus showed maximum catabolism of associated molecules at 6, and 24 hpi [Figure 4.2-A8(I)]. Comparatively the highest amounts of the aforesaid molecules appeared at 4, and 36 hpi [Figure 4.2-A8(II)].

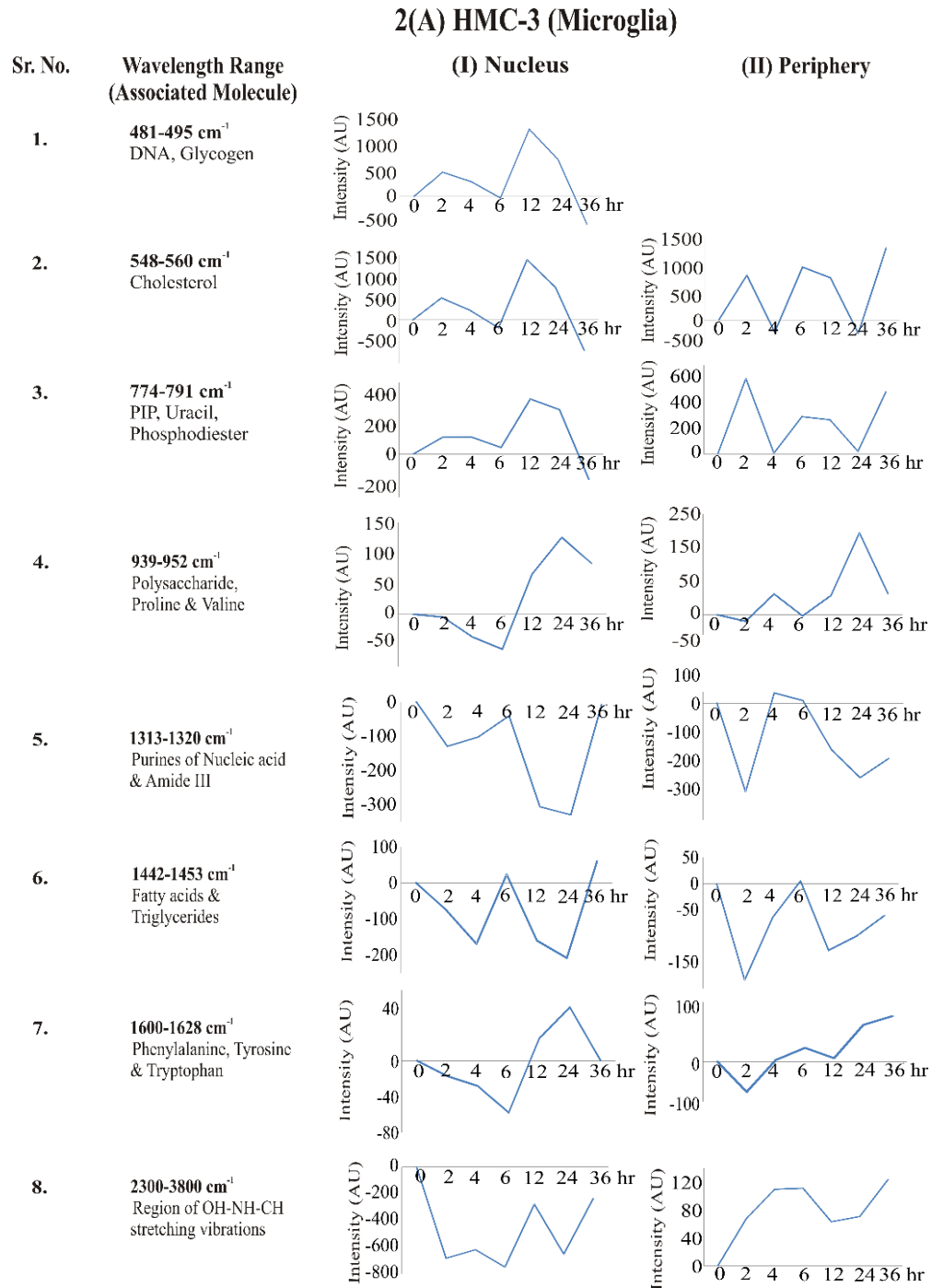


Figure 4.2 Expression of various biomolecules at different time points post EBV infection in HMC-3 cells. The intensity levels of each biomolecule group upon EBV infection are plotted separately in comparison to that of uninfected cells. The data was recorded at the time intervals of 2, 4, 6, 12, 24, 36 hpi for HMC-3 cells.

Changes in the Raman intensity related to nucleic acid, amino acids, lipids, and carbohydrates were observed in microglial cell line.

Table 1. The Raman signature of the biomolecules that are known to be altered on infection with different viruses and how the virus utilizes them.

Wavenumber Range (cm ⁻¹)	Wavenumber (cm ⁻¹)	Associated Biomolecule	Probable function in cell metabolism	Reports on association with virus infection
460-480	481	DNA	Genetic Material	
	484-490	Glycogen	Energy storage molecule	<ol style="list-style-type: none"> 1. HCMV enhances glycolytic flux to fuel fatty acid synthesis. [89] 2. HSV-1 gears glycolytic metabolism toward the production of pyrimidine nucleotide components. [89] 3. EBV infected NPC cell lines show increased glycolysis levels; LMP-1 of EBV induces Hexokinase-2 to induce glycolysis and upregulation of GLUT-1. [96]
540-560	548	Cholesterol/ Cholesterol esters	Cell membrane constituent (maintains membrane fluidity), Involved in cell signalling, transport processes and nerve conduction	<ol style="list-style-type: none"> 1. Cellular Cholesterol Facilitates the Post-entry Replication Cycle of HSV 1 [81] 2. EBV: LMP-2A is secreted in exosomes in Cholesterol dependent manner [97] 3. KSHV- decreased cholesterol synthesis. [98]

	540	Glucose-saccharide band	Energy currency of the cell	1. HBV - Increased Gluconeogenesis & glycolysis. [99]
	573	Tryptophan	Essential amino acid, involved in synthesis of brain serotonin and kynurenine	1. Conserved Tryptophan Motifs in the Large Tegument Protein pUL36 Are Required for Efficient Secondary Envelopment of HSV Capsids [100] 2. Indoleamine-2,3-Dioxygenase (IDO) plays role in IFN-gamma mediated Antiviral Effects against HSV Infections [101]
776-800	776	Phosphatidylinositol	Interacts with proteins, involved in cell signalling cascades and intracellular membrane trafficking; primary source of arachidonic acid (in brain)	1. KSHV induces PI-3K/AKT/mTOR pathway to facilitate its survival and proliferation in B-cells. [71] 2. Inhibition of the phosphatidylinositol 3-kinase-Akt pathway enhances gamma-2 herpesvirus (HHV-8/KSHV) lytic replication and facilitates reactivation from latency [102]
	782	Thymine/ Cytosine, Guanine	Basic unit of genetic material, molecules like ATP, NADH etc.	
	784	Phosphodiester,		

		Cytosine	Components of the genetic material (forming backbone of DNA/RNA)	
	786	Pyrimidine ring		
	787	Phosphatidyl serine		
	788	O-P-O stretching DNA		
850-855	852	Proline/ Hydroxyproline, Tyrosine	Involved in cell signalling pathways regulating cell proliferation, mTOR pathway; can scavenge ROS	
	852	Glycogen	Energy storage molecule	
1112-1124	1117	Glucose and Saccharide band	Energy currency of the cell	
	1122	Polysaccharides	Energy storage or structural support	

	1124	C-C stretching mode of lipids	Conformational structure of lipids; involved in long term energy storage, cell membrane constitution, and intercellular transmembrane transport	<ol style="list-style-type: none"> 1. HCMV- increased lipid biosynthesis. [103] 2. KSHV- Increased lipid synthesis [104]
1257-1263	1258-60	Amide III	Structural constituent of proteins in the body	<ol style="list-style-type: none"> 1. HCMV- increased anaplerotic use of glutamine. [105]
	1260	Protein band	Plays multiple roles in the cells; involved in cell signalling, proliferation etc; structural role.	
Second amide				
1270-1280	1264	Triglycerides	Main component of dietary fats, act as long-term energy storage molecule	<ol style="list-style-type: none"> 1. HSV, EBV and CMV- Infection facilitates cytokine-induced alterations in lipid and lipoprotein metabolism, leading to decreased serum levels of total cholesterol (TC), HDL-C, LDL-C, apoA1, apoB and Lp(a), as well as increased triglyceride (TG) and apoE concentrations. [106]
	1270	Unsaturated fatty acids		<ol style="list-style-type: none"> 1. DENV- increased fatty acid biosynthesis [107]

	1270	Phospholipids		
2860-2880	2853-2881	Lipids and proteins	Structural constitution of the cell; involved in signalling and transport	<ol style="list-style-type: none"> 1. Vaccinia virus- Increased de-novo fatty acid biosynthesis and β-oxidation [108] 2. HBV- Disturbed lipid synthesis [109] 3. HCV- Decreased lipid secretion [110]

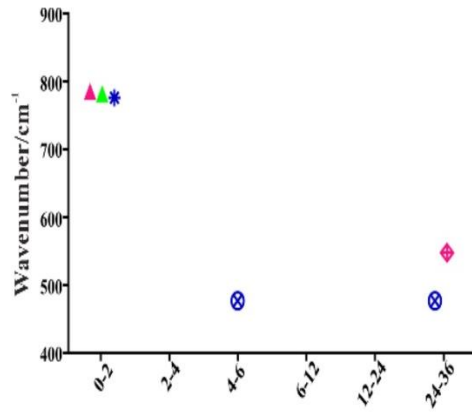
[†]HCMV - Human cytomegalovirus; HSV-1 - Herpes simplex virus-1; EBV - Epstein-Barr virus; KSHV - Kaposi's sarcoma associated herpes virus; HBV - Hepatitis B virus; DENV - Dengue virus.

4.4.3 Varying biomolecular expression at nucleus and periphery of glial cells with continuing EBV infection

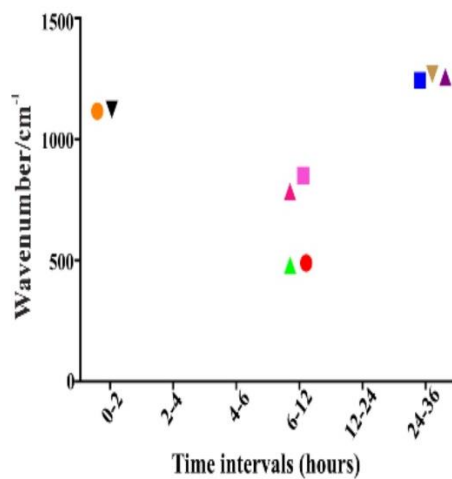
To understand the alterations happening in biomolecular expression on continuous cycle of infection progression, we compared the signal intensities at subsequent time points. The gradual increase in intensity was analyzed at successive time frames throughout the infection, in terms of predefined intervals, i.e., 0-2; 2-4; 4-6; 6-12 hpi; and 24-36 hpi for HMC-3 cells.

For HMC-3 cells, in the interval of 0-2 hpi, we observed an increment in the signal intensities of glucose and lipids [Figure 4.3-A] in the nucleus. Whereas, on the cell periphery an increase in the intensity of PIP, DNA and its phosphodiester backbone was obtained [Figure 4.3-B]. In the time span of 4-6 hpi, the amount of polysaccharide was increased at the cell periphery [Figure 4.3-B]. Later during 6-12 hpi, nucleus of microglial cells showed maximum activity with increased levels of DNA and its phosphodiester backbone, glycogen, nucleotides (guanine and cytosine) and amino acids like proline and tyrosine [Figure 4.3-A]. However, the peripheral region maintained its *status-quo* without any changes [Figure 4.3-B]. However, during the last leg of our experimental infection from 24 to 36 hpi the activity of amide III, nucleotides of DNA (guanine, cytosine, adenine, and thymine), and fatty acids was highest in the nucleus [Figure 4.3-A]. Contrary to that the amount of cholesterol and polysaccharides was highest on the peripheral region [Figure 4.3-B].

A) Periphery (HMC-3)



B) Nucleus (HMC-3)



Sign	Molecules
▲	DNA
▲	Phosphodiester backbone of DNA
▲	Nucleotides of DNA
●	Glycogen
●	Glucose
⊗	Polysaccharides
○	Lactic acid
■	Proline, tyrosine and RNA
■	Amide I, II, III
■	Tryptophan
⊠	Phenylalanine
□	Proline
⊠	Protein stretch
▼	Lipids
▼	Fatty acids
▼	Triglycerides
+	Lipids & proteins (mixed signals)
*	PIP
◇	Cholesterol
◇	Cholesterol esters
★	OH-NH-CH stretch

Figure 4.3. Representative view of changes in biomolecular activity upon continuous infection progression. Briefly, the biomolecules represented by their corresponding wavenumber values are plotted against the time interval of their occurrence. The recorded data was plotted for consequent time intervals of 0-2, 2-4, 4-6, 6-12, 12-24, and 24-36 for HMC-3 at both cellular locations (nucleus and periphery) separately. Maximum molecular activity was recorded (A) at the nucleus of HMC-3 cells during 0-2, 6-12, and 24-36 hpi, (B) at the periphery of HMC-3 cells during 0-2, 4-6, and 24-36 hpi.

4.4.4 Pathway Analysis of selected biomolecules

Further the information regarding the biomolecules was uploaded to Qiagen's IPA system. The global molecular network available in the Ingenuity pathway knowledge base (IPKB) identified canonical pathways, and gene networks associated with particular biomolecule related neuropathologies. We obtained a connectome with the set filters of virus infection and associated diseases

including neurodegeneration suggesting high involvement of cholesterol in various pathways.

Prominent molecules obtained on infection of microglia (HMC-3) were, cholesterol, cholesterol esters, phosphatidylinositol, 3-nitrotyrosine, lactic acid, lipids, and glucose [Figure 4.4]. Notably, cholesterol trafficking is prominently affected in AD and MS pathology via ABCA-1 (ATP binding cassette subfamily A member 1) transporter and modulation of apolipoprotein (APOA and APOE) metabolism [55]. Yet another group of molecules involved in cholesterol metabolism and implicated in MS, AD and PD pathologies are those involved in membrane trafficking, namely SOAT-1 (Sterol-O-Acyltransferase-1) [56], SGPL-1 (Sphingosine-1-phosphate lyase-1) [57] and SNCA (Synuclein alpha) [58] respectively. These molecules are involved in cholesterol transport in and out of the cell as well as, in presynaptic signaling. The connectome indicated various other membrane proteins like MAP-2 (matrix associated protein-2), CD-44 (a cell surface marker), PLP-1 (proteolipid protein-1), and APP (amyloid precursor protein) directly or indirectly related to cholesterol metabolism in development of neurodegenerative pathologies. These molecules mainly act as cell surface receptors and are responsible for maintaining the cell integrity, cell-cell interactions, adhesion and migration. APP, PLP-1 and MAP-2 are widely recognized in AD. Whereas, MBP (myelin basic protein) linked with lipid metabolism, is a primary marker for neurodegeneration observed in MS and ALS. Cell damage caused by oxidative stress generated due to reactive oxygen species (ROS) is one of the prevailing hypotheses of neurodegenerative pathology. Being rich in peroxidation susceptible substrates and having high oxygen consumption, the brain is more prone to damage caused by ROS. Molecules involved in the oxidative stress hypothesis of neurodegeneration were also interlinking the ones we found in our study. For example, PSEN-1 (presenilin-1) which is thoroughly studied in MS [59], AD [60] and PD [61] pathology is the connecting link between phosphatidylinositol (PIP), 3-nitrotyrosine, lactic acid, cholesterol ester and cholesterol. Additionally, molecules involved in the oxidative stress hypothesis such as BACE-1 (beta site APP cleaving enzyme-1) and A β PP are also interlinking with the cholesterol metabolism.

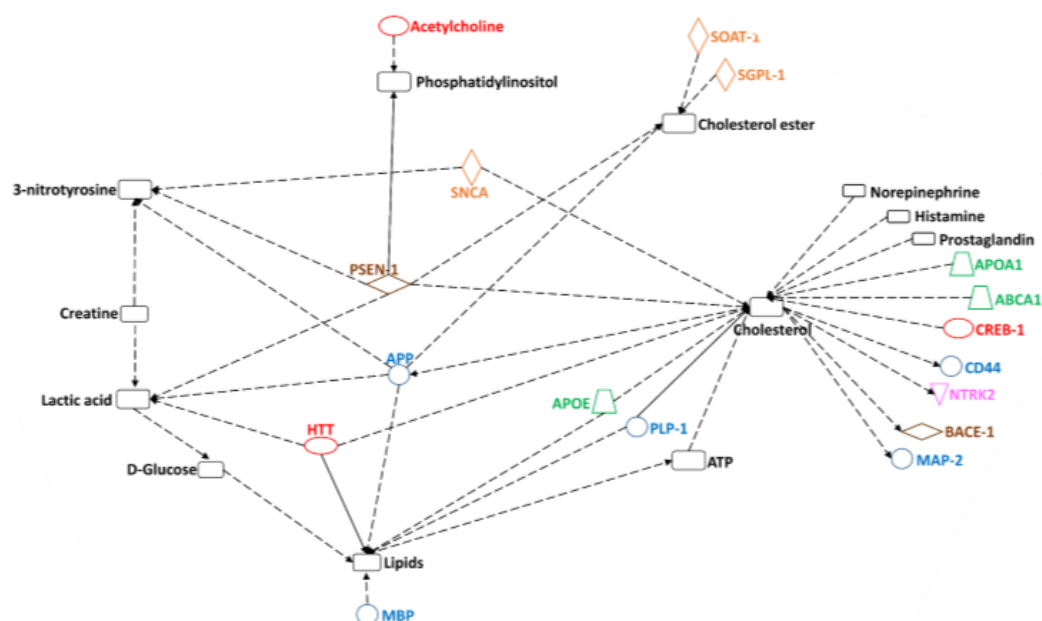


Figure 4.4. Connectome representing the interlinks of biomolecules observed to be modulated on EBV infection in HMC-3 (Microglia). The network depicts the molecules implicated in various neurodegenerative pathologies (according to the IPA knowledge database). Molecular metabolism related to (A) cholesterol, lipids, lactic acid metabolism, and PIP signaling cascade were recorded to be modulated in HMC-3 cells.

4.5 Discussion

Traces of EBV has been consistently found in the CSF samples of patients suffering from various NDDs such as AD [62], PD [63], MS and ALS [64]. Although the biochemistry of the processes involved in the viral entry and propagation inside the cell is still ambiguous. Traditional techniques of viral detection rely on the presence of viral transcripts and proteins in the host cell to ascertain infection [65]. Thereby, making the diagnosis organ and individual-specific, costly, time-consuming, handling-dependent, and with low reproducibility rate. On the contrary, RS is a non-invasive, robust, less time-consuming diagnostic technique with lesser handling constraints [66]. These qualities make RS a state-of-the-art diagnostic tool that could be utilized for early detection of infection initiation and progress inside a cell. As mentioned previously, while infecting a cell a virus goes through the sequential process of attachment, penetration, uncoating, genome replication, assembly ultimately followed by egress. All these processes are biochemically driven and can be monitored using Raman signals with respect to biochemical changes happening

inside the host cell [67]. Using RS, we recorded sequential changes at biomolecular level happening inside the microglial cells upon EBV infection, probably reflecting the aforementioned processes. The information thus obtained provides an insightful glance at the virus driven biomolecular changes inside the host cells.

During the initial stages of infection, i.e., from the time of infection to healthy cells till first 2hpi the recorded Raman signals showed an increased levels of glucose and lipid molecules in the nucleus and enhanced DNA and PIP activity at the periphery of the microglial cells. It suggested that lipids might be involved in the process of cell membrane modulation to facilitate EBV entry in the cells. In addition, until the elapse of 2 hpi, EBV (a DNA virus) was present at the cell periphery of the glial cells, and alterations in the signalling processes involving PIP were ongoing. Implying that, signaling molecules such as PIP might be helping in attachment and entry of the EBV inside the glial cells. Many viruses have developed mechanism to take advantage of phosphatidylinositol (PI)-mediated signaling cascade to gain entry inside and trigger modulations in the cell micro-environment beforehand to favor the virus's survival [68]. Although PI is the least abundant phospholipid in the cell membrane yet plays a crucial role in modulating the traffic in and out of the cell. It does so by getting differentially phosphorylated and giving rise to various PIP species [69]. Class-I PI-3 kinase (PI-3K) is the most extensively exploited signaling pathway by various viruses during the entry process. For example HIV-1 is known to employ the PI-3K mediated micropinocytosis mechanism to modulate the cell cytoskeleton for gaining entry inside the cell [70]. Various other studies have also reported the alteration of pathways involving PIP in the successful establishment of virus infection of KSHV, Human Herpesvirus-8 (HHV-8) [71] [91], HSV-1 [68] [88], HCV [72] [92], Zaire Ebola Virus [73] [93], and VZV [74]. Thus, our experiments suggested its role in EBV's entry inside the glial cells. Interestingly, PIP is implicated in the processing of APP as well and thereby in the development of AD pathologies like plaque formation or neurofibrillary tangle (NFT) deposition [75]. It also suggested a probable PIP mediated role of EBV in neurodegeneration. Our experiments also indicated that EBV infection manipulates sterol metabolism in astroglial cells on entry.

Interestingly, the brain is the most cholesterol-rich organ, consisting of about 20-25% of the total cholesterol content of the whole body. Sterol metabolism naturally being one of the cornerstones of the energy cycle in the brain plays an important role in numerous neural metabolic pathways. Disruption of sterol homeostasis in the brain may be linked with multiple neurodegenerative pathologies such as MS, AD, PD, HD, and ALS [76]–[78]. Any disturbance in the enzymatic mechanism of cholesterol synthesis, trafficking, or dissolution would lead to abnormal deposition of various sterol moieties in intracellular or extracellular matrix. This might cause hindrance in impulse transmission through neurons leading to atypical pathology of neurodegenerative diseases as AD [79], PD, or Lewy body dementia [80]. The capacity of EBV to modulate sterol homeostasis in astroglia is observed in our study and therefore it suggested that EBV could also mediate neurodegeneration by dysregulation of the cholesterol metabolism.

By the end of 2 hpi the Raman signals obtained from periphery of microglial cells coincides with that obtained at the nucleus. In addition to the continued glucose and lipid metabolism signals from the nucleus, we observed an increase in the expression of PIP and DNA at both locations. The nuclear signals decline slightly thereafter till 4 hpi. These observations point towards an early start of an increase in the DNA activity inside the nucleus of microglial cells by 2 hpi, accompanied by an enhancement in signaling processes throughout the cell, as indicated by the increased signals for PIP, or lipid molecules such as cholesterol. Moreover, by the end of 4 hpi, signals from the periphery showed the presence of polysaccharide and protein-related moieties and purines of nucleic acids. Most biomolecular signals from the nucleus showed a decline in the period of 4 to 6 hpi, except for a slight rise in the expression of fatty acids at 6 hpi. However, we noticed a probable increase in cellular traffic at the periphery during 4-6 hpi based on the increased activity of cholesterol, PIP, and amino acids (Phe, Tyr, and Trp) at the periphery of microglia. Besides, few reports suggest the exploitation of cholesterol and saccharide moieties to attach and gain entry inside the host cell, by the Herpes virus family [81].

We speculated that after entering the nucleus of a microglial cell, during 6-12 hpi the virus is most likely manipulating nuclear metabolism of glycogen [82]

and amino acids [83] to facilitate its replication cycle. It is noteworthy to state that an abnormal glucose metabolism is often associated with various neuro-inflammatory disorders [84]. The microglial nucleus showed maximum activity post 6 hpi till 12 hpi. Enhanced signals for amino acids (Pro and Tyr), glycogen, and DNA metabolism (in the form of signals for DNA, phosphodiester bond, and purines-guanine and cytosine) are observed past 6 hours in the nucleus of microglial cells and are maintained till the end of 12 hpi. It coincided with the presence of polysaccharides and amino acids in the nucleus. Nonetheless, in microglia the activity of most biomolecules at the periphery was downregulated from 6-12 hpi except a slight increase in polysaccharides and amino acids (Pro, and Val) signals. Various viruses like Dengue (DENV) [85], HCMV [86], HSV-1 [87], and EBV [88] are known to manipulate the glycolytic pathway for their benefit. These viruses could either utilize glycogen for glycogenolysis to sustain increased energy requirements during replication or fuel fatty acid synthesis (HCMV), or enhance pyrimidine production (HSV-1) as required [89]. The manipulation of glycogen metabolism by various viruses to facilitate their replication cycle enabled us to conclude that EBV may be modulating the glycogen metabolism for aiding its replication cycle in the microglia occurring at 6-12 hpi. Importantly, proline and tyrosine are involved in the cell signaling pathways such as those, regulating proliferation [90], and ROS scavenging [91]. Modulation of amino acid metabolism like that of tyrosine, and phenylalanine are known to be associated with HIV-1 [92], and HBV infections [93].

After that, in the duration of 12-24 hpi, we hypothesized the successive steps of the virus packaging and transport to be occurring in the astrocytes indicated by the presence of nucleotide molecules at periphery. However, the virus replication cycle repeated after completion of 24 hpi, as suggested by the repetition of signals obtained for PIP and cholesterol from the nucleus. Whereas, signals collected from the periphery indicate the presence of nucleotides and proteins which might be denoting the viral egress from the cell at later time points (36-48 hpi). Thereafter, in the microglial cell line, plausibly, the process of viral packaging is initiated (periphery) at 24 hpi and is carried until 36 hpi. Enhancements in signals produced from amide bond and amino acids (Phe, Tyr, and Trp), nucleotides and fatty acids corroborate our speculations; as the

molecules falling in the broad category of protein and lipids are believed to be utilized by certain viruses like HCMV to facilitate their survival inside the host. In fact, a wide variety of viruses reportedly alter fatty acid metabolism, such as HCMV, HSV, EBV, DENV, Hepatitis-B Virus (HBV), Hepatitis-C Virus (HCV), Vaccinia virus, and KSHV to name a few [93], [94]. Lipids and fatty acids being the second preferable energy source after glucose for the brain play a major role in neurophysiology. Thus, any disturbance in the homeostasis of the lipid metabolism in the brain could result in grave consequences. For instance, impaired enzymatic cascades (such as sphingolipid pathway) or oxidative stress resulting in dysregulation of lipid metabolism and lipid rafts are well described to be associated with amyloid plaque and NFT deposition causing AD [77], PD or HD [95]. After 36 hpi, we suspect that many cellular processes are simultaneously happening as the Raman signals thus obtained are mixed (pertaining to the obtained signals corresponding to the molecules like phosphodiester, proline, tyrosine, and lipids). These processes may be occurring to facilitate the initiation of the next virus replication cycle and/or carrying on the ongoing cycle.

4.6 Materials and Methods

4.6.1 Cell culture

HMC-3 cell lines (SV-40 transformed, immortalized microglial cell lines were obtained from Dr. Anirban Basu's laboratory, National Brain Research Centre, Delhi) were cultured in high glucose-containing Dulbecco's modified eagle medium (HiMedia) supplemented with 10% fetal bovine serum (Invitrogen), 50 units/mL penicillin and 100 ug/mL streptomycin (Invitrogen) over coverslips. The cells were incubated at 37°C with 5% CO₂.

4.6.2 Virus isolation and purification

HEK-293T cells (a kind gift from Prof. Erle S. Robertson's lab, University of Pennsylvania) transformed with GFP tagged virus-containing bacmid were used to obtain EBV particles [93]. Briefly to obtain the virus particles, lytic induction was given to cells with 20 ng/ml tetradecanoyl phorbol acetate and 3mM butyric

acid at 60% cell confluence for 4-5 days. The cell suspension was centrifuged at 775 g for 20 min, and the supernatant was then filtered through a 0.45 μ membrane (Millipore). The filtrate was ultra-centrifuged at 65,291 g, for 90 min at 4°C. The concentrated virus pellet was resuspended in a suitable amount of culture media and stored at -80°C until further use.

4.6.3 EBV infection in glial cells

The HMC-3 cells cultured onto the cover-slips were infected with EBV at MOI of 5.0 and incubated for the duration of 2, 4, 6, 12, 24, and 36 H. After collecting the coverslips at respective time points, the cells grown on these coverslips were fixed using 4% paraformaldehyde (PFA) for 20 min at room temperature. The coverslips were mounted onto glass slides before visualization on the Raman spectrometer.

4.6.4 Raman Spectroscopy

Raman spectroscopy was performed on LabRAM HR Evolution (Horiba-Jobin Yvon) spectrometer using a 633 nm excitation source of He-Ne laser. The sample was focused with the help of 100X optical lens to probe the nucleus and periphery of cell with greater accuracy. The Raman measurement was performed at the minimum laser power nearly about 10mW, at which laser power was not destroying the cell and providing the clear Raman spectra. Each Raman spectra were recorded for keeping 30 sec integration time to improve the quality of Raman spectra. Accumulation time was fixed for 2 sec to protect the Raman data from the noise (disturbances and cosmic shower). The Raman study was performed on uninfected (UI) and 2, 4, 6, 12, 24, and 36 hpi of respective cells. The laser was focused onto the nuclei and cell body (periphery) separately as visualised on the microscope to acquire signals from respective places.

4.6.5 Data Analysis

4.6.5.1. Graphical analysis: All the raw data of Raman vibrational intensity obtained from Raman spectroscope within wavenumber range of 400-4000 cm^{-1} were smoothed by 20 points for better visibility. Signals from common cell culture artifacts like culture medium, phosphate-buffered saline (PBS),

PFA, coverslips and glass slides were subtracted from all the samples. Thereafter, we selected the most relevant wavenumber peaks from the graph based on intensity.

4.6.5.2. Statistical analysis: Dimensionality of the raw data was reduced using principal component analysis (PCA) on SPSS software. The total numbers of selected peaks were verified through PCA. Mann-Whitney U test ($\alpha=0.05$) was applied to the screened data consisting of wavenumber ranges corresponding to the peaks for comparison of Raman intensities at subsequent time points. Additionally, we also included the odds ratio (OR) analysis to enhance data confidence.

4.6.6 Interactome study

The selected wavenumber peaks were cross referenced with the available literature to verify the corresponding biomolecules. The biomolecules were then uploaded on Qiagen's Ingenuity Pathway Analysis (IPA) software to obtain interconnection between them. Thereafter, a global molecular network available on IPKB was used as reference to perform analysis of canonical pathways, diseases and functions, and gene networks. The analysis gave us hits which are most significantly related to the biomolecular changes occurring in viral infection and neurodegenerative diseases.

4.7 References

- [1] N. Kuhar, S. Sil, T. Verma, and S. Umapathy, "Challenges in application of Raman spectroscopy to biology and materials," *RSC Adv.*, vol. 8, no. 46, pp. 25888–25908, 2018, doi: 10.1039/C8RA04491K.
- [2] A. J. Barr, "The biochemical basis of disease," *Essays Biochem.*, vol. 62, no. 5, pp. 619–642, Dec. 2018, doi: 10.1042/EBC20170054.
- [3] H. L. Taylor, C.-L. Wu, Y.-C. Chen, P.-G. Wang, J. T. Gonzalez, and J. A. Betts, "Post-Exercise Carbohydrate-Energy Replacement Attenuates Insulin Sensitivity and Glucose Tolerance the Following Morning in Healthy Adults," *Nutrients*, vol. 10, no. 2, p. E123, Jan. 2018, doi: 10.3390/nu10020123.
- [4] S. W. Boyer, L. J. Barclay, and L. C. Burrage, "Inherited Metabolic Disorders: Aspects of Chronic Nutrition Management," *Nutr. Clin. Pract. Off.*

Publ. Am. Soc. Parenter. Enter. Nutr., vol. 30, no. 4, pp. 502–510, Aug. 2015, doi: 10.1177/0884533615586201.

[5] K. G. Parhofer, “The Treatment of Disorders of Lipid Metabolism,” *Dtsch. Ärztebl. Int.*, Apr. 2016, doi: 10.3238/arztebl.2016.0261.

[6] R. de C. F. Borges, R. S. Navarro, H. E. Giana, F. G. Tavares, A. B. Fernandes, and L. Silveira Junior, “Detecting alterations of glucose and lipid components in human serum by near-infrared Raman spectroscopy,” *Res. Biomed. Eng.*, vol. 31, no. 2, pp. 160–168, Jun. 2015, doi: 10.1590/2446-4740.0593.

[7] J. W. Kang *et al.*, “Direct observation of glucose fingerprint using *in-vivo* Raman spectroscopy,” *Sci. Adv.*, vol. 6, no. 4, p. eaay5206, Jan. 2020, doi: 10.1126/sciadv.aay5206.

[8] M. Javanmard and R. W. Davis, “Surface-enhanced Raman scattering (SERS) for detection of phenylketonuria for newborn screening,” San Francisco, California, United States, Feb. 2014, p. 89540R. doi: 10.1117/12.2040845.

[9] R. Manoharan *et al.*, “Raman Spectroscopy and Fluorescence Photon Migration for Breast Cancer Diagnosis and Imaging,” *Photochem. Photobiol.*, vol. 67, no. 1, pp. 15–22, Jan. 1998, doi: 10.1111/j.1751-1097.1998.tb05160.x.

[10] M. V. P. Chowdary, K. K. Kumar, J. Kurien, S. Mathew, and C. M. Krishna, “Discrimination of normal, benign, and malignant breast tissues by Raman spectroscopy,” *Biopolymers*, vol. 83, no. 5, pp. 556–569, Dec. 2006, doi: 10.1002/bip.20586.

[11] I. J. Pence *et al.*, “Clinical characterization of *in-vivo* inflammatory bowel disease with Raman spectroscopy,” *Biomed. Opt. Express*, vol. 8, no. 2, p. 524, Feb. 2017, doi: 10.1364/BOE.8.000524.

[12] K. Czamara, K. Majzner, A. Selmi, M. Baranska, Y. Ozaki, and A. Kaczor, “Unsaturated lipid bodies as a hallmark of inflammation studied by Raman 2D and 3D microscopy,” *Sci. Rep.*, vol. 7, no. 1, p. 40889, Feb. 2017, doi: 10.1038/srep40889.

[13] S. P. Singh *et al.*, “Identification of early inflammatory changes in the tympanic membrane with Raman spectroscopy,” *The Analyst*, vol. 144, no. 22, pp. 6721–6728, 2019, doi: 10.1039/C9AN01772K.

[14] S. K. Patel *et al.*, “Rapid Discrimination of Malaria- and Dengue-Infected Patients Sera Using Raman Spectroscopy,” *Anal. Chem.*, vol. 91, no. 11, pp. 7054–7062, Jun. 2019, doi: 10.1021/acs.analchem.8b05907.

- [15] K. E. Hamden, B. A. Bryan, P. W. Ford, C. Xie, Y.-Q. Li, and S. M. Akula, "Spectroscopic analysis of Kaposi's sarcoma-associated herpesvirus infected cells by Raman tweezers," *J. Virol. Methods*, vol. 129, no. 2, pp. 145–151, Nov. 2005, doi: 10.1016/j.jviromet.2005.05.018.
- [16] P. R. T. Jess, D. D. W. Smith, M. Mazilu, K. Dholakia, A. C. Riches, and C. S. Herrington, "Early detection of cervical neoplasia by Raman spectroscopy," *Int. J. Cancer*, vol. 121, no. 12, pp. 2723–2728, Dec. 2007, doi: 10.1002/ijc.23046.
- [17] J. D. Driskell, Y. Zhu, C. D. Kirkwood, Y. Zhao, R. A. Dluhy, and R. A. Tripp, "Rapid and Sensitive Detection of Rotavirus Molecular Signatures Using Surface Enhanced Raman Spectroscopy," *PLoS ONE*, vol. 5, no. 4, p. e10222, Apr. 2010, doi: 10.1371/journal.pone.0010222.
- [18] S. Sehrawat, D. Kumar, and B. T. Rouse, "Herpesviruses: Harmonious Pathogens but Relevant Cofactors in Other Diseases?," *Front. Cell. Infect. Microbiol.*, vol. 8, p. 177, May 2018, doi: 10.3389/fcimb.2018.00177.
- [19] L. Zanella, I. Riquelme, K. Buchegger, M. Abanto, C. Ili, and P. Brebi, "A reliable Epstein-Barr Virus classification based on phylogenomic and population analyses," *Sci. Rep.*, vol. 9, no. 1, p. 9829, Dec. 2019, doi: 10.1038/s41598-019-45986-3.
- [20] M. K. Smatti, D. W. Al-Sadeq, N. H. Ali, G. Pintus, H. Abou-Saleh, and G. K. Nasrallah, "Epstein-Barr Virus Epidemiology, Serology, and Genetic Variability of LMP-1 Oncogene Among Healthy Population: An Update," *Front. Oncol.*, vol. 8, p. 211, Jun. 2018, doi: 10.3389/fonc.2018.00211.
- [21] Y.-F. Chiu and B. Sugden, "Epstein-Barr Virus: The Path from Latent to Productive Infection," *Annu. Rev. Virol.*, vol. 3, no. 1, pp. 359–372, Sep. 2016, doi: 10.1146/annurev-virology-110615-042358.
- [22] Y. Yang and F. Gao, "Clinical characteristics of primary and reactivated Epstein-Barr virus infection in children," *J. Med. Virol.*, vol. 92, no. 12, pp. 3709–3716, Dec. 2020, doi: 10.1002/jmv.26202.
- [23] H. C. Jha, Y. Pei, and E. S. Robertson, "Epstein-Barr Virus: Diseases Linked to Infection and Transformation," *Front. Microbiol.*, vol. 7, p. 1602, 2016, doi: 10.3389/fmicb.2016.01602.
- [24] I. Carbone *et al.*, "Herpes virus in Alzheimer's disease: relation to progression of the disease," *Neurobiol. Aging*, vol. 35, no. 1, pp. 122–129, Jan. 2014, doi: 10.1016/j.neurobiolaging.2013.06.024.

- [25] X.-L. Bu *et al.*, “The association between infectious burden and Parkinson’s disease: A case-control study,” *Parkinsonism Relat. Disord.*, vol. 21, no. 8, pp. 877–881, Aug. 2015, doi: 10.1016/j.parkreldis.2015.05.015.
- [26] S. Jakhmola, A. Upadhyay, K. Jain, A. Mishra, and H. C. Jha, “Herpesviruses and the hidden links to Multiple Sclerosis neuropathology,” *J. Neuroimmunol.*, vol. 358, p. 577636, Sep. 2021, doi: 10.1016/j.jneuroim.2021.577636.
- [27] S. Burnard, J. Lechner-Scott, and R. J. Scott, “EBV and MS: Major cause, minor contribution or red-herring?,” *Mult. Scler. Relat. Disord.*, vol. 16, pp. 24–30, Aug. 2017, doi: 10.1016/j.msard.2017.06.002.
- [28] J. Schneider-Schaulies, “Cellular receptors for viruses: links to tropism and pathogenesis,” *J. Gen. Virol.*, vol. 81, no. 6, pp. 1413–1429, Jun. 2000, doi: 10.1099/0022-1317-81-6-1413.
- [29] J. J. Miner and M. S. Diamond, “Zika Virus Pathogenesis and Tissue Tropism,” *Cell Host Microbe*, vol. 21, no. 2, pp. 134–142, Feb. 2017, doi: 10.1016/j.chom.2017.01.004.
- [30] V. G. Puelles *et al.*, “Multiorgan and Renal Tropism of SARS-CoV-2,” *N. Engl. J. Med.*, vol. 383, no. 6, pp. 590–592, Aug. 2020, doi: 10.1056/NEJMc2011400.
- [31] C. Shannon-Lowe and M. Rowe, “Epstein-Barr virus entry; kissing and conjugation,” *Curr. Opin. Virol.*, vol. 4, pp. 78–84, Feb. 2014, doi: 10.1016/j.coviro.2013.12.001.
- [32] D. Tiwari, S. Jakhmola, D. K. Pathak, R. Kumar, and H. C. Jha, “Temporal *In Vitro* Raman Spectroscopy for Monitoring Replication Kinetics of Epstein–Barr Virus Infection in Glial Cells,” *ACS Omega*, vol. 5, no. 45, pp. 29547–29560, Nov. 2020, doi: 10.1021/acsomega.0c04525.
- [33] O. Indari, R. Chandramohanadas, and H. C. Jha, “Epstein–Barr virus infection modulates blood–brain barrier cells and its co-infection with *Plasmodium falciparum* induces RBC adhesion,” *Pathog. Dis.*, vol. 79, no. 1, p. ftaa080, Jan. 2021, doi: 10.1093/femspd/ftaa080.
- [34] A. Rani, S. Jakhmola, S. Karnati, H. S. Parmar, and H. Chandra Jha, “Potential entry receptors for human γ -herpesvirus into epithelial cells: A plausible therapeutic target for viral infections,” *Tumour Virus Res.*, vol. 12, p. 200227, Dec. 2021, doi: 10.1016/j.tvr.2021.200227.

- [35] G. R. Nemerow, R. A. Houghten, M. D. Moore, and N. R. Cooper, "Identification of an epitope in the major envelope protein of Epstein-Barr virus that mediates viral binding to the B lymphocyte EBV receptor (CR2)," *Cell*, vol. 56, no. 3, pp. 369–377, Feb. 1989, doi: 10.1016/0092-8674(89)90240-7.
- [36] H. C. Jha *et al.*, "Gammaherpesvirus Infection of Human Neuronal Cells," *mBio*, vol. 6, no. 6, Dec. 2015, doi: 10.1128/mBio.01844-15.
- [37] C. M. Borza and L. M. Hutt-Fletcher, "Alternate replication in B cells and epithelial cells switches tropism of Epstein–Barr virus," *Nat. Med.*, vol. 8, no. 6, pp. 594–599, Jun. 2002, doi: 10.1038/nm0602-594.
- [38] N. A. Ilyushina *et al.*, "Comparative Study of Influenza Virus Replication in MDCK Cells and in Primary Cells Derived from Adenoids and Airway Epithelium," *J. Virol.*, vol. 86, no. 21, pp. 11725–11734, Nov. 2012, doi: 10.1128/JVI.01477-12.
- [39] H. Chu *et al.*, "Comparative tropism, replication kinetics, and cell damage profiling of SARS-CoV-2 and SARS-CoV with implications for clinical manifestations, transmissibility, and laboratory studies of COVID-19: an observational study," *Lancet Microbe*, vol. 1, no. 1, pp. e14–e23, May 2020, doi: 10.1016/S2666-5247(20)30004-5.
- [40] P. Mrozek-Gorska *et al.*, "Epstein–Barr virus reprograms human B lymphocytes immediately in the prelatent phase of infection," *Proc. Natl. Acad. Sci.*, vol. 116, no. 32, pp. 16046–16055, Aug. 2019, doi: 10.1073/pnas.1901314116.
- [41] S. Halder, M. Murakami, S. C. Verma, P. Kumar, F. Yi, and E. S. Robertson, "Early Events Associated with Infection of Epstein-Barr Virus Infection of Primary B-Cells," *PLoS ONE*, vol. 4, no. 9, p. e7214, Sep. 2009, doi: 10.1371/journal.pone.0007214.
- [42] L. E. Kamemoto *et al.*, "Near-Infrared Micro-Raman Spectroscopy for *in Vitro* Detection of Cervical Cancer," *Appl. Spectrosc.*, vol. 64, no. 3, pp. 255–261, Mar. 2010, doi: 10.1366/000370210790918364.
- [43] N. Stone, C. Kendall, N. Shepherd, P. Crow, and H. Barr, "Near-infrared Raman spectroscopy for the classification of epithelial pre-cancers and cancers," *J. Raman Spectrosc.*, vol. 33, no. 7, pp. 564–573, Jul. 2002, doi: 10.1002/jrs.882.
- [44] C. Krafft, L. Neudert, T. Simat, and R. Salzer, "Near infrared Raman spectra of human brain lipids," *Spectrochim. Acta. A. Mol. Biomol. Spectrosc.*, vol. 61, no. 7, pp. 1529–1535, May 2005, doi: 10.1016/j.saa.2004.11.017.

- [45] C. Kendall *et al.*, “Evaluation of Raman probe for oesophageal cancer diagnostics,” *The Analyst*, vol. 135, no. 12, p. 3038, 2010, doi: 10.1039/c0an00536c.
- [46] G. Shetty, C. Kendall, N. Shepherd, N. Stone, and H. Barr, “Raman spectroscopy: elucidation of biochemical changes in carcinogenesis of oesophagus,” *Br. J. Cancer*, vol. 94, no. 10, pp. 1460–1464, May 2006, doi: 10.1038/sj.bjc.6603102.
- [47] A. J. Ruiz-Chica, M. A. Medina, F. Sánchez-Jiménez, and F. J. Ramírez, “Characterization by Raman spectroscopy of conformational changes on guanine–cytosine and adenine–thymine oligonucleotides induced by aminoxy analogues of spermidine,” *J. Raman Spectrosc.*, vol. 35, no. 2, pp. 93–100, Feb. 2004, doi: 10.1002/jrs.1107.
- [48] D. P. Lau *et al.*, “Raman spectroscopy for optical diagnosis in the larynx: Preliminary findings,” *Lasers Surg. Med.*, vol. 37, no. 3, pp. 192–200, Sep. 2005, doi: 10.1002/lsm.20226.
- [49] M. Gniadecka, H. C. Wulf, N. Nymark Mortensen, O. Faurskov Nielsen, and D. H. Christensen, “Diagnosis of Basal Cell Carcinoma by Raman Spectroscopy,” *J. Raman Spectrosc.*, vol. 28, no. 2–3, pp. 125–129, Feb. 1997, doi: 10.1002/(SICI)1097-4555(199702)28:2/3<125::AID-JRS65>3.0.CO;2-#.
- [50] I. Rehman, R. Smith, L. L. Hench, and W. Bonfield, “Structural evaluation of human and sheep bone and comparison with synthetic hydroxyapatite by FT-Raman spectroscopy,” *J. Biomed. Mater. Res.*, vol. 29, no. 10, pp. 1287–1294, Oct. 1995, doi: 10.1002/jbm.820291016.
- [51] R. K. Dukor, “Vibrational Spectroscopy in the Detection of Cancer,” in *Handbook of Vibrational Spectroscopy*, J. M. Chalmers and P. R. Griffiths, Eds. Chichester, UK: John Wiley & Sons, Ltd, 2006, p. s8107. doi: 10.1002/0470027320.s8107.
- [52] L. Silveira, S. Sathaiyah, R. A. Zângaro, M. T. T. Pacheco, M. C. Chavantes, and C. A. G. Pasqualucci, “Correlation between near-infrared Raman spectroscopy and the histopathological analysis of atherosclerosis in human coronary arteries: RAMAN ANALYSIS OF ATHEROSCLEROSIS,” *Lasers Surg. Med.*, vol. 30, no. 4, pp. 290–297, Apr. 2002, doi: 10.1002/lsm.10053.
- [53] Z. Huang, A. McWilliams, H. Lui, D. I. McLean, S. Lam, and H. Zeng, “Near-infrared Raman spectroscopy for optical diagnosis of lung cancer,” *Int. J. Cancer*, vol. 107, no. 6, pp. 1047–1052, Dec. 2003, doi: 10.1002/ijc.11500.

- [54] R. J. Lakshmi, V. B. Kartha, C. Murali Krishna, J. G. R. Solomon, G. Ullas, and P. Uma Devi, "Tissue Raman Spectroscopy for the Study of Radiation Damage: Brain Irradiation of Mice," *Radiat. Res.*, vol. 157, no. 2, pp. 175–182, Feb. 2002, doi: 10.1667/0033-7587(2002)157[0175:TRSFTS]2.0.CO;2.
- [55] V. Hirsch-Reinshagen *et al.*, "Deficiency of ABCA1 Impairs Apolipoprotein E Metabolism in Brain," *J. Biol. Chem.*, vol. 279, no. 39, pp. 41197–41207, Sep. 2004, doi: 10.1074/jbc.M407962200.
- [56] Y. Shibuya, C. C. Chang, and T.-Y. Chang, "ACAT1/SOAT1 as a therapeutic target for Alzheimer's disease," *Future Med. Chem.*, vol. 7, no. 18, pp. 2451–2467, Dec. 2015, doi: 10.4155/fmc.15.161.
- [57] S. Cosconati and E. Novellino, "The First Sphingosine 1-Phosphate Lyase Inhibitors against Multiple Sclerosis: A Successful Drug Discovery Tale," *J. Med. Chem.*, vol. 57, no. 12, pp. 5072–5073, Jun. 2014, doi: 10.1021/jm500845y.
- [58] L. Stefanis, "-Synuclein in Parkinson's Disease," *Cold Spring Harb. Perspect. Med.*, vol. 2, no. 2, pp. a009399–a009399, Feb. 2012, doi: 10.1101/cshperspect.a009399.
- [59] M. Cummings *et al.*, "Presenilin1 regulates Th1 and Th17 effector responses but is not required for experimental autoimmune encephalomyelitis," *PLoS One*, vol. 13, no. 8, p. e0200752, 2018, doi: 10.1371/journal.pone.0200752.
- [60] R. J. Kelleher and J. Shen, "Presenilin-1 mutations and Alzheimer's disease," *Proc. Natl. Acad. Sci.*, vol. 114, no. 4, pp. 629–631, Jan. 2017, doi: 10.1073/pnas.1619574114.
- [61] L. Ibanez *et al.*, "Pleiotropic Effects of Variants in Dementia Genes in Parkinson Disease," *Front. Neurosci.*, vol. 12, p. 230, Apr. 2018, doi: 10.3389/fnins.2018.00230.
- [62] S.-Y. Huang *et al.*, "Herpesvirus infections and Alzheimer's disease: a Mendelian randomization study," *Alzheimers Res. Ther.*, vol. 13, no. 1, p. 158, Dec. 2021, doi: 10.1186/s13195-021-00905-5.
- [63] J. M. Woulfe *et al.*, "Absence of elevated anti- α -synuclein and anti-EBV latent membrane protein antibodies in PD," *Neurology*, vol. 58, no. 9, pp. 1435–1435, May 2002, doi: 10.1212/WNL.58.9.1435.
- [64] K. Bjornevik *et al.*, "Longitudinal analysis reveals high prevalence of Epstein-Barr virus associated with multiple sclerosis," *Science*, vol. 375, no. 6578, pp. 296–301, Jan. 2022, doi: 10.1126/science.abj8222.

- [65] D. R. Peaper and M. L. Landry, "Laboratory diagnosis of viral infection," *Handb. Clin. Neurol.*, vol. 123, pp. 123–147, 2014, doi: 10.1016/B978-0-444-53488-0.00005-5.
- [66] S. Uskoković-Marković, M. Jelikić-Stankov, I. Holclajtner-Antunović, and P. Đurđević, "Raman Spectroscopy as a New Biochemical Diagnostic Tool," *J. Med. Biochem.*, vol. 32, no. 2, pp. 96–103, Apr. 2013, doi: 10.2478/jomb-2013-0004.
- [67] K. W. Short, S. Carpenter, J. P. Freyer, and J. R. Mourant, "Raman Spectroscopy Detects Biochemical Changes Due to Proliferation in Mammalian Cell Cultures," *Biophys. J.*, vol. 88, no. 6, pp. 4274–4288, Jun. 2005, doi: 10.1529/biophysj.103.038604.
- [68] K. Zheng *et al.*, "Epidermal Growth Factor Receptor-PI3K Signaling Controls Cofilin Activity To Facilitate Herpes Simplex Virus 1 Entry into Neuronal Cells," *mBio*, vol. 5, no. 1, pp. e00958-13, Feb. 2014, doi: 10.1128/mBio.00958-13.
- [69] G. D. Prestwich, "Phosphoinositide Signaling," *Chem. Biol.*, vol. 11, no. 5, pp. 619–637, May 2004, doi: 10.1016/j.chembiol.2004.03.025.
- [70] V. Rocha-Perugini, M. Gordon-Alonso, and F. Sánchez-Madrid, "PIP2: choreographer of actin-adaptor proteins in the HIV-1 dance," *Trends Microbiol.*, vol. 22, no. 7, pp. 379–388, Jul. 2014, doi: 10.1016/j.tim.2014.03.009.
- [71] A. P. Bhatt and B. Damania, "AKTivation of PI3K/AKT/mTOR signaling pathway by KSHV," *Front. Immunol.*, vol. 3, 2013, doi: 10.3389/fimmu.2012.00401.
- [72] K. L. Berger *et al.*, "Roles for endocytic trafficking and phosphatidylinositol 4-kinase III alpha in hepatitis C virus replication," *Proc. Natl. Acad. Sci.*, vol. 106, no. 18, pp. 7577–7582, May 2009, doi: 10.1073/pnas.0902693106.
- [73] M. F. Saeed, A. A. Kolokoltsov, A. N. Freiberg, M. R. Holbrook, and R. A. Davey, "Phosphoinositide-3 Kinase-Akt Pathway Controls Cellular Entry of Ebola Virus," *PLoS Pathog.*, vol. 4, no. 8, p. e1000141, Aug. 2008, doi: 10.1371/journal.ppat.1000141.
- [74] R. Izmailyan *et al.*, "Integrin β 1 Mediates Vaccinia Virus Entry through Activation of PI3K/Akt Signaling," *J. Virol.*, vol. 86, no. 12, pp. 6677–6687, Jun. 2012, doi: 10.1128/JVI.06860-11.

- [75] E. Morel *et al.*, “Phosphatidylinositol-3-phosphate regulates sorting and processing of amyloid precursor protein through the endosomal system,” *Nat. Commun.*, vol. 4, no. 1, p. 2250, Oct. 2013, doi: 10.1038/ncomms3250.
- [76] U. Jin, S. J. Park, and S. M. Park, “Cholesterol Metabolism in the Brain and Its Association with Parkinson’s Disease,” *Exp. Neurobiol.*, vol. 28, no. 5, pp. 554–567, Oct. 2019, doi: 10.5607/en.2019.28.5.554.
- [77] R. S. Yadav and N. K. Tiwari, “Lipid Integration in Neurodegeneration: An Overview of Alzheimer’s Disease,” *Mol. Neurobiol.*, vol. 50, no. 1, pp. 168–176, Aug. 2014, doi: 10.1007/s12035-014-8661-5.
- [78] R. W. Browne *et al.*, “High-density lipoprotein cholesterol is associated with multiple sclerosis fatigue: A fatigue-metabolism nexus?,” *J. Clin. Lipidol.*, vol. 13, no. 4, pp. 654-663.e1, Jul. 2019, doi: 10.1016/j.jacl.2019.06.003.
- [79] T.-Y. Chang, Y. Yamauchi, M. T. Hasan, and C. Chang, “Cellular cholesterol homeostasis and Alzheimer’s disease,” *J. Lipid Res.*, vol. 58, no. 12, pp. 2239–2254, Dec. 2017, doi: 10.1194/jlr.R075630.
- [80] I. Alecu and S. A. L. Bennett, “Dysregulated Lipid Metabolism and Its Role in α -Synucleinopathy in Parkinson’s Disease,” *Front. Neurosci.*, vol. 13, p. 328, Apr. 2019, doi: 10.3389/fnins.2019.00328.
- [81] G. A. Wudiri *et al.*, “Molecular Requirement for Sterols in Herpes Simplex Virus Entry and Infectivity,” *J. Virol.*, vol. 88, no. 23, pp. 13918–13922, Dec. 2014, doi: 10.1128/JVI.01615-14.
- [82] G. A. Gualdoni *et al.*, “Rhinovirus induces an anabolic reprogramming in host cell metabolism essential for viral replication,” *Proc. Natl. Acad. Sci.*, vol. 115, no. 30, Jul. 2018, doi: 10.1073/pnas.1800525115.
- [83] N. Boodhoo, N. Kamble, S. Sharif, and S. Behboudi, “Glutaminolysis and Glycolysis Are Essential for Optimal Replication of Marek’s Disease Virus,” *J. Virol.*, vol. 94, no. 4, pp. e01680-19, Jan. 2020, doi: 10.1128/JVI.01680-19.
- [84] R. S. Jope, C. J. Yuskaitis, and E. Beurel, “Glycogen Synthase Kinase-3 (GSK3): Inflammation, Diseases, and Therapeutics,” *Neurochem. Res.*, vol. 32, no. 4–5, pp. 577–595, Mar. 2007, doi: 10.1007/s11064-006-9128-5.
- [85] K. A. Fontaine, E. L. Sanchez, R. Camarda, and M. Lagunoff, “Dengue Virus Induces and Requires Glycolysis for Optimal Replication,” *J. Virol.*, vol. 89, no. 4, pp. 2358–2366, Feb. 2015, doi: 10.1128/JVI.02309-14.

- [86] J. Munger, S. U. Bajad, H. A. Collier, T. Shenk, and J. D. Rabinowitz, “Dynamics of the Cellular Metabolome during Human Cytomegalovirus Infection,” *PLoS Pathog.*, vol. 2, no. 12, p. e132, 2006, doi: 10.1371/journal.ppat.0020132.
- [87] J. L. Abrantes *et al.*, “Herpes simplex type 1 activates glycolysis through engagement of the enzyme 6-phosphofructo-1-kinase (PFK-1),” *Biochim. Biophys. Acta BBA - Mol. Basis Dis.*, vol. 1822, no. 8, pp. 1198–1206, Aug. 2012, doi: 10.1016/j.bbadis.2012.04.011.
- [88] W.-W. Sung, P.-R. Chen, M.-H. Liao, and J.-W. Lee, “Enhanced aerobic glycolysis of nasopharyngeal carcinoma cells by Epstein-Barr virus latent membrane protein 1,” *Exp. Cell Res.*, vol. 359, no. 1, pp. 94–100, Oct. 2017, doi: 10.1016/j.yexcr.2017.08.005.
- [89] L. Vastag, E. Koyuncu, S. L. Grady, T. E. Shenk, and J. D. Rabinowitz, “Divergent Effects of Human Cytomegalovirus and Herpes Simplex Virus-1 on Cellular Metabolism,” *PLoS Pathog.*, vol. 7, no. 7, p. e1002124, Jul. 2011, doi: 10.1371/journal.ppat.1002124.
- [90] U. Y. Choi *et al.*, “Oncogenic human herpesvirus hijacks proline metabolism for tumorigenesis,” *Proc. Natl. Acad. Sci.*, vol. 117, no. 14, pp. 8083–8093, Apr. 2020, doi: 10.1073/pnas.1918607117.
- [91] Y. Jiang, Y. Li, L. Zhou, and D. Zhang, “Comparative metabolomics unveils molecular changes and metabolic networks of syringin against hepatitis B mice by untargeted mass spectrometry,” *RSC Adv.*, vol. 10, no. 1, pp. 461–473, 2020, doi: 10.1039/C9RA06332C.
- [92] J. M. Gostner, K. Becker, K. Kurz, and D. Fuchs, “Disturbed Amino Acid Metabolism in HIV: Association with Neuropsychiatric Symptoms,” *Front. Psychiatry*, vol. 6, Jul. 2015, doi: 10.3389/fpsyt.2015.00097.
- [93] Q. Xie *et al.*, “Multi-omics analyses reveal metabolic alterations regulated by hepatitis B virus core protein in hepatocellular carcinoma cells,” *Sci. Rep.*, vol. 7, no. 1, p. 41089, Feb. 2017, doi: 10.1038/srep41089.
- [94] P. Lange, M. Lagunoff, and V. Tarakanova, “Chewing the Fat: The Conserved Ability of DNA Viruses to Hijack Cellular Lipid Metabolism,” *Viruses*, vol. 11, no. 2, p. 119, Jan. 2019, doi: 10.3390/v11020119.
- [95] R. E. Estes, B. Lin, A. Khera, and M. Y. Davis, “Lipid Metabolism Influence on Neurodegenerative Disease Progression: Is the Vehicle as Important as the Cargo?,” *Front. Mol. Neurosci.*, vol. 14, p. 788695, Dec. 2021, doi: 10.3389/fnmol.2021.788695.

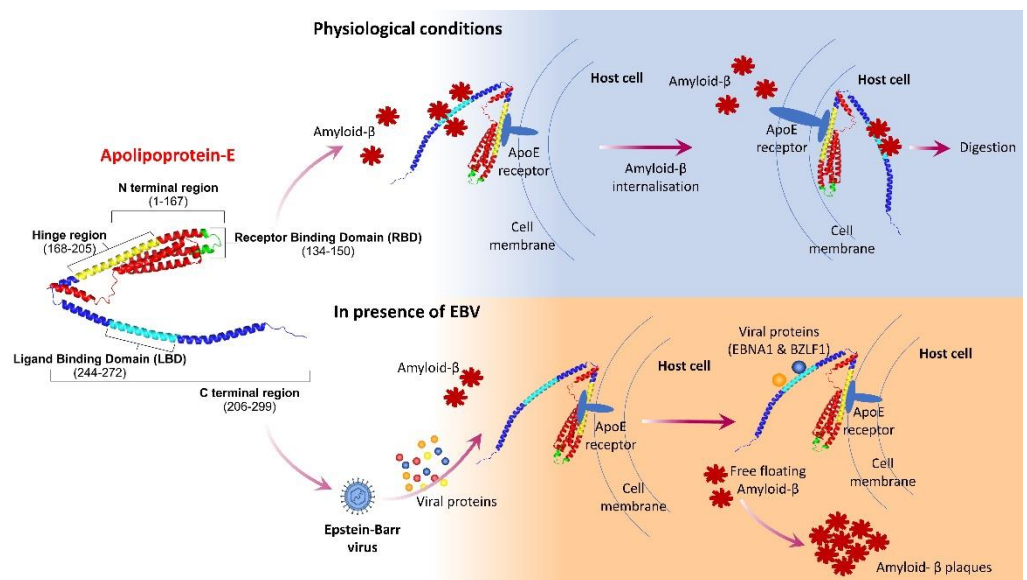
- [96] L. Xiao et al., “Targeting Epstein–Barr virus oncoprotein LMP1-mediated glycolysis sensitizes nasopharyngeal carcinoma to radiation therapy,” *Oncogene*, vol. 33, no. 37, pp. 4568–4578, Sep. 2014, doi: 10.1038/onc.2014.32.
- [97] M. Ikeda and R. Longnecker, “Cholesterol is critical for Epstein-Barr virus latent membrane protein 2A trafficking and protein stability,” *Virology*, vol. 360, no. 2, pp. 461–468, Apr. 2007, doi: 10.1016/j.virol.2006.10.046.
- [98] A. K. P. Serquiña, D. M. Kambach, O. Sarker, and J. M. Ziegelbauer, “Viral MicroRNAs Repress the Cholesterol Pathway, and 25-Hydroxycholesterol Inhibits Infection,” *mBio*, vol. 8, no. 4, pp. e00576-17, Sep. 2017, doi: 10.1128/mBio.00576-17.
- [99] H.-J. Shin et al., “Hepatitis B Virus X Protein Regulates Hepatic Glucose Homeostasis via Activation of Inducible Nitric Oxide Synthase,” *J. Biol. Chem.*, vol. 286, no. 34, pp. 29872–29881, Aug. 2011, doi: 10.1074/jbc.M111.259978.
- [100] L. Ivanova et al., “Conserved Tryptophan Motifs in the Large Tegument Protein pUL36 Are Required for Efficient Secondary Envelopment of Herpes Simplex Virus Capsids,” *J. Virol.*, vol. 90, no. 11, pp. 5368–5383, Jun. 2016, doi: 10.1128/JVI.03167-15.
- [101] O. Adams, K. Besken, C. Oberdörfer, C. R. MacKenzie, O. Takikawa, and W. Däubener, “Role of Indoleamine-2,3-Dioxygenase in Alpha/Beta and Gamma Interferon-Mediated Antiviral Effects against Herpes Simplex Virus Infections,” *J. Virol.*, vol. 78, no. 5, pp. 2632–2636, Mar. 2004, doi: 10.1128/JVI.78.5.2632-2636.2004.
- [102] L. Peng et al., “Inhibition of the phosphatidylinositol 3-kinase-Akt pathway enhances gamma-2 herpesvirus lytic replication and facilitates reactivation from latency,” *J. Gen. Virol.*, vol. 91, no. 2, pp. 463–469, Feb. 2010, doi: 10.1099/vir.0.015073-0.
- [103] Y. Yu, T. G. Maguire, and J. C. Alwine, “Human Cytomegalovirus Infection Induces Adipocyte-Like Lipogenesis through Activation of Sterol Regulatory Element Binding Protein 1,” *J. Virol.*, vol. 86, no. 6, pp. 2942–2949, Mar. 2012, doi: 10.1128/JVI.06467-11.
- [104] T. Delgado, E. L. Sanchez, R. Camarda, and M. Lagunoff, “Global Metabolic Profiling of Infection by an Oncogenic Virus: KSHV Induces and Requires Lipogenesis for Survival of Latent Infection,” *PLoS Pathog.*, vol. 8, no. 8, p. e1002866, Aug. 2012, doi: 10.1371/journal.ppat.1002866.

- [105] J. W. Chambers, T. G. Maguire, and J. C. Alwine, "Glutamine Metabolism Is Essential for Human Cytomegalovirus Infection," *J. Virol.*, vol. 84, no. 4, pp. 1867–1873, Feb. 2010, doi: 10.1128/JVI.02123-09.
- [106] I. F. Gazi and M. S. Elisaf, "Effect of infection on lipid profile: focus on Epstein–Barr virus," *Clin. Lipidol.*, vol. 5, no. 5, pp. 607–610, Oct. 2010, doi: 10.2217/clp.10.53.
- [107] N. S. Heaton et al., "Dengue virus nonstructural protein 3 redistributes fatty acid synthase to sites of viral replication and increases cellular fatty acid synthesis," *Proc. Natl. Acad. Sci.*, vol. 107, no. 40, pp. 17345–17350, Oct. 2010, doi: 10.1073/pnas.1010811107.
- [108] M. D. Greseth and P. Traktman, "De novo Fatty Acid Biosynthesis Contributes Significantly to Establishment of a Bioenergetically Favorable Environment for Vaccinia Virus Infection," *PLoS Pathog.*, vol. 10, no. 3, p. e1004021, Mar. 2014, doi: 10.1371/journal.ppat.1004021.
- [109] C.-F. Teng, H.-C. Wu, W.-C. Hsieh, H.-W. Tsai, and I.-J. Su, "Activation of ATP Citrate Lyase by mTOR Signal Induces Disturbed Lipid Metabolism in Hepatitis B Virus Pre-S2 Mutant Tumorigenesis," *J. Virol.*, vol. 89, no. 1, pp. 605–614, Jan. 2015, doi: 10.1128/JVI.02363-14.
- [110] G. Perlemuter et al., "Hepatitis C virus core protein inhibits microsomal triglyceride transfer protein activity and very low density lipoprotein secretion: a model of viral-related steatosis," *FASEB J.*, vol. 16, no. 2, pp. 185–194, Feb. 2002, doi: 10.1096/fj.01-0396com.

Chapter 5

An *in-silico* insight into the predictive interaction of Apolipoprotein-E with Epstein-Barr virus proteins and their probable role in mediating Alzheimer's disease

5.1 Graphical abstract



5.2 Abstract

The prevailing viral hypothesis of AD implicates the presence of neurotropic viruses in the CNS as an initiating factor of AD pathophysiology. Recent reports suggest that persistent infection of Epstein-Barr virus, a member of the Herpesviridae family, and its recurrent reactivation could potentially instigate the formation of proteinaceous plaques in the brain: a hallmark of AD. Interestingly, a genetic risk factor of AD, namely ApoE, has been reported to influence the outcome of EBV infection in an individual; and states that EBV infection in an individual could predispose them to develop AD later in life. The presence of persistent EBV infection in a genetically predisposed individual could create a perfect recipe for severe consequences like AD. Further, ApoE also influences the clearance of proteinaceous plaques, and its defective functioning could result in aggregate depositions in the brain. Therefore, we have

investigated the possible interaction between ApoE and various EBV proteins in the present study using computational tools. Our results showed possibly stable de-novo interactions between the C-terminal domain of ApoE3 and EBV proteins: EBNA1 and BZLF1. The EBNA1 protein of EBV plays a crucial role in establishing latency and carrying out replication of the virus. At the same time, BZLF1 is involved in the lytic replication cycle. The proposed interaction of EBV proteins at the ligand-binding site of ApoE3 on CTD could interfere with its capability to sequester amyloid fragments and hence their clearance from the brain giving rise to AD pathology. This study provides a new outlook on EBV's role in AD development and paves the way for novel avenues of investigation which could further our understanding of AD pathogenesis.

Keywords: Epstein-Barr Virus, Alzheimer's disease, Apolipoprotein E, EBNA-1, BZLF1

5.3 Introduction

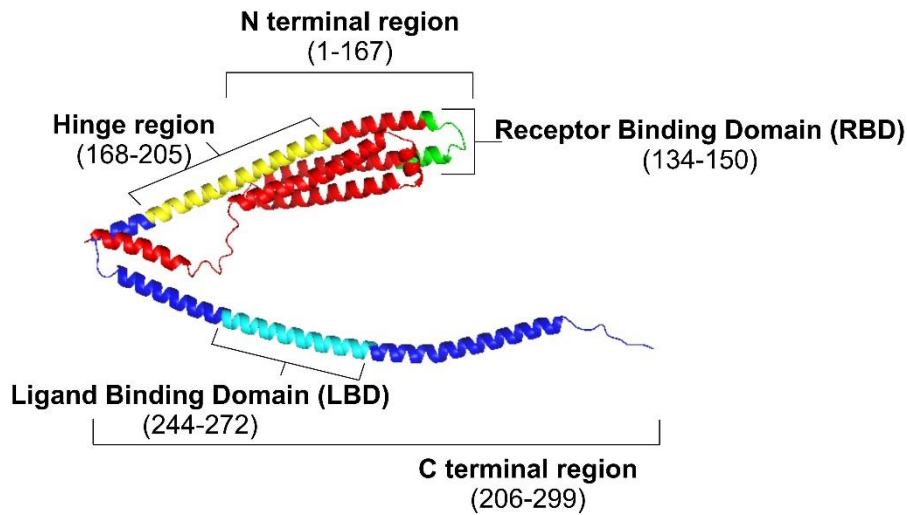
AD is the most prevalent kind of dementia caused due to progressive neurodegeneration [1]. A predictive analysis based on the data obtained from the Global Burden of Disease (GBD) study forecasted an estimated increase from 57.4 million cases globally to 152.8 million cases in mere 30 years, from 2019 to 2050 [2]. The disease presents as a gradual loss of memory, executive functions, and cognition, ultimately resulting in the loss of identity of an individual. Pathological symptoms of the disease include the deposition of proteinaceous plaques made from $A\beta_{42}$ and tau proteins in the brain, accompanied by neuroinflammation and neuronal loss leading to brain atrophy [1]. Prevalent hypotheses implicate Apolipoprotein E as a major genetic risk factor for late-onset AD in an individual, accounting for >99% of cases [3]. Physiologically, ApoE carries out lipid transport across the cell by facilitating the binding of lipoproteins or lipid complexes to specific cell-surface receptors [4]. The receptors then internalize these ApoE-bound lipids, thus assisting the ApoE-mediated lipid transportation across the cells and tissues.

The human ApoE is a 299 amino acid long protein with a molecular mass of ~34 kDa. Structurally, it comprises two domains separated by ~20-30 long stretch of

amino acids making the hinge region (residue 168-205th) [Figure 5.1 (a)]. The N-terminal domain (1-167th residue) consists of four helix-antiparallel bundles containing a receptor-binding region ranging from 134-150th amino acid residues [Figure 5.1 (a)]. The residue at the 158th position also forms a part of the NTD receptor binding region. At the same time, the C-terminal domain (206-299th residue) contains a major lipid-binding region from the 244-272nd amino acid residue [5], [6] [Figure 5.1 (a)]. Genetic polymorphism in the ApoE gives rise to three isoforms, namely, ApoE2, ApoE3, and ApoE4 [7]. These isoforms differ in amino acid residue at the 112th and 158th positions. ApoE3, considered the wild type (WT) form is the most abundant among the three variants in the global population with ~77.9% prevalence and contains a cysteine residue at 112th and arginine at 158th positions [Figure 5.1 (b)]. Whereas, ApoE2, which is linked with hyperproteinemia type III and decreased risk of AD, is the least prevalent form with ~8.4% occurrence in the global population. ApoE2 contains cysteine residues at both positions. However, the ApoE4, the most potent genetic risk factor for AD, occurs in ~13.7% of the global population and contains arginine residues at both positions [8] [Figure 5.1 (b)]. Research attempts in the last few decades have clearly shown that ApoE variants could differentially affect cholesterol-dependent modification of APP metabolism [9], enhance A β aggregation and toxicity [10], or hinder the clearance of A β peptides from the brain [11]. Interestingly, several *in-vitro* studies demonstrated that both the binding sites at NTD and CTD of the ApoE are involved in binding with A β . It was observed that the 13-17th residue of A β is involved in its interaction with the 144-148th residue at NTD as a part of the receptor-binding domain along with the 244-272nd residue forming the lipid-binding domain at the CTD [12], [13]. However, different isoforms of ApoE show varied binding affinity with A β . Several studies have demonstrated the binding efficiency of ApoE isoforms with A β in order ApoE2 \geq ApoE3>ApoE4 [14], [15]. The WT isoform ApoE3 has the optimum tendency to bind with A β . It is believed that defective clearance of A β due to improper functioning of ApoE variants could cause an increase in A β deposition and thus giving rise to AD pathology [16].

Figure 5.1

a). Structure of human Apolipoprotein E



b). Polymorphism in human Apolipoprotein E

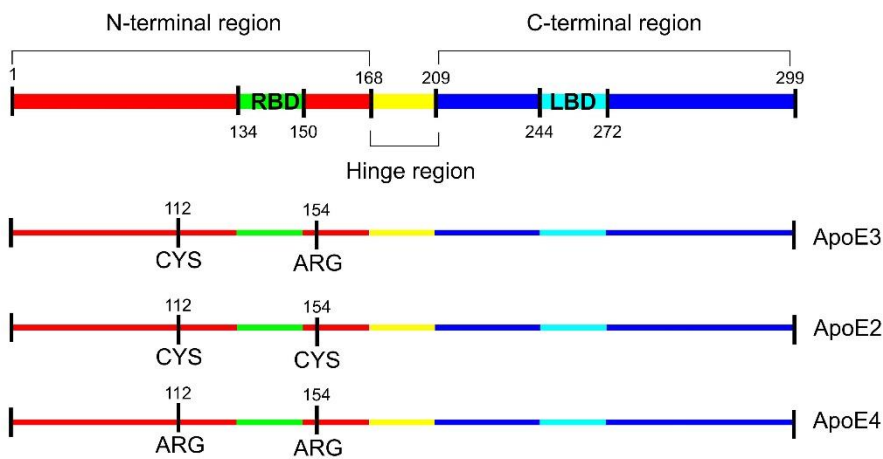


Figure 5.1 a) Structure of human Apolipoprotein E. The N-terminal region (red), ranging from the 1-167th amino acid, consists of four helices arranged in anti-parallel bundles and contains the receptor-binding domain (134-150 residue; yellow). The C-terminal region (blue), ranging from the 206-299th residue, contains a ligand-binding domain (244-272 residue; cyan). The two regions are connected by a hinge (168-205). b) Polymorphism in human ApoE. The three isoforms of human ApoE differ at 112th and 154th residue with ApoE3, the healthy isoform having a Cys at 112nd and an Arg residue at 154th position. The disease-associated isoforms ApoE2 and ApoE4, respectively, contain Cys and Arg at both positions.

Additionally, ApoE has long been known to associate with viral infections such as the Human Immunodeficiency Virus (HIV) [17], [18], Hepatitis virus-B [19], and C (HBV, HCV) [20], Herpes-Simplex virus-1 (HSV-1) [21], and recently been linked to severe acute respiratory syndrome causing Corona virus-2

(SARS-CoV2) [22]. It has been a long-standing notion that ApoE variants could influence an individual's susceptibility to chronic systemic infectious agents like HSV-1 and various other Herpesviruses, including Human Herpesvirus-4 (HHV-4) aka Epstein-Barr virus (EBV) [23]–[25]. In particular, ApoE variants have been reported to differentially facilitate neurotropic viruses such as Herpes Simplex Virus-1 (HSV-1) in establishing latency in the cerebral milieu by regulating the expression of HSV-1 immediate-early (IE) genes [26], [27]. After establishing latency, these viruses (HSV-1 and EBV) could reactivate periodically, causing cold sores and infectious mononucleosis in ~20-40% of the people. Interestingly, severe neurodegenerative consequences like AD are supposed to be associated with the reactivation of Herpesviruses [28], [29]. However, the factors responsible for developing neurodegenerative pathology in selective individuals are still under exploration.

Interestingly, seropositivity and EBV's presence in the CNS have been linked with an increased risk of developing AD in an individual [30], [31]. Although, the neurotropic potential of EBV has only been brought to light in the recent decade by Jha et al., who demonstrated successful *in-vitro* infection of EBV in neurons (SH-Sy5y, Ntera2) [32], astrocytes (U-87 MG) [33], and microglial (HMC-3) cells [34]. A recent study also implicated an EBV peptide in mediating amyloidogenesis which could probably initiate A β plaque formation [35]. Further, through various studies, it is well known that upon infecting the host cell, EBV can modulate its lipid profile through BZLF1 and transcription factors IE protein BRLF-1 [36]. Our previous study also observed significant alterations in the lipid and cholesterol metabolism by EBV infection in glial cells [34]. Notably, lipid metabolism is closely linked with neurodegeneration via ApoE [37]. It is thus suggested that viral infection in amalgamation with the genetic risk factor ApoE could create a suitable platform for AD development.

Therefore, studying the “*how and when*” of the EBV infection leading to neurodegenerative changes associated with AD is imperative. Our current investigation is based on the hypothesis that persistent EBV infection in an otherwise healthy individual could trigger AD neurodegenerative pathogenesis by interacting with ApoE3. The viral interaction with ApoE3 could interfere with ApoE-A β binding, causing modulated A β clearance, thereby influencing AD

pathogenesis. To understand the role of EBV in mediating AD development, we have investigated the interaction of various EBV proteins with the healthy variant of ApoE, i.e., ApoE3 using an *in-silico* approach. We have examined the probable protein-protein interactions (PPI) occurring at two different binding regions of ApoE3 at the NTD and CTD, respectively, with various EBV proteins.

5.4 Results and Discussion

The Herpesvirus family has been linked with neurodegeneration for decades. However, the neurotropic potential of HHV-4 (EBV) is only recently being explored in relation to neurodegenerative diseases like AD and PD. Although the association of EBV with multiple sclerosis is well studied, the virus's links with AD are still ambiguous. The viral hypothesis of AD implicates neurotropic herpesviruses such as EBV, HSV-1, and HCMV in initiating the A β deposition cascade, thus giving rise to neuroinflammatory responses resulting in neurodegeneration. It is believed that A β is seeded as a part of the innate immune response by the host to physically trap the viral pathogens and thus hinder the spread of infection and its aftereffects. Various studies reporting colocalization of viral pathogens and their transcripts with A β plaques corroborated the claim. Interestingly, amyloid plaques have also been reported to contain ApoE and cholesterol along with A β fragments, further hinting at possible links between the three: A β , ApoE, and viral pathogens. We propose that the binding of EBV proteins at Ligand Binding Domain (LBD) and Receptor Binding Domain (RBD) of ApoE3 could interfere and competitively hinder its binding to A β , thus increasing the levels of free-floating A β . This free-floating A β is more prone to forming aggregates, thereby enhancing the chances of AD pathogenesis. Therefore, we conducted the following *in-silico* analysis to test the probable interactions occurring between the healthy variant of ApoE, i.e., ApoE3, and various EBV proteins.

5.4.1 Structure modelling & Docking

To check the interaction between EBV proteins and host ApoE3 protein, we obtained the available 3D structure of concerned proteins from RCSB-PDB and modeled the rest using iTASSER. The resulting modeled structure of ApoE3-

CTD (hereon referred to as “CTD” only) was evaluated by subjecting it to the SAVES tool, which shows that the modeled structure passes through the checks for all the parameters [Figure S5. 1]. Thereafter, both the ApoE3-NTD (hereon referred to as “NTD” only) and CTD structures were docked against all the thirteen EBV proteins [Table 2]. Twenty-six possible complexes, predicted individually by HADDOCK and HDOCK, were formed between all the thirteen viral proteins and NTD and CTD, respectively. We then sorted the complexes according to geometric shape and their 3D orientation. Based on overlapping structural orientation and similar interactions involved in complex formation between the host and viral proteins, we shortlisted two EBV proteins, EBNA1 and BZLF1, as potential interactors of ApoE3 at both the NTD and CTD domains. Out of fifty-two predicted complexes, four complexes formed between NTD + EBNA1, NTD + BZLF1, CTD + EBNA1, and CTD + BZLF1 were chosen for further analysis. The HADDOCK server predicts the docked transformations based on the HADDOCK score and z-score [Table 2]. “The HADDOCK score is a weighted sum of various energy terms including van der Waals, electrostatic, desolvation, and restraint violation energies (E_{vdw} , E_{elec} , E_{desol} , and E_{air} , respectively).” Whereas “the z-score represents how many standard deviations the HADDOCK score of a given cluster is separated from the mean of all clusters, the lower the z-score is, the better.”

As predicted by HADDOCK, EBNA1 binds to NTD with the binding energy of -83.2 (+/-4.9) kJ/mol and a Z-score of -1.7. The complex formed between CTD + EBNA1 showed binding energy of -60.1 (+/-3) kJ/mol and -1.3 Z-score. The NTD + BZLF1 complex had binding energy of -41.2 (+/-0.8) kJ/mol and a Z-score of -1.3, and the CTD + BZLF1 complex showed slightly increased binding efficiency with binding energy of -90.2 (+/-11.9) kJ/mol and Z-score of -1.3 [Table 2]. Further, these complexes were subjected to molecular dynamics simulations to understand the complexes’ interaction dynamics in an environment through a fixed time interval.

Table 2 The binding energy of various EBV proteins with NTD and CTD of ApoE3 based on docking by HADDOCK and HDOCK.

EBV Proteins (PDB ID)	HADDOCK				HDOCK			
	With ApoE3-NTD		With ApoE3-CTD		With ApoE3-NTD		With ApoE3-CTD	
	Binding Energy	Z-score	Binding Energy	Z-score	Binding Energy	Ligand rmsd	Binding Energy	Ligand rmsd
1 BARF1 (2CH8)	-84.4 ± 1.0	-1.8	-89.6 ± 5.8	-2.1	-248.28	105.37	-305.75	126.41
2 BBRF1 (6LQN)	-64.1 ± 8.0	-1.6	-66.5 ± 10.1	-1.4	-238.78	38.1	-301.73	57.42
3 BCRF1 (1VLK)	-81.1 ± 3.5	-1.8	-76.6 ± 8.4	-1.7	-217.98	89.95	-276.05	114.25
4 BHRF1 (2WH6)	-105.4 ± 9.1	-2.3	-98.1 ± 5.9	-2.3	-201.94	74.36	-300.37	71.81
5 BMRF1 (2ZOL)	-88.7 ± 7.4	-1.9	-90.2 ± 11.9	-2.1	-257.27	126.89	-310.33	185.78
6 BZLF1 (2C9L)	-41.2 ± 0.8	-1.2	-98.4 ± 7.0	-1.2	-258.75	115.45	-251.59	95.37
7 dUTPase (2BSY)	-58.0 ± 10.3	-1.3	-43.8 ± 5.2	-1.3	-227.08	55	-271.36	70.64
8 EBNA1 (6VHZ)	-83.2 ± 4.9	-1.8	-83.5 ± 16.8	-1.9	-219.74	88.74	-269.73	33.26
9 gH (7CZE)	-77.9 ± 5.6	-1.7	-76.1 ± 19.0	-1.5	-234.4	81.88	-301.33	65.81
10 gL (7CZE)	-75.6 ± 3.0	-1.7	-73.6 ± 2.3	-1.4	-228.41	99.94	-357.57	61.73
11 gp42 (6LYJ)	-61.6 ± 2.9	-1.5	-60.1 ± 3.0	-1.3	-240.66	96.64	-291.07	40.91
12 p40 (3FD4)	-96.7 ± 12.0	-2	-93.4 ± 12.9	-2.3	-213.55	76.98	-284.31	86.77
13 UDG (1O6E)	-58.2 ± 12.6	-1.3	-53.1 ± 9.0	-1.3	-228.26	71.24	-272.75	70.68

BARF1 Secreted protein BARF1; BBRF1 Portal protein BBRF1; BCRF1 Viral interleukin-10 homolog; BHRF1 Apoptosis regulator BHRF1; BMRF1 DNA polymerase processivity factor BMRF1; BZLF1 Trans-activator protein BZLF1; *dUTPase* EBV- deoxyuridine 5'-triphosphate nucleotidohydrolase; EBNA1 Epstein-Barr nuclear antigen 1; gH Envelope glycoprotein H; gL Envelope glycoprotein L; gp42 Glycoprotein 42; p40 Capsid scaffolding protein 40; UDG Uracil-DNA glycosylase.

5.4.2 Trajectory Analysis of MD Simulations

To understand the binding and structural dynamics of ApoE3 in complex with EBV proteins, we performed molecular dynamics simulations for 100 ns of all the four systems mentioned above. The RMSD values of the complexes revealed the stability and convergence of each system compared to their initial conformations. The entire trajectory of 100ns was divided into equal intervals of 20ps, and RMSD values were measured for each segment. The RMSD of NTD + EBNA1 and NTD + BZLF1 complexes remained comparatively more stable, around ~ 0.5 Å and 1.1 Å, respectively, throughout the 100ns simulation. However, the CTD + EBNA1 and CTD + BZLF1 stabilized only after approximately 30 and 25ns, with average RMSD values of 1.8 Å and 2.1 Å, respectively [Figure 5.2 (a)]. The average deviations in NTD were 0.3 Å in both the complexes, whereas the CTD showed deviations of ~ 2.5 Å [Figure 5.2 (b)]. Whereas EBV proteins EBNA1 and BZLF1 in the complex individually showed average deviations of 0.2 Å and ~ 1 Å, respectively [Figure 5.2 (c)].

Figure 5.2

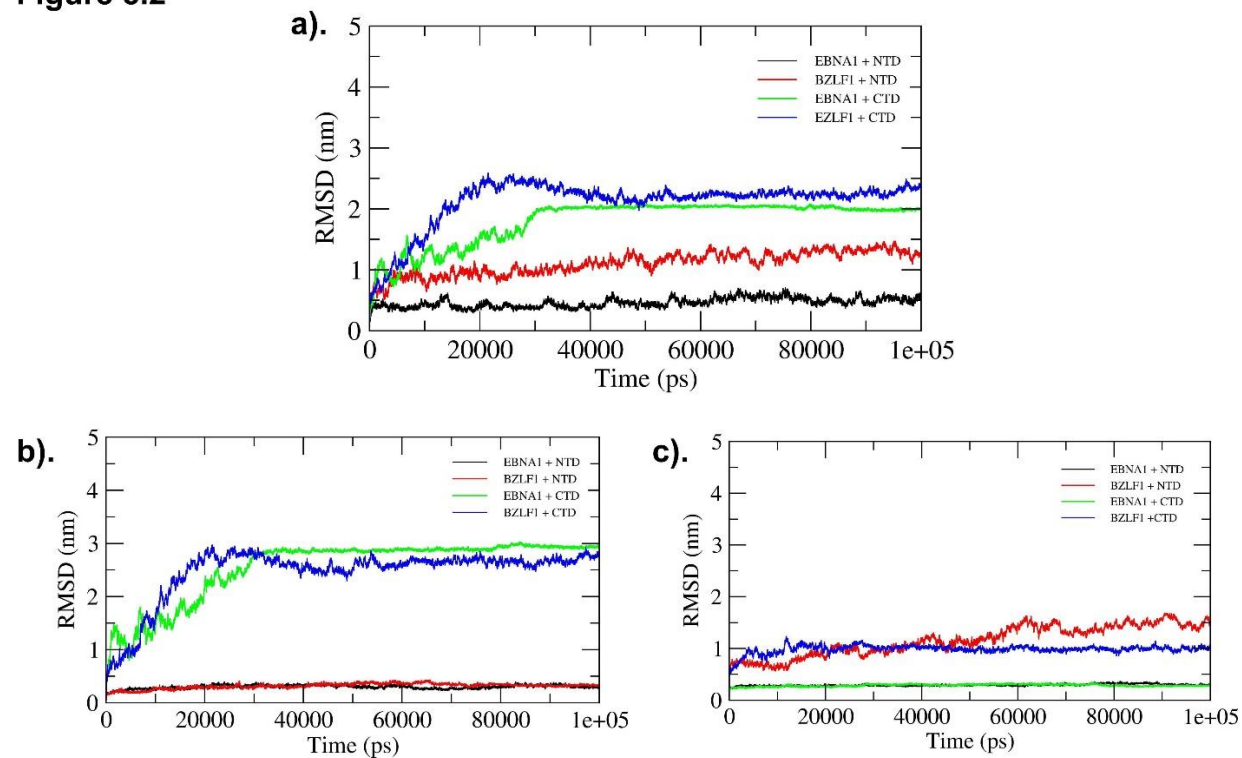


Figure 5.2 . Root mean square deviations (RMSD) in the bound complexes throughout MD simulation (100ns). a) RMSD of the entire bound complexes, b) RMSD of the ApoE (NTD/CTD) in the bound complex, and c) RMSD of the EBV proteins (EBNA1/BZLF1) in the bound complex.

Further, to study the flexibility of the specific residues around their average positions during simulations, the RMSF of protein backbone atoms for each system was calculated. We identified residues in the regions around 164-6 of NTD [Figure 5.3 (a)], 123-7 of CTD [Figure 5.3 (b)], 471-5 of EBNA1 [Figure 5.3 (c)]; and 426-30 of BZLF1 [Figure 5.3 (d)], showing highest fluctuations in the respective complexes.

Figure 5.3

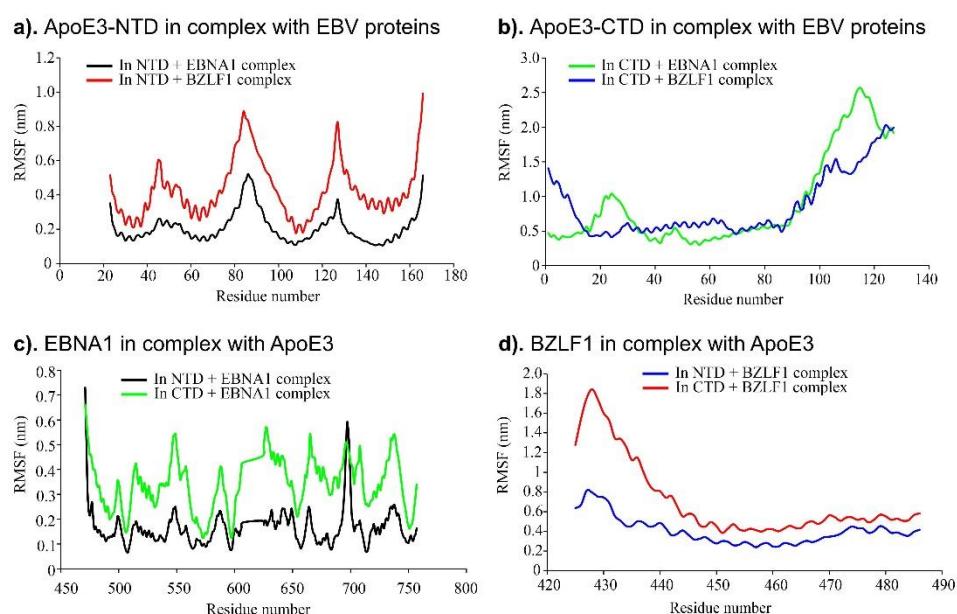


Figure 5.3 Root mean square fluctuations (RMSF) plots of respective chains in the bound complexes. a) RMSF of various residues of a) NTD in complex with EBNA1 and BZLF1, b) CTD in complex with EBNA1 and BZLF1, c) EBNA1 in complex with NTD and CTD, d) BZLF1 in complex with NTD and CTD of ApoE3.

For estimating the structural compactness of the system, the Rg was calculated. The complexes NTD + EBNA1, NTD + BZLF1, and CTD + BZLF1 showed similar pattern with average Rg values ~ 2.8 Å. However, the average Rg for CTD + EBNA1 complex was observed to be comparatively lower, with a value of ~ 2.4 Å [Figure 5.4 (a)]. To ascertain the compactness of the complexes formed further, SASA was also determined individually for each of the complexes. The average SASA values for EBNA1 in bound to ApoE3 at NTD and CTD ranged from ~ 90 - 95 nm², and for the BZLF1, the value was observed to be between 74 - 78 nm². Lesser deviation in the SASA values of the complexes throughout the simulation reflected that the structural compactness of these complexes is maintained [Figure 5.4 (b)]. The decreasing value of Rg in combination with

SASA values indicates that as the complexes enter into equilibrium through the simulation time, they tend to become more compact.

Figure 5.4

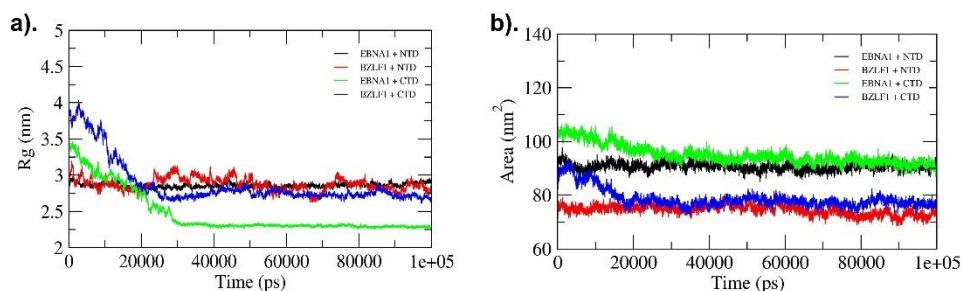


Figure 5.4 a) Radius of gyration (Rg), b) Solvent accessible surface area (SASA) plots.

5.4.3 Binding Free Energy

As calculated by MM-PBSA, the binding energy of all the complexes is listed in [Table 3]. It was observed that complex formation between EBV proteins (EBNA1 and BZLF1) at CTD of the ApoE3 was more energetically favorable, as reflected by the highly negative binding energy of the complexes. The complex formed between CTD and EBNA1 showed binding energy of -1307.95 kJ/mol, whereas the binding energy of the complex formed with BZLF1 had binding energy of -1742.77 kJ/mol. Electrostatic energy contributed the most, followed by van der Waal's energy in forming both the complexes.

However, the binding energy of the EBV proteins in complex with NTD of ApoE3 was comparatively way higher, indicating that their formation is energetically less favored. The NTD + EBNA1 complex and NTD + BZLF1 complex showed binding energy of approximately -35 kJ/mol and -40 kJ/mol, respectively.

Table 3. Binding free energy decomposition

Protein-Protein complexes	van der Waal energy	Electrostatic energy	Polar solvation energy	SASA energy	Binding energy
EBNA1 + NTD	-258.961	-680.593	939.931	-35.227	-34.848
BZLF1 + NTD	-159.783	-118.708	256.527	-18.186	-40.149
EBNA1 + CTD	-632.575	-2438.544	1846.063	-82.89	-1307.947
BZLF1 + CTD	-537.615	-3655.62	2524.269	-73.806	-1742.772

5.4.4 Hydrogen Bond Analysis

Further, hydrogen bond (H-bond) formations were investigated to corroborate the energetic analysis of the binding interactions between the host and viral proteins. The complexes NTD + EBNA1, CTD + EBNA1, and CTD + BZLF1 showed an increase in hydrogen bonding compared to their initial state through the simulation time, with an average of approximately 8, 14, and 21 H-bonds, respectively [Figure 5.5]. However, a decrease in H-bond interactions was observed in the complex formed between NTD + BZLF1 with average H-bonds ~2 throughout the simulation period of 100 ns. Percentage occupancy of the topmost H-bonds throughout the simulation was in the order of complex CTD+EBNA1 > CTD+BZLF1 > NTD+EBNA1 > NTD+BZLF1. In the case of the complex NTD + EBNA1 complex, the primary H-bonding residues are Arg142, Arg145 from the NTD side, and Arg486 from the EBNA1 side. Similarly, for the NTD + BZLF1 complex, the residues observed in H-bonding are Arg 114, Arg136, Ser139, and Arg142 from the NTD side, and BZLF1 contributed through Arg474. For the CTD + EBNA-1 complex, the CTD side contributed Arg6, Arg56 along with Gln471, and Arg491 of EBNA-1 in H-bonding. Further, the residues involved in H-bonding within the CTD + BZLF1 complex were Arg45 and Arg52 from the CTD side, along with Arg179, Arg183, Arg187, Arg190, and Arg451 from the BZLF1. Interestingly, the region involved in binding both the EBV proteins at either CTD or NTD were almost overlapping.

Figure 5.5

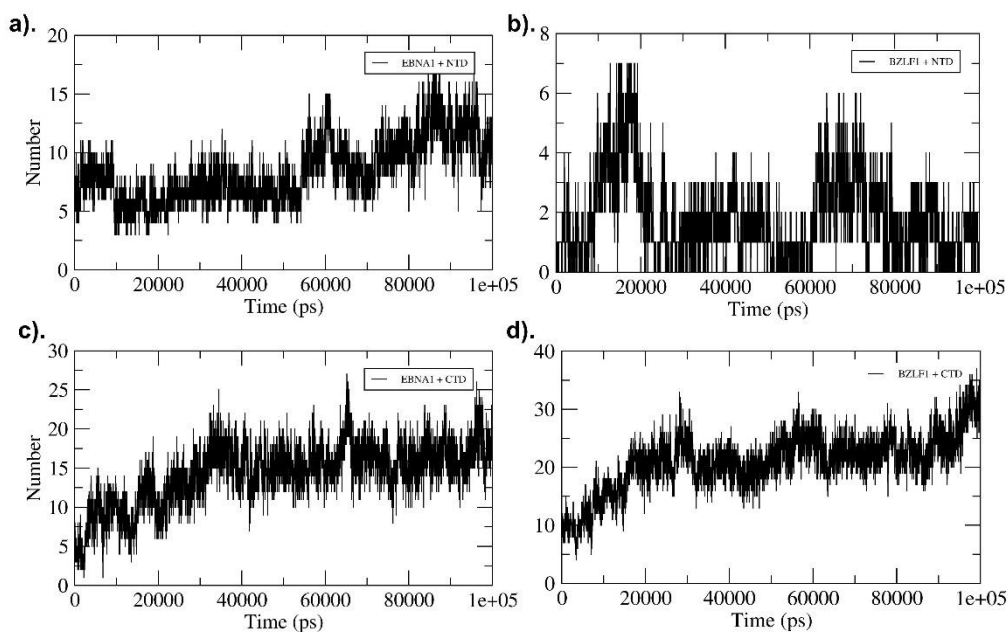


Figure 5.5 Hydrogen Bond Analysis of the respective complexes. The average number of H-bonds in complex a) EBNA1 + NTD were 8, b) BZLF1 + NTD were 2, c) EBNA1 + CTD were 14, and d) BZLF1 + CTD were 21 throughout the duration of MD simulation.

5.5 Conclusions

The involvement of EBV in AD development is still debated in the scientific community. However, recent evidence suggests that latent EBV infection could play a role in AD pathogenesis. Still, the current knowledge about EBV's involvement in mediating AD lacks mechanistic understanding. Besides, an interesting report linking the two implicates Apolipoprotein-E, a well-known genetic risk factor for AD, as a possible element modulating the outcome of EBV infection in an individual. Interestingly, ApoE is also involved in the clearance of amyloid- β fragments from the brain, and its defective functioning is linked with disease development. Additionally, several population-based studies have suggested that persistent EBV infection and its timely reactivation increase AD development chances in individuals at later stages of life. Nonetheless, the precise interplay happening between ApoE and EBV is unexplored.

Therefore, in this study, we attempted to examine the possibility of interaction between ApoE and various EBV proteins. For this analysis, we chose to examine

the interactions of EBV proteins with ApoE3, the healthy isoform. The current investigation evaluates the interaction of various viral proteins at both the binding sites on ApoE: RBD at the N-terminal and LBD at the C-terminal regions. Our analysis showed that EBV proteins BZLF1 and EBNA-1 have a higher affinity toward the ligand-binding region at the CTD of ApoE3. Based on our findings, we propose that this interaction of EBV proteins might interfere with ApoE's A β binding capability and hinder its normal functioning. Defective A β clearance from the brain by ApoE3 could increase the chances of plaque deposition, thereby initiating AD pathogenesis. For the first time, our study suggests a novel interaction between EBV and the host protein strongly implicated in AD development, i.e., ApoE. The current investigation opens up novel avenues of exploration to determine the role of EBV, which has been so far considered only a bystander in AD development.

5.6 Materials and methods

5.6.1 3D structure retrieval and preparation of host and viral proteins

The X-ray crystallographic structure of human apolipoprotein E: NTD from 41-184th amino acid (PDB ID: 1LPE) of 2.5 Å resolution was obtained from the RCSB-PDB database. Further, for obtaining the CTD structure of ApoE3, the FASTA sequence (UniProt ID: 00001124AF) was retrieved from UniProt. The structure of CTD, ranging from the 192-299th amino acid, was built using the AF-P02649-F1 as a template through the iTASSER. Before proceeding, the homology model validation was carried out using the SAVES v.6.0 server (SAVES v6.0 – DOE-MBI Structure Lab UCLA). The 3D structures of various viral proteins were obtained from the RCSB-PDB database. The details of the same are listed in [Table 2].

5.6.2 Molecular Docking

As determined by existing literature, the docking of EBV proteins at ApoE3 was done at both the binding sites located at 136-150th residue on NTD and 244-278th residues at CTD. *Ab-initio* docking-based tools, HADDOCK 2.4 (<https://wenmr.science.uu.nl/haddock2.4/>) and HDOCK

(<http://hdock.phys.hust.edu.cn/>) were utilized for the purpose. The 3D structure of various EBV proteins was pre-processed for submitting to HADDOCK using PDBTOOLS (<https://wenmr.science.uu.nl/pdbtools/>).

5.6.3 Molecular Dynamic Simulations

An MD simulation study was done to validate the stability of all the docked complexes. MD simulation was performed for 100ns with Gromacs 4.6 [38], [39]. Topology files of macromolecules were prepared using the Amber99sb-ildn force field and ANTECHAMBER module of AMBER Tools [40], [41]. Initially, docked complexes were placed in the center of a cubic box, having a distance of 1.0 Å between the protein and edge of the simulation box. Further, systems were solvated with TIP3P [42] explicit water molecules. Systems were neutralized by adding the required numbers of CL or NA ions. Each system was minimized by using the steepest descent approach. Further NVT and NPT were performed for 2ns each to equilibrate the systems for constant volume, pressure (1 atm), and temperature (300K). Generated trajectories were used for further analysis using Xmgrace [43].

5.7 References

- [1] S. Karantzoulis and J. E. Galvin, “Distinguishing Alzheimer’s disease from other major forms of dementia,” *Expert Rev. Neurother.*, vol. 11, no. 11, pp. 1579–1591, Nov. 2011, doi: 10.1586/ern.11.155.
- [2] E. Nichols *et al.*, “Estimation of the global prevalence of dementia in 2019 and forecasted prevalence in 2050: an analysis for the Global Burden of Disease Study 2019,” *Lancet Public Health*, vol. 7, no. 2, pp. e105–e125, Feb. 2022, doi: 10.1016/S2468-2667(21)00249-8.
- [3] K. H. Weisgraber and R. W. Mahley, “Human apolipoprotein E: the Alzheimer’s disease connection,” *FASEB J.*, vol. 10, no. 13, pp. 1485–1494, Nov. 1996, doi: 10.1096/fasebj.10.13.8940294.
- [4] J. Kim, J. M. Basak, and D. M. Holtzman, “The Role of Apolipoprotein E in Alzheimer’s Disease,” *Neuron*, vol. 63, no. 3, pp. 287–303, Aug. 2009, doi: 10.1016/j.neuron.2009.06.026.

- [5] J. Chen, Q. Li, and J. Wang, "Topology of human apolipoprotein E3 uniquely regulates its diverse biological functions," *Proc. Natl. Acad. Sci. U. S. A.*, vol. 108, no. 36, pp. 14813–14818, Sep. 2011, doi: 10.1073/pnas.1106420108.
- [6] D. M. Hatters, C. A. Peters-Libeu, and K. H. Weisgraber, "Apolipoprotein E structure: insights into function," *Trends Biochem. Sci.*, vol. 31, no. 8, pp. 445–454, Aug. 2006, doi: 10.1016/j.tibs.2006.06.008.
- [7] H. K. Das, J. McPherson, G. A. Bruns, S. K. Karathanasis, and J. L. Breslow, "Isolation, characterization, and mapping to chromosome 19 of the human apolipoprotein E gene.," *J. Biol. Chem.*, vol. 260, no. 10, pp. 6240–6247, May 1985, doi: 10.1016/S0021-9258(18)88963-3.
- [8] P. P. Singh, M. Singh, and S. S. Mastana, "APOE distribution in world populations with new data from India and the UK," *Ann. Hum. Biol.*, vol. 33, no. 3, pp. 279–308, Jan. 2006, doi: 10.1080/03014460600594513.
- [9] A. R. Koudinov, T. T. Berezov, and N. V. Koudinova, "Alzheimer's amyloid beta and lipid metabolism: a missing link?," *FASEB J.*, vol. 12, no. 12, pp. 1097–1099, Sep. 1998, doi: 10.1096/fasebj.12.12.1097.
- [10] D. M. Holtzman, "Role of apoE/A β Interactions in the Pathogenesis of Alzheimer's Disease and Cerebral Amyloid Angiopathy," *J. Mol. Neurosci.*, vol. 17, no. 2, pp. 147–155, 2001, doi: 10.1385/JMN:17:2:147.
- [11] D.-S. Yang *et al.*, "Apolipoprotein E promotes the binding and uptake of β -amyloid into Chinese hamster ovary cells in an isoform-specific manner," *Neuroscience*, vol. 90, no. 4, pp. 1217–1226, Jun. 1999, doi: 10.1016/S0306-4522(98)00561-2.
- [12] S. Deroo *et al.*, "Chemical Cross-Linking/Mass Spectrometry Maps the Amyloid β Peptide Binding Region on Both Apolipoprotein E Domains," *ACS Chem. Biol.*, vol. 10, no. 4, pp. 1010–1016, Apr. 2015, doi: 10.1021/cb500994j.
- [13] Q. Liu *et al.*, "Mapping ApoE/A β binding regions to guide inhibitor discovery," *Mol. Biosyst.*, vol. 7, no. 5, p. 1693, 2011, doi: 10.1039/c1mb05019b.
- [14] J. Petrlova *et al.*, "A differential association of Apolipoprotein E isoforms with the amyloid- β oligomer in solution: Association of apoE Isoforms with a TOAC-Ab," *Proteins Struct. Funct. Bioinforma.*, vol. 79, no. 2, pp. 402–416, Feb. 2011, doi: 10.1002/prot.22891.

- [15] T. Kanekiyo, H. Xu, and G. Bu, "ApoE and A β in Alzheimer's Disease: Accidental Encounters or Partners?," *Neuron*, vol. 81, no. 4, pp. 740–754, Feb. 2014, doi: 10.1016/j.neuron.2014.01.045.
- [16] K. R. Wildsmith, M. Holley, J. C. Savage, R. Skerrett, and G. E. Landreth, "Evidence for impaired amyloid β clearance in Alzheimer's disease," *Alzheimers Res. Ther.*, vol. 5, no. 4, p. 33, 2013, doi: 10.1186/alzrt187.
- [17] R. Siddiqui *et al.*, "Apolipoprotein E is an HIV-1-inducible inhibitor of viral production and infectivity in macrophages," *PLOS Pathog.*, vol. 14, no. 11, p. e1007372, Nov. 2018, doi: 10.1371/journal.ppat.1007372.
- [18] N. Khan, G. Datta, J. D. Geiger, and X. Chen, "Apolipoprotein E isoform dependently affects Tat-mediated HIV-1 LTR transactivation," *J. Neuroinflammation*, vol. 15, no. 1, p. 91, Dec. 2018, doi: 10.1186/s12974-018-1129-1.
- [19] L. Qiao and G. G. Luo, "Human apolipoprotein E promotes hepatitis B virus infection and production," *PLoS Pathog.*, vol. 15, no. 8, p. e1007874, Aug. 2019, doi: 10.1371/journal.ppat.1007874.
- [20] J. Jiang, W. Cun, X. Wu, Q. Shi, H. Tang, and G. Luo, "Hepatitis C Virus Attachment Mediated by Apolipoprotein E Binding to Cell Surface Heparan Sulfate," *J. Virol.*, vol. 86, no. 13, pp. 7256–7267, Jul. 2012, doi: 10.1128/JVI.07222-11.
- [21] M. Linard, L. Letenneur, I. Garrigue, A. Doize, J.-F. Dartigues, and C. Helmer, "Interaction between *APOE4* and herpes simplex virus type 1 in Alzheimer's disease," *Alzheimers Dement.*, vol. 16, no. 1, pp. 200–208, Jan. 2020, doi: 10.1002/alz.12008.
- [22] S. N. Kurki *et al.*, "APOE ϵ 4 associates with increased risk of severe COVID-19, cerebral microhaemorrhages and post-COVID mental fatigue: a Finnish biobank, autopsy and clinical study," *Acta Neuropathol. Commun.*, vol. 9, no. 1, p. 199, Dec. 2021, doi: 10.1186/s40478-021-01302-7.
- [23] M. A. Wozniak *et al.*, "Does apolipoprotein E determine outcome of infection by varicella zoster virus and by Epstein-Barr virus?," *Eur. J. Hum. Genet.*, vol. 15, no. 6, pp. 672–678, Jun. 2007, doi: 10.1038/sj.ejhg.5201812.
- [24] LONG Yan, ZUO Li, and Li Guang-rong, "Influences of EBV infection and single nucleotide polymorphism of apolipoprotein E gene on Alzheimer's

disease,” *Chin. J. Public Health*, vol. 24, no. 5, pp. 573–574, 2008, doi: 10.11847/zgggws2008-24-05-30.

[25] J. S. Burgos, C. Ramirez, I. Sastre, M. J. Bullido, and F. Valdivieso, “ApoE4 is more efficient than E3 in brain access by herpes simplex virus type 1;,” *NeuroReport*, vol. 14, no. 14, pp. 1825–1827, Oct. 2003, doi: 10.1097/00001756-200310060-00013.

[26] J. S. Burgos, C. Ramirez, I. Sastre, and F. Valdivieso, “Effect of Apolipoprotein E on the Cerebral Load of Latent Herpes Simplex Virus Type 1 DNA,” *J. Virol.*, vol. 80, no. 11, pp. 5383–5387, Jun. 2006, doi: 10.1128/JVI.00006-06.

[27] J. S. Burgos and F. Valdivieso, “Understanding the relationship between ApoE and HSV-1 and its possible significance in Alzheimer’s disease,” *Future Virol.*, vol. 2, no. 3, pp. 239–242, May 2007, doi: 10.2217/17460794.2.3.239.

[28] J. Hogestyn, D. Mock, and M. Mayer-Proschel, “Contributions of neurotropic human herpesviruses herpes simplex virus 1 and human herpesvirus 6 to neurodegenerative disease pathology,” *Neural Regen. Res.*, vol. 13, no. 2, p. 211, 2018, doi: 10.4103/1673-5374.226380.

[29] N. Zhang, Y. Zuo, L. Jiang, Y. Peng, X. Huang, and L. Zuo, “Epstein-Barr Virus and Neurological Diseases,” *Front. Mol. Biosci.*, vol. 8, p. 816098, Jan. 2022, doi: 10.3389/fmolb.2021.816098.

[30] I. Carbone *et al.*, “Herpes virus in Alzheimer’s disease: relation to progression of the disease,” *Neurobiol. Aging*, vol. 35, no. 1, pp. 122–129, Jan. 2014, doi: 10.1016/j.neurobiolaging.2013.06.024.

[31] M. A. Allnutt *et al.*, “Human Herpesvirus 6 Detection in Alzheimer’s Disease Cases and Controls across Multiple Cohorts,” *Neuron*, vol. 105, no. 6, pp. 1027-1035.e2, Mar. 2020, doi: 10.1016/j.neuron.2019.12.031.

[32] H. C. Jha *et al.*, “Gammaherpesvirus Infection of Human Neuronal Cells,” *mBio*, vol. 6, no. 6, Dec. 2015, doi: 10.1128/mBio.01844-15.

[33] S. Jakhmola and H. C. Jha, “Glial cell response to Epstein-Barr Virus infection: A plausible contribution to virus-associated inflammatory reactions in the brain,” *Virology*, vol. 559, pp. 182–195, Jul. 2021, doi: 10.1016/j.virol.2021.04.005.

[34] D. Tiwari, S. Jakhmola, D. K. Pathak, R. Kumar, and H. C. Jha, “Temporal *In Vitro* Raman Spectroscopy for Monitoring Replication Kinetics of

Epstein–Barr Virus Infection in Glial Cells,” *ACS Omega*, vol. 5, no. 45, pp. 29547–29560, Nov. 2020, doi: 10.1021/acsomega.0c04525.

[35] D. Tiwari *et al.*, “Indication of Neurodegenerative Cascade Initiation by Amyloid-like Aggregate-Forming EBV Proteins and Peptide in Alzheimer’s Disease,” *ACS Chem. Neurosci.*, vol. 12, no. 20, pp. 3957–3967, Oct. 2021, doi: 10.1021/acchemneuro.1c00584.

[36] Y. Li, J. Webster-Cyriaque, C. C. Tomlinson, M. Yohe, and S. Kenney, “Fatty acid synthase expression is induced by the Epstein-Barr virus immediate-early protein BRLF1 and is required for lytic viral gene expression,” *J. Virol.*, vol. 78, no. 8, pp. 4197–4206, Apr. 2004, doi: 10.1128/jvi.78.8.4197-4206.2004.

[37] E. Hone, F. Lim, and I. J. Martins, “Fat and Lipid Metabolism and the Involvement of Apolipoprotein E in Alzheimer’s Disease,” in *Neurodegeneration and Alzheimer’s Disease*, R. N. Martins, C. S. Brennan, W. M. A. D. B. Fernando, M. A. Brennan, and S. J. Fuller, Eds. Chichester, UK: John Wiley & Sons, Ltd, 2019, pp. 189–231. doi: 10.1002/9781119356752.ch7.

[38] B. Hess, C. Kutzner, D. van der Spoel, and E. Lindahl, “GROMACS 4: Algorithms for Highly Efficient, Load-Balanced, and Scalable Molecular Simulation,” *J. Chem. Theory Comput.*, vol. 4, no. 3, pp. 435–447, Mar. 2008, doi: 10.1021/ct700301q.

[39] D. Van Der Spoel, E. Lindahl, B. Hess, G. Groenhof, A. E. Mark, and H. J. C. Berendsen, “GROMACS: Fast, flexible, and free,” *J. Comput. Chem.*, vol. 26, no. 16, pp. 1701–1718, Dec. 2005, doi: 10.1002/jcc.20291.

[40] K. Lindorff-Larsen *et al.*, “Improved side-chain torsion potentials for the Amber ff99SB protein force field: Improved Protein Side-Chain Potentials,” *Proteins Struct. Funct. Bioinforma.*, vol. 78, no. 8, pp. 1950–1958, Jun. 2010, doi: 10.1002/prot.22711.

[41] A. W. Sousa da Silva and W. F. Vranken, “ACPYPE - AnteChamber PYthon Parser interfacE,” *BMC Res. Notes*, vol. 5, no. 1, p. 367, Dec. 2012, doi: 10.1186/1756-0500-5-367.

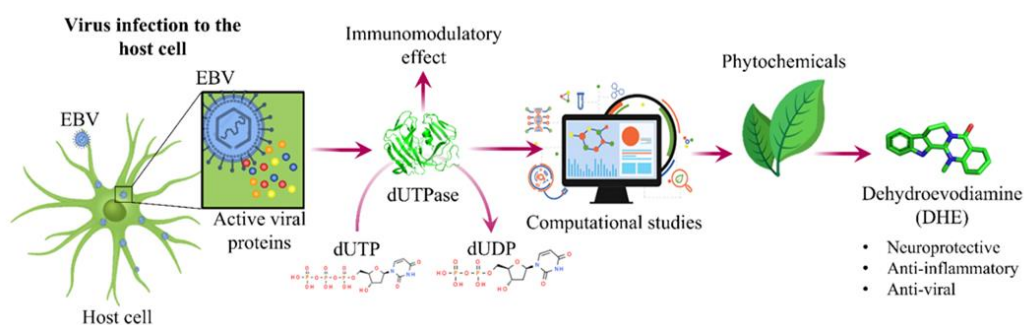
[42] W. L. Jorgensen, J. Chandrasekhar, J. D. Madura, R. W. Impey, and M. L. Klein, “Comparison of simple potential functions for simulating liquid water,” *J. Chem. Phys.*, vol. 79, no. 2, pp. 926–935, Jul. 1983, doi: 10.1063/1.445869.

[43] S. S. Soman, K. C. Sivakumar, and E. Sreekumar, "Molecular dynamics simulation studies and *in-vitro* site directed mutagenesis of avian beta-defensin Apl_AvBD2," *BMC Bioinformatics*, vol. 11 Suppl 1, p. S7, Jan. 2010, doi: 10.1186/1471-2105-11-S1-S

Chapter 6

Targeting Epstein-Barr virus *dUTPase*, an immunomodulatory protein using anti-viral, anti-inflammatory and neuroprotective phytochemicals

6.1 Graphical abstract



6.2 Abstract

Although primary infection of EBV is generally considered non-lethal, viral reactivation is often associated with fatal outcomes such as oncogenesis and various neurological pathologies. Regardless, there are no FDA-approved therapeutics available to treat this omnipresent viral infection. The current investigation utilized phytochemicals to target viral maintenance and reactivation at the early stages by inhibiting the functioning of viral deoxyuridine-triphosphatase (*dUTPase*). The EBV-*dUTPase* protein is essential for the maintenance of nucleotide balance and thus, plays a vital role in the viral replication cycle. Additionally, the protein has been shown to induce neuromodulatory/neuroinflammatory effects. To selectively target the protein activity and thereby possibly altering its after effects, we utilized a virtual screening approach and screened 45 phytochemicals reported to have anti-viral, anti-inflammatory, and neuroprotective properties. The analysis revealed Kaempferol-3-rutinoside (K3R), Mangiferin (MANG), Sarsasapogenin (SARA), and Dehydroevodiamine (DHED) bound to the target protein with high affinity. In-silico ADMET and Lipinski's rule analysis predicted favorable

druggability of DHED among all the phytochemical candidates. Further, we corroborated our findings by molecular dynamic simulation and binding affinity estimation by the molecular mechanics Poisson-Boltzmann surface area (MM-PBSA) algorithm. Our outcomes ascertained a stable binding of DHED to EBV-*dUTPase* primarily through electrostatic interactions. We identified that the protein-ligand binding involves the region around His71, which is previously reported as a potent drug target site. Interestingly, DHED is an alkaloid compound known to have applications as anti-dementia medication. Conclusively, the phytochemical DHED showed a promising future as a drug development candidate against EBV-*dUTPase*.

Keywords: Epstein-Barr virus (EBV), Deoxyuridine-triphosphatase (*dUTPase*), Dehydroevodiamine (DHE), Molecular docking study, MD simulation.

6.3 Introduction

EBV is a ubiquitous pathogen primarily responsible for causing IM in the teenage population. The virus establishes latent infection in >95% of the world population and resides asymptotically in the host's B-cells [1]. However, recent studies have indicated its multitrophic potential towards neurons, glial cells, etc. After successfully establishing latent infection in a cell, the virus may reactivate multiple times during a person's lifespan resulting in abortive/lytic replication. The lytic replication cycle of the virus leads to the production of progeny virions, thus helping in the transmission and maintenance of persistent infection. Reactivation of EBV at later stages of life is associated with various pathologies such as Burkitt's lymphoma (BL), nasopharyngeal carcinoma (NPC), lymphoproliferative disorders, etc. [2]. Interestingly, clinical reports have also suggested the role of EBV in various NDDs, including AD [3]–[5]. In particular, the genetic material of EBV and anti-viral antibodies against the virus has been prevalent in the CSF samples of patients suffering from NDs [5]. Our earlier study successfully established EBV infection in neural cells (namely neurons, astroglia, and microglial cells) *in-vitro*, thus corroborating the

neurovirulent properties of the virus [6]–[8]. However, the mechanistic details of the EBV infection leading to neurodegeneration are still elusive.

Upon establishing infection successfully, EBV expresses and employs multiple proteins to hijack and drive the cellular machinery for its replication. One of the crucial proteins involved in this process is a 278 aa long the viral *dUTPase* (deoxyuridine triphosphatase) encoded by the BLLF3 gene [9]. The viral protein is expressed early during lytic replication [10], [11]. It catalyzes the conversion of dUTP (deoxyuridine triphosphate) to dUDP (deoxyuridine diphosphate), thus helping in the maintenance of the dUTP/dTTP ratio and decreasing the misincorporation of uracil into newly synthesized DNA [12]. The enzyme *dUTPases* are classified under three families based on their oligomerization state and specificity for dUTP: homotrimeric, homodimeric, and monomeric [13]. The mammalian and avian herpesviruses like HSV, HCMV, Varicella-Zoster virus (VZV), and EBV exclusively encode for the monomeric form of the enzyme [13]. The monomeric *dUTPases* are believed to have derived from trimeric *dUTPases* by gene duplication. Despite different subunit organizations from the trimeric forms, the catalytic mechanism of the monomeric form of the enzyme remains unchanged. A study of the crystal structure of the EBV-*dUTPase* in complex with a non-hydrolyzable substrate analog (α , β -imino-dUTP) or the product dUMP revealed that its single catalytic site mimics that of homotrimeric *dUTPases* [14]. The catalytic site of the monomeric EBV-*dUTPase* is made up of three domains comprising five highly conserved motifs (I, II, III, IV, and V), as depicted in [Error! Reference source not found. [13]. These three domains are structurally and functionally similar to one of the three active sites of the trimeric *dUTPases*. Domain I and II form the *dUTPase* fold, while domain III contributes only a little secondary structure to form a unique active site. The catalytic site of EBV-*dUTPase* is formed at the interface of domains I and II containing motifs I-IV, whereas motif V is disordered. Domain I contribute motif III, while motifs I, II, and IV are contributed by domain II [14].

Figure 6.1

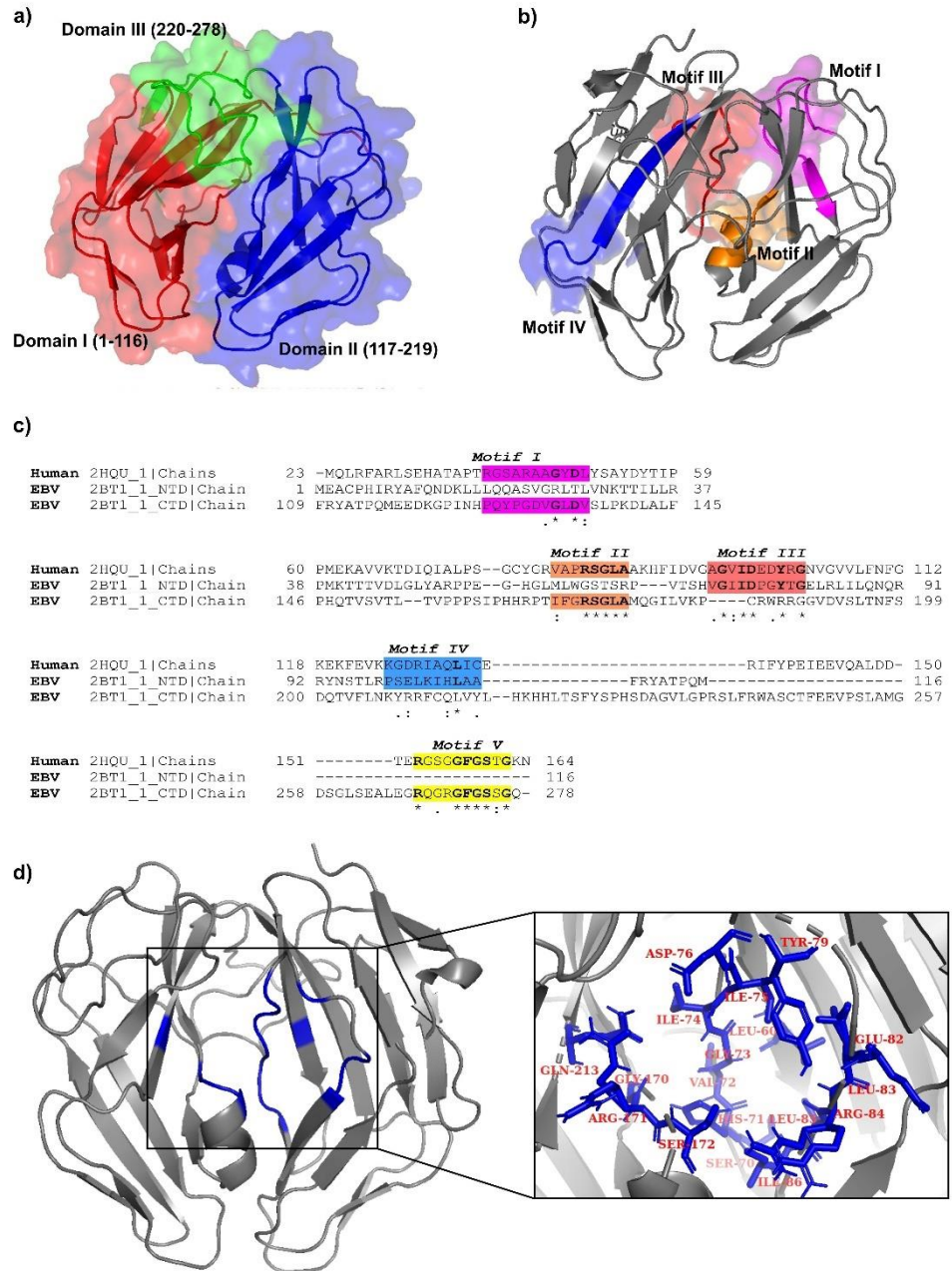


Figure 6.1 Structural details of the EBV-dUTPase. a) Location and orientation of the domains I (1-116), II (117-219), and III (220-278) forming the secondary structure of EBV-dUTPase is shown in red, blue, and green color, respectively. b) The conserved motifs I (magenta), II (orange), III (red), and IV (blue) constitute the active site of the EBV-dUTPase. Due to its flexibility and disordered structure, motif V is generally invisible. c) The sequence alignment of the human dUTPase with that of EBV. The location of each of the motifs I, II, III, IV, and V is highlighted respectively in magenta, yellow, cyan, green, and grey. d) The active site of EBV-dUTPase is depicted in blue residues; inset: The residues involved in the active site formation are shown in red.

Further, owing to its role in nucleotide metabolism, inhibition of *dUTPases* is hypothesized to result in uracil misincorporation-induced double-stranded DNA

breaks in the viral genome, thereby hindering the viral replication cycle. A report describing reduced viral replication of murine gammaherpesvirus (MHV-68) lacking its viral *dUTPase* corroborates the claim [15]. Clinically, the presence of EBV-*dUTPase* has been detected in the lesions from epithelial layers of oral hairy leukoplakia (HL) in the lymphocytes from the tonsils of IM patients and NPC tissue. Apart from playing a role in maintaining the nucleotide balance, the viral *dUTPase* is also reported to play immunomodulatory functions in the host suffering from encephalitis like neurological ailments [16], [17]. Recent studies have shown that EBV-*dUTPase* could induce inflammation via NF- κ B activation through TLR2 [18]. The study demonstrated that dendritic cells (DCs) and monocytes/macrophages serve as primary cellular targets for EBV-*dUTPase*. A study by Ariza *et al.* demonstrated that chemically induced Raji cells produce exosomes containing EBV-*dUTPase* that can induce NF- κ B activation and secretion of pro-inflammatory cytokines from DCs and PBMCs [19]. William *et al.* showed that mRNA expression of pro-inflammatory cytokines such as IL-1b and IL-6 increased rapidly upon treating human cerebral microvascular endothelial cells with EBV-*dUTPase* compared to the vehicle-treated control. Interestingly, a parallel increase in NF- κ B and TLR-2 was also observed in these cells. Similarly, treatment of EBV-*dUTPase* to microglial cells resulted in an increase in the mRNA expression of IL-1b and IL-6 [20] and induced upregulation of TNF α , culminating at 2-hour post-treatment [21]. Furthermore, it was observed that in normally dividing cells, cellular *dUTPase* would be hijacked by the EBV to carry out the function. However, as neurons are non-dividing cells, viral *dUTPase* would be functional, and therefore targeting the viral *dUTPase* in neurons would be more feasible [22].

Thus, to target the EBV infection-mediated neuropathologies, we sought to target EBV-*dUTPase*, by using phytochemicals reported to have anti-inflammatory, anti-viral, and/or neuroprotective effects. Plants contain a plethora of medicinally potent compounds that can be exploited for their low toxicity and susceptibility to microbial resistance. The compounds with the properties mentioned above taken under investigation in this study are listed in [Table]. In this current study, about 45 compounds were selected based on their known anti-herpesviral, neuroprotective and anti-inflammatory properties; and

are used to target the EBV-*dUTPase* employing an *in-silico* approach. Molecular docking was performed to find these phytochemicals' binding affinities and essential structural insights toward the target protein's active site. The top-scoring compounds were subjected to MD simulations and the MM-PBSA method to assess the binding energy of the ligands and the viral protein. Additionally, the prediction of toxicity, physicochemical characteristics, and pharmacokinetic factors were also investigated to ascertain the druggable nature of these compounds.

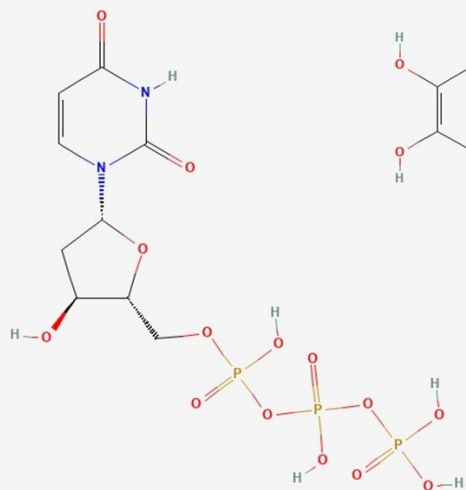
6.4 Results

6.4.1 Molecular Docking of EBV-*dUTPase* with dUTP and other phytochemicals

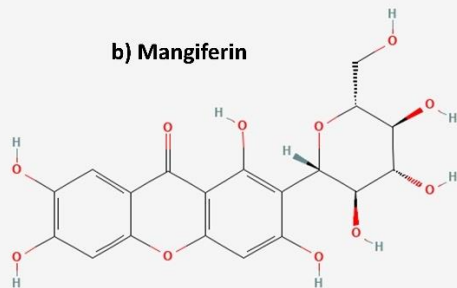
The site-specific docking of all the phytochemicals was done in the grid defined earlier. All the phytochemicals were binding within the active site lying in the grid. We selected the most reliable binding pose of the phytochemicals with the target protein *dUTPase*, based on the lowest RMSD values of binding. The chemical structure of the top four ligands along with *dUTP* is depicted in [Figure 6.2], and their respective binding free energies are listed in [Table]. These ligands interacted with *dUTPase* through various strong (conventional H bonding, C-H bonding) and weak (alkyl, π -alkyl, π -anion, π - π T shaped, van-der Waal's, unfavorable donor-donor) interactions. The binding free energy of the top four ligands, i.e., K3R, MANG, SARA, DHED, ranges from -9.1 to -8.5 kCal/mol, and -7.6 kCal/mol for the natural ligand dUTP.

Figure 6.2

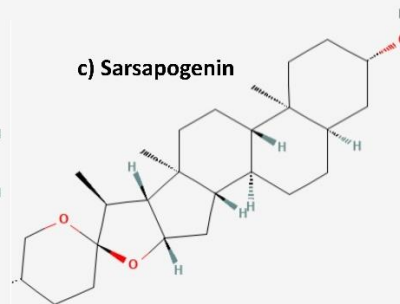
a) Deoxyuridine triphosphate (dUTP)



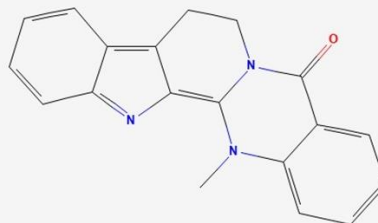
b) Mangiferin



c) Sarsapogenin



d) Dehydroevodiamine



e) Kaempferol-3-rutinoside

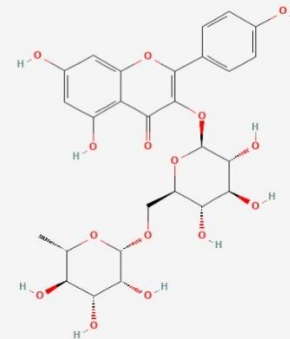


Figure 6.2. Structural representation of the phytochemicals: (a) Deoxyuridine triphosphate (dUTP), (b) Mangiferin, (c) Sarsapogenin, (d) Dehydroevodiamine, and (e) Kaempferol-3-O-Rutinoside.

Table 6.1. A detailed description of the natural ligand of dUTPase (dUTP) and the top 5 phytochemicals possessing anti-viral and neuroprotective properties with the highest binding affinities towards EBV-dUTPase based on a molecular docking study; Dehydrouridine triphosphate (dUTP), Kaempferol-3-rutinoside (K3R), Mangiferin (MANG), Sarsasapogenin (SARA), Dehydroevodiamine (DHED).

Sr. No.	Class	Compound Name (mol. wt.)	Molecular formula	Compound identifier (PubChem)	Binding Energy (kCal/mol)
	Natural substrate	dUTP	C₉H₁₅N₂O₁₄P₃	CID-65070	-7.6
1	Anti-inflammatory [28]	K3R (902.8g/mol)	C ₂₇ H ₃₀ O ₁₅	CID-122173234	-9.1
2	Neuroprotective [29], Anti-inflammatory [30], Anti-viral [31]	MANG (422.3g/mol)	C ₁₉ H ₁₈ O ₁₁	CID-5281647	-9
3	Neuroprotective [32]	SARA (416.6g/mol)	C ₂₇ H ₄₄ O ₃	CID-92095	-8.8
4	Neuroprotective [33], Anti-viral [34]	DHED (301.3g/mol)	C ₁₉ H ₁₅ N ₃ O	CID-9817839	-8.6

6.4.2 Molecular Dynamic (MD) Simulations Analysis

The docked complexes were subjected to MD simulations for 100 ns to assess their structural stability. The stability of the simulated systems was further evaluated by calculating RMSD, RMSF, hydrogen bonds, Rg, and SASA from the trajectories obtained after the successful completion of the simulations.

6.4.3 Root-Mean-Square Deviation

RMSD is one of the commonly used quantitative measures to assess the stability of the docked complexes [35]–[37]. It calculates the difference between the protein backbone from its initial position to its final conformation. The smaller deviations signify more stability of the docked complexes. As evident from [Figure 6.3 (a)], the complex with MANG (green) showed an average RMSD value of around 0.1 nm, the least among all the five complexes. The average RMSD values for complexes with dUTP (cyan), K3R (red), DHED (blue), and SARA (purple) were estimated to be ~0.3, ~1.0, ~1.0, and 2 nm, respectively. The complex with K3R has shown major fluctuation around 20 ns and two slight fluctuations around 50 and 60 ns before reaching a constant RMSD value of ~1 nm at 70 ns, where it overlaps with the DHED. The compound SARA showed fluctuations throughout the simulation. The first stable conformation was observed at the starting point between 2 and 10 ns on 0.3 nm, followed by two significant fluctuations around 10 ns and 25 ns. The next stable conformation was noted around 60 ns with an average RMSD value of ~2 nm, comparatively higher than other complexes. Based on these observations, we assume that EBV-*dUTPase* has more conformational changes in SARA, followed by K3R and DHED and then by MANG and dUTP. These fluctuations were further confirmed by observing their local changes at the residues level by the RMSF plot discussed below.

6.4.4 Root-Mean-Square Fluctuation

RMSF helps to know which protein regions are responsible for the fluctuations. It is used to measure the flexibility of the individual residue of the system with respect to time. The higher score signifies unstable and flexible bonds, whereas

the lower score indicates stable regions in the protein-ligand complexes [36]. The RMSF of $C\alpha$ atoms of all the five complexes and the control was determined. The average RMSF values of control and complexes formed with K3R, MANG, DHED, SARA, and dUTP were ~ 0.09 , ~ 0.084 , ~ 0.078 , ~ 0.074 , ~ 0.084 , and ~ 0.075 nm respectively, as depicted in [Figure 6.3 (b)]. These values indicate that all the docked complexes demonstrate comparatively fewer fluctuations in their conformations than the control. The fewer fluctuations of the complexes indicate the significant interactions between the phytochemicals and the residues distributed across the active site of the protein.

Figure 6.3

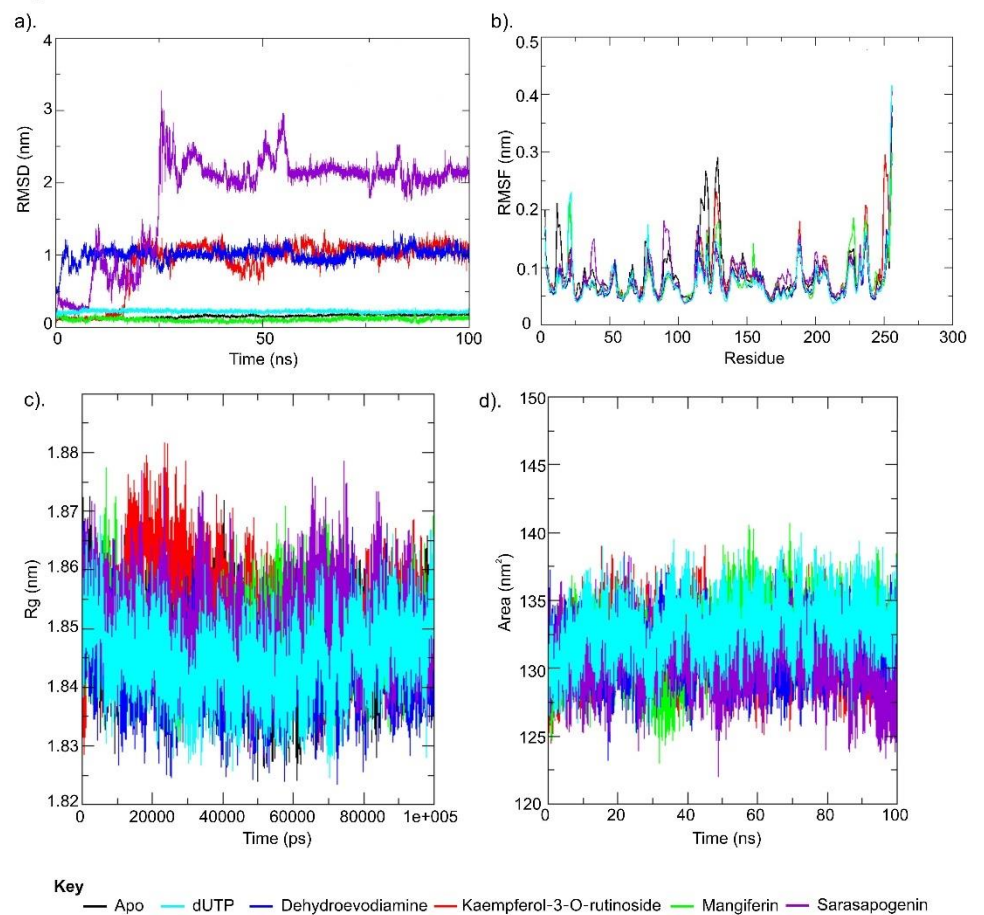


Figure 6.3. a) Root-mean-square deviations (RMSDs) of the EBV-dUTPase backbone atoms during MD simulation, b) RMSF analysis of $C\alpha$ during MD simulation, c) Solvent accessible surface area (SASA) analysis, and d) Rg plot of EBV-dUTPase bound and unbound with phytochemicals.

6.4.5 Radius of Gyration (Rg) and Solvent Accessible Surface Area (SASA) Analysis

The Rg of a structure is the measure of its compactness. The Rg represents the atomic distribution from their mutual center of mass in terms of mass-weighted root mean square distance [38], [39]. The Rg depicts the compactness and inclusive dimension of the protein and protein-ligand complexes that may comprise their appropriate interactions. Protein-ligand complexes displayed the least radius of gyration, indicating their compact packing and stability. SASA is another significant measure that calculates the accessible area of the solvent molecule. SASA was also computed for 100 ns for all the proteins. SASA is an important measure to determine the area of the receptor exposed to the solvents during the simulation. Stably folded protein can maintain a relatively steady value of Rg. All five complexes were subjected to Rg and SASA analysis. As evident from **[Figure 6.3 (c)]**, all the five systems and control showed similar Rg values with a very narrow range between 1.842 and 1.852 nm throughout the simulation, which is in agreement with the previous reports [40]. The estimated SASA values also have a similar pattern between 130.5 and 133 nm² as shown in **[Figure 6.3 (d)]**. These observations affirm the stability of all the systems.

6.4.6 Hydrogen Bond Analysis

The intermolecular H-bonds between interacting atom pairs in a protein-ligand complex play a vital role in the stability and molecular recognition process [41]. The intermolecular H-bonds were calculated with respect to time during the 100 ns MD simulations to ascertain each complex's dynamics stability. The hydrogen bond analysis is essential in determining the specificity of the interactions and the binding strength of the protein-ligand complex. The molecular interactions between the receptor protein and phytochemicals were explored to investigate the number of hydrogen bonds formed throughout the MD simulation, as represented in [Figure 6.4]. The complex formed with dUTP and MANG showed a consistently higher number of hydrogen bonds, followed by K3R, throughout the simulation of 100 ns. The former two even showed more than ten hydrogen bonds at the different timescale of the simulation. On the other hand, SARA showed a decrease in the number of hydrogen bonds compared to the simulation's starting point. Whereas, DHED comparatively showed a stable number of hydrogen bonds throughout the simulation.

Figure 6.4

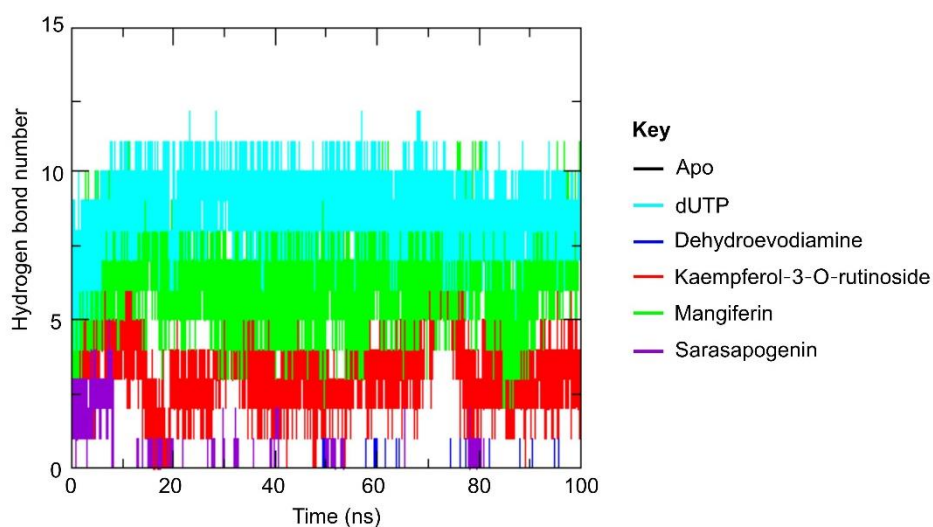


Figure 6.4. Hydrogen bond analysis of the docked complexes.

6.4.7 Binding Free Energy Estimation

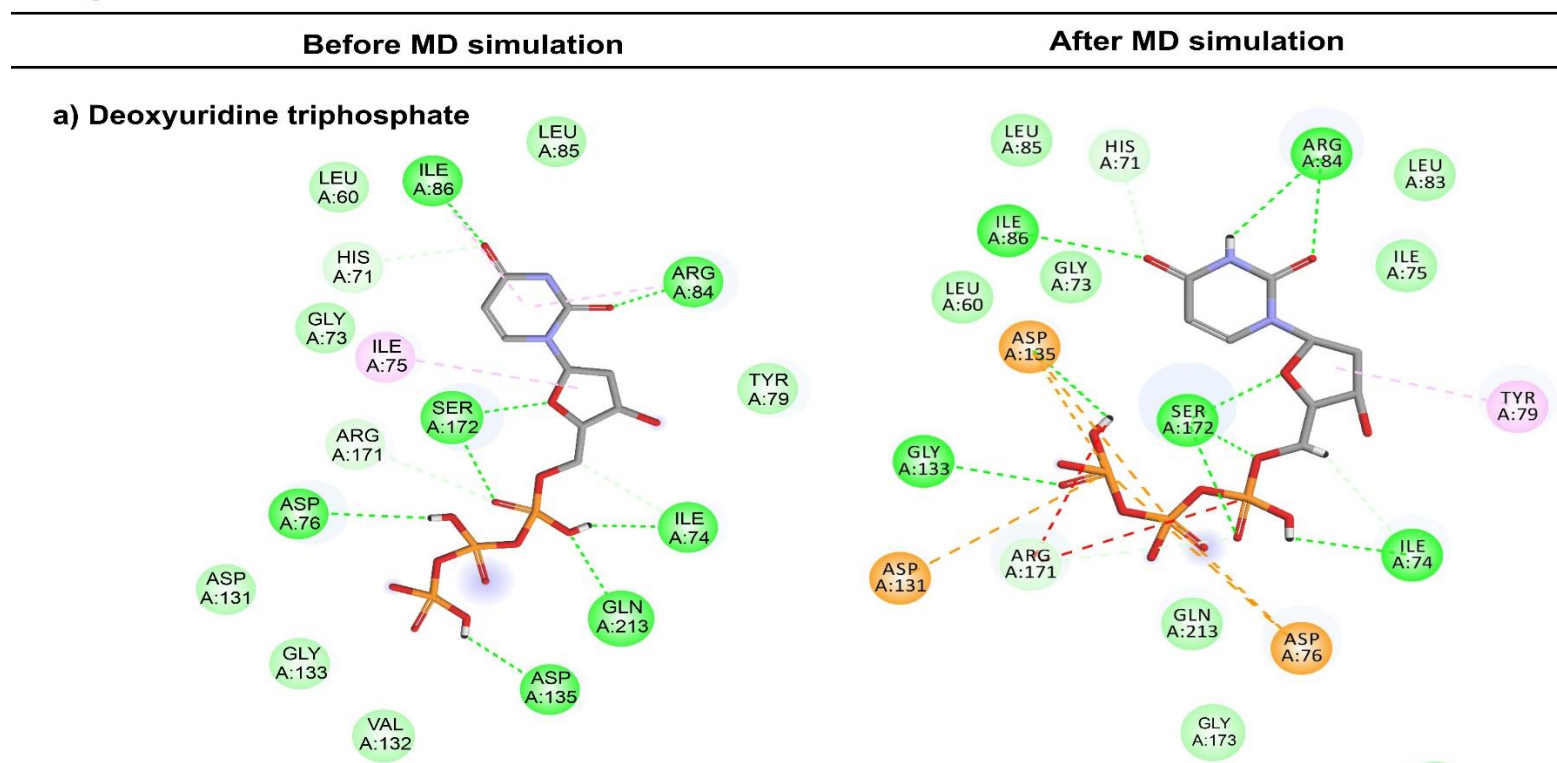
MM-PBSA method was used to estimate the binding free energy for each of the complexes. The lower the binding energy of the complex, the more is its stability. [Table] shows each complex's binding energy and other components that contribute to the molecular interactions such as van der Waals energy, electrostatic energy, and solvation energy. The results clearly suggest that all types of energy contributed significantly to the interactions. The selected phytochemicals with the highest negative binding energy could be used as the potential modulator for the EBV-*dUTPase* receptor.

Table 6.2. MM-PBSA analysis of the bound complexes

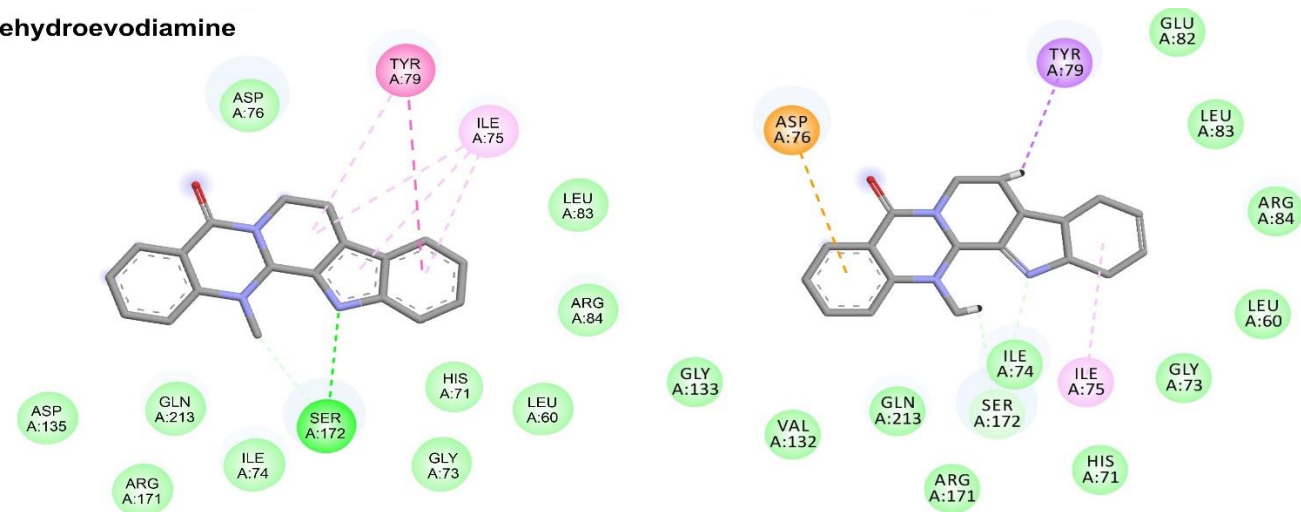
Complex	Binding Energy (kJ/mol)	van der Waals Energy (kJ/mol)	Electrostatic energy (kJ/mol)	Solvation Energy (kJ/mol)
<i>dUTPase/dUTP</i>	-65956.70	-7515.65	-45758.80	-12682.25
<i>dUTPase/DHED</i>	-69358.97	-7519.74	-48210.74	-13799.67
<i>dUTPase/SARA</i>	-68777.60	-7492.05	-48945.86	-12339.68
<i>dUTPase/K3R</i>	-68746.01	-7472.04	-48802.74	-12471.24
<i>dUTPase/MANG</i>	-68194.67	-7472.45	-47749.60	-12972.63

The binding free energy & their components (kJ/mol) post-simulation.

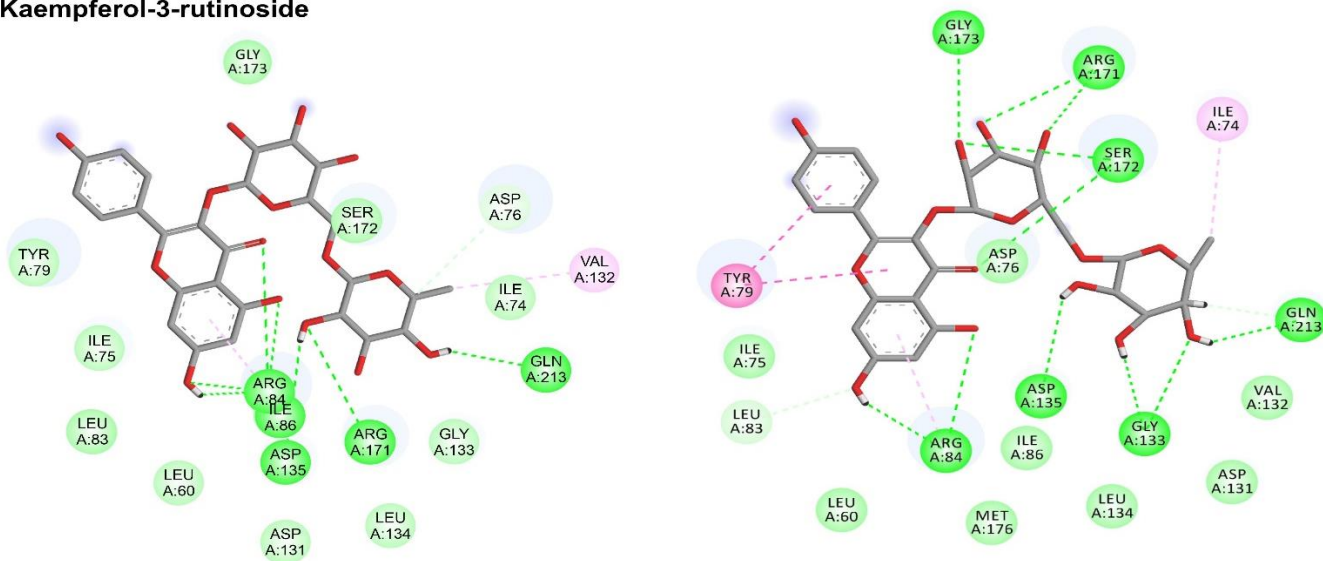
Figure 6.5



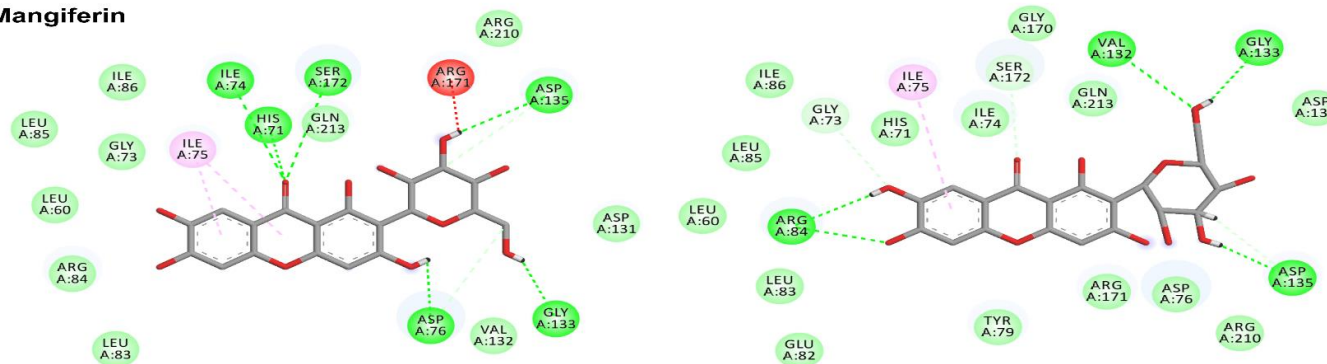
b) Dehydroevodiamine



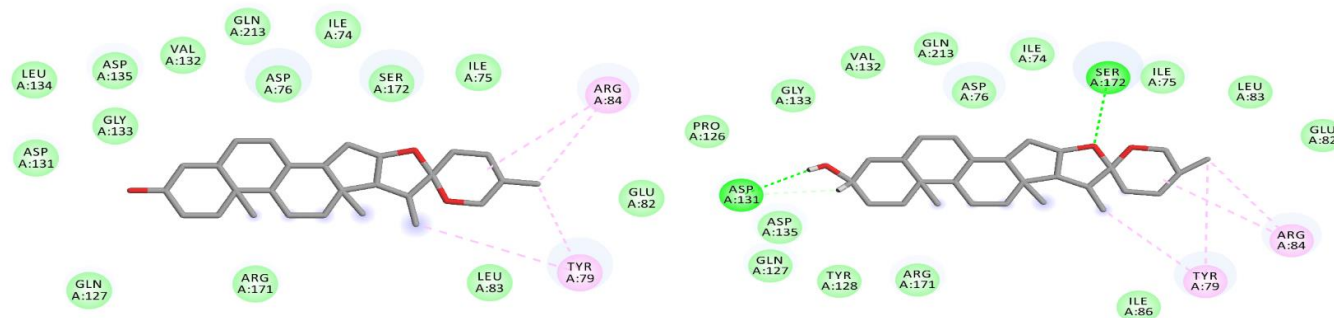
c) Kaempferol-3-rutinoside



d) Mangiferin



e) Sarasapogenin



KEY

Carbon Hydrogen Bond	Unfavourable Positive-Positive	Pi-Anion	Pi-Alkyl
van der Waals	Unfavourable Donor-Donor	Attractive Charges	Pi-Sigma
Conventional Hydrogen Bond	Unfavourable Aceptor-Aceptor	Alkyl	Pi-Pi stacked
			Pi-Pi T-shaped

Figure 6.5. 2D visualization of ligand-bound protein before and after MD simulation. Various types of interactions taking part in the protein-ligand binding are listed below, with the key. Throughout the simulation, the ligands remain bound to the protein EBV-*dUTPase*, establishing a stable connection towards the end of 100 ns.

6.4.8. ADMET Analysis

A good drug candidate is one that is not hindered by the physical factors, namely, absorption, distribution, metabolism, and excretion (ADME), to reach the target. Additionally, the compound should be non-toxic to the host [42]. Thus, evaluation of the ADMET properties of a compound is a crucial step towards establishing its drug likeliness. Therefore, we screened all four phytochemicals *in-silico* for their ADMET properties and drug-likeliness predictions. We observed that only DHED among all the phytochemicals evaluated followed all the rules for drug likeliness. Most importantly, DHED satisfies Lipinski's rule of 5 (Ro5), i.e., having a molecular mass less than 500 Da (286 Da), high lipophilicity with LogP value less than 5 (0.46), less than five hydrogen bond donors, less than ten hydrogen bond acceptor (3), and molar refractivity value in between 40-130 (74.77). ADMET results for all of the phytochemicals are enlisted in [Table 4].

Table 4.3 Pharmacokinetic properties and toxicity prediction of phytocompounds through the pkCSM and SwissADMET server.

Property	Model Name (Unit)	Predicted Value			
		DHED	K3R	MANG	SARA
Absorption	Water solubility (log mol/L)	-3.6	-2.891	-2.918	-5.485
	Caco2 permeability (log Papp in 10 ⁻⁶ cm/s)	1.741	-1.668	-0.926	1.301
	Intestinal absorption (human) (% Absorbed)	98.443	0	46.135	95.856
	Skin Permeability (log Kp)	-2.703	-2.735	-2.735	-2.973
	P-glycoprotein substrate (Yes/No)	No	Yes	Yes	No
	P-glycoprotein I inhibitor (Yes/No)	No	No	No	Yes
	P-glycoprotein II inhibitor (Yes/No)	No	No	No	Yes

Distribution	VDss (human) (log L/kg)	0.46	0.31	1.364	0.174
	Fraction unbound (human) (Fu)	0.062	0.241	0.289	0
	BBB permeability (log BB)	0.353	-2.707	-1.573	0.17
	CNS permeability (log PS)	-1.475	-6.562	-4.211	-2.576
Metabolism	CYP2D6 substrate (Yes/No)	No	No	No	No
	CYP3A4 substrate (Yes/No)	Yes	No	No	Yes
	CYP1A2 inhibitor (Yes/No)	Yes	No	No	No
	CYP2C19 inhibitor (Yes/No)	Yes	No	No	No
	CYP2C9 inhibitor (Yes/No)	No	No	No	No
	CYP2D6 inhibitor (Yes/No)	No	No	No	No
	CYP3A4 inhibitor (Yes/No)	No	No	No	No
Excretion	Total Clearance (log ml/min/kg)	0.615	-0.418	0.347	0.322
	Renal OCT2 substrate (Yes/No)	Yes	No	No	No
Toxicity	AMES toxicity (Yes/No)	No	No	No	No
	Max. tolerated dose (human) (log mg/kg/day)	-0.361	0.4	0.58	-0.492
	hERG I inhibitor (Yes/No)	No	No	No	No
	hERG II inhibitor (Yes/No)	Yes	Yes	No	No
	Hepatotoxicity (Yes/No)	No	No	No	No
	Skin Sensitisation (Yes/No)	No	No	No	No
Drug likeness	Lipinski (Yes/No)	Yes	No	No	Yes
	Ghose (Yes/No)	Yes	No	No	No
	Veber (Yes/No)	Yes	No	No	Yes
	Egan (Yes/No)	Yes	No	No	Yes
	Muegge (Yes/No)	Yes	No	No	No
	Bioavailability Score	0.55	0.17	0.17	0.55
Medicinal Chemistry	Lead likeness (Yes/No)	Yes	No	No	No

6.5 Discussion

The Epstein-Barr virus is considered a ubiquitous pathogen in the human population. Though the primary infection of EBV is often asymptomatic and establishes persistent latency, the host immune system keeps it in check. However, if the host-virus balance is not maintained, it results in viral reactivation, driving potentially lethal pathologies such as multiple oncogenic disorders. It has also been linked to neurological manifestations such as encephalitis, aseptic meningitis, transverse myelitis, MS, AD, and GBS, owing to its recently discovered neurotropic potential [43]–[46]. Despite such cataclysmic consequences, no FDA-approved therapeutic intervention is available for EBV infection and related pathologies. Currently, available treatment regimens do not target EBV selectively and specifically. Therefore, we tried to target the EBV infection by inhibiting a specific protein of the virus, the *dUTPase*. The protein is crucial for the viral replication cycle [47]. To target the viral *dUTPase* protein, we employed an *in-silico* approach using various phytochemicals. The plant-based compounds included in this study were selected based on their known anti-viral, anti-inflammatory, and neuroprotective properties.

In the present study, molecular docking of the EBV-*dUTPase* protein was done with all the 45 phytochemical ligands in the predefined active-site pocket. Subsequently, the top five protein-ligand complexes with the lowest binding energy values, namely K3R, MANG, SARA, DHED, and the natural ligand dUTP, were subjected to MD simulation analysis. The RMSD analysis of the ligand-bound protein showed the least RMSD value for MANG, followed by the natural ligand dUTP and, after that, DHED. DHED and MANG were revealed to bind most stably to the target protein EBV-*dUTPase* throughout the 100 ns simulation out of the four phytochemical ligands. The lower RMSF of C α atoms for DHED and MANG corroborated their stable binding to EBV-*dUTPase*. Surprisingly, the RMSF of C α atoms for DHED (0.74 nm) and MANG (0.78 nm) lies near that of dUTP (0.75 nm). Smaller deviations in average Rg and SASA values also indicate greater compactness and sturdy binding of the protein-ligand complexes. The binding of DHED with the EBV-*dUTPase* primarily involved electrostatic interactions. The 2D analysis of interactions

revealed that binding of the DHE-*dUTPase* complex occurs through His71 of the EBV-*dUTPase*. The histidine residue at the 71st position is conserved among the gamma-herpesviruses, whereas the human counterpart of the enzyme contains an alanine residue at its place [14]. Therefore, the region around His71 residue is considered a crucial target site for drug development against EBV. Further, the ADMET analysis of these top five phytochemical ligands revealed that only DHED is a potential drug candidate adhering to Lipinski's rule of 5. Thus, DHED could be a potential drug candidate to target EBV-*dUTPase*. The stable binding of DHED at the protein's active site will act competitively to inhibit the binding of natural ligand dUTP, thus hindering the virus's nucleotide metabolism and thereby viral replication and propagation.

Interestingly, recent investigations have revealed DHED as a potential treatment for Alzheimer's disease [48], [49]. It is demonstrated to bind with cholinesterases (ChE) and hinder their enzyme-degrading activity towards acetylcholine (ACh) and butyrylcholine (BCh) [49]. ACh and BCh are essential neurotransmitters that play a crucial role in normal brain function, such as attention, arousal, memory, and motivation [50]. The enzyme AChE rapidly degrades the excess of ACh released at the synaptic cleft. Previous studies have predominantly reported lower levels of acetylcholine in AD patients [51]. Interestingly, the current FDA-approved treatment regime for AD includes AChE inhibitors, namely Donepezil, Rivastigmine, and Galantamine [52]. DHED treatment has also shown cognitive improvement in mice, owing to its antioxidant activity towards A β -induced ROS and inhibition of neurotoxicity [48]. It is thereby proclaimed to attenuate A β -mediated amnesia [53] and tau hyperphosphorylation [54]. Additionally, a recent *in-silico* study successfully demonstrated DHED as a potent candidate to target EBV infection by inhibiting a viral protease [34].

Our current study demonstrates the use of phytochemical DHED to target the viral *dUTPase* to subdue virus-mediated neurodegenerative consequences. Here it is noteworthy to recount the neuroprotective properties of the phytochemical as mentioned earlier. The additive effects of neuroprotective and anti-viral properties of DHED make it an ideal candidate for drug development against EBV-mediated neuropathologies. However, further *in-vitro* evaluations are

required to establish the validity of the predicted anti-EBV *dUTPase* activity of DHED.

6.6 Methodology

6.6.1 Retrieval of protein-ligand structure and preparation for molecular docking

A high resolution (1.25 Å) crystal structure of the protein EBV-*dUTPase* (PDB ID: 2bsy) was obtained from the RCSB-PDB database. The ligand structures were downloaded from PubChem as structure data files (SDF) and converted to PDF using PyMOL before proceeding ahead. The details of ligands are listed in [Table and Table S6. 1]. The protein and ligand preparation were done using AutoDockTools 1.5.6 (ADT) for molecular docking. Briefly, the protein preparation involved removing water molecules and adding polar hydrogens and Kollmans' charges. Whereas ligand preparation for docking included adding Gasteiger charges, merging of non-polar hydrogens, identification of aromatic carbons and rotatable bonds, and setting of the torsion tree.

6.6.2 Active site validation and Molecular docking studies

Previous studies have already reported some residues (Leu60, Ser70, His71, Val72, Gly73, Ile74, Ile75, Asp76, Tyr79, Glu82, Leu83, Arg84, Leu85, Ile86, Gly170, Arg171, Ser172, and Gln213) to be involved in ligand binding on EBV-*dUTPase* [Figure 6.1 (d)]. These amino acid residues were reported to be involved in various interactions, including hydrogen bonds, C-H bonds, Pi-sigma, and Pi-alkyl bonds with the ligands. To validate the active binding site of the protein, we subjected the protein structure to Computed Atlas of Surface Tomography of Protein (CASTp) 3.0 and FTmap servers. Based on the literature survey and the data obtained from both the software, a docking grid was constructed around the protein such that it covers all the amino acid residues of the active binding site, as depicted in [Figure 6.1 (d)]. The grid was centered at $x=54.719$, $y=22.173$, and $z=26.211$ with the xyz dimensions 48X52X44 and spacing 0.375 Å.

6.6.3 MD Simulations

MD simulations of dUTP and four phytochemicals viz., K3R, MANG, DHED, and SARA with EBV-*dUTPase* were performed to assess the stabilities of the docked conformation of the respective complexes using GROMACS 2021 package [23]. These compounds were screened based on their molecular docking scores. The topology parameter of the ligand was built using the CGenFF server. All the complexes were immersed in a cubic box of TIP3P water models. The distance between the edge of the box and the protein was 1nm to maintain the periodic boundary conditions. A strength of 0.15M NaCl was added to neutralize both the systems. Energy minimization was performed using the steepest descent method of 1000 kJ/mol and 50,000 iteration steps, followed by the conjugate gradient method to release conflicting contacts. The Particle Mesh Ewald (PME) method was applied to calculate long-range interactions [24]. The neutralized system was then equilibrated in two phases. In the first phase, the temperature was equilibrated with the NVT ensemble where N is the constant number of particles, V is the volume, and T is the temperature, with 50000 number of iterations and 2 femtoseconds (fs) each. In the second phase, pressure is equilibrated at 300 K with NPT ensemble where N is the constant number of particles, P is the pressure and T is the temperature. V-rescale, a modified Berendsen thermostat, was used to regulate the temperature inside the system. Parrinello-Rahman, a pressure coupling method, was used in the NPT ensemble to maintain the pressure. After equilibrating the system with desired temperature and pressure, a production run of 100 ns was finally established to get an insight into the motional behavior of the complex.

6.6.4 Trajectory Analysis

Upon completion of the MD simulations, the obtained trajectories were analyzed for RMSD, RMSF, intermolecular hydrogen bond, the Rg, and SASA calculations using in-built tools of GROMACS package. The rms module of GROMACS was used to calculate the RMSD in the protein backbone, whereas the RMSF in the atomic positions of the protein C α backbone was computed using RMSF module. Other modules such as H-bond, gyrate, and SASA were

utilized to determine the number of hydrogen bonds, Rg and SASA, respectively.

6.6.5 Binding Free Energy Calculations

The MM-PBSA method was employed using the gmx_MMPBSA tool to estimate the binding free energy of interactions between the docked complexes from GROMACS MD trajectories of 100 ns [25], [26]. The binding energy (kJ/mol), non-bonded potentials such as van der Waals energy and electrostatic energy, and polar solvation energy are the major components that contributed to estimating the MM-PBSA relative binding affinity [27]. The binding free energy for a given complex of protein and ligand can be calculated using the following equation:

$$\Delta G_{bind} = G_{complex} - G_{protein} - G_{ligand}$$

where G_{bind} is the binding affinity of the complex, $G_{complex}$ depicts the total free energy of the docked complex, whereas $G_{protein}$ and G_{ligand} represents the total free energies of the unbound protein and ligand in the water or solvent, respectively.

6.6.6 ADMET/Drug Likelihood Properties

ADMET collectively stands for the pharmacokinetic properties of a chemical compound, namely, adsorption, distribution, metabolism, excretion, and toxicity. The given properties of the top 5 phytochemicals (based on docking score) were determined using the pk-CSM pharmacokinetics web server. Further, the drug likelihood of the physiochemical was evaluated according to Lipinski's rule using the SwissADME server.

6.7 References

- [1] L. S. Young and A. B. Rickinson, “Epstein–Barr virus: 40 years on,” *Nat. Rev. Cancer*, vol. 4, no. 10, pp. 757–768, Oct. 2004, doi: 10.1038/nrc1452.
- [2] Y. Yang and F. Gao, “Clinical characteristics of primary and reactivated Epstein-Barr virus infection in children,” *J. Med. Virol.*, vol. 92, no. 12, pp. 3709–3716, Dec. 2020, doi: 10.1002/jmv.26202.
- [3] M. A. Allnutt *et al.*, “Human Herpesvirus 6 Detection in Alzheimer’s Disease Cases and Controls across Multiple Cohorts,” *Neuron*, vol. 105, no. 6, pp. 1027–1035.e2, Mar. 2020, doi: 10.1016/j.neuron.2019.12.031.
- [4] S.-M. Shim, H.-S. Cheon, C. Jo, Y. H. Koh, J. Song, and J.-P. Jeon, “Elevated Epstein-Barr Virus Antibody Level is Associated with Cognitive Decline in the Korean Elderly,” *J. Alzheimers Dis.*, vol. 55, no. 1, pp. 293–301, Nov. 2016, doi: 10.3233/JAD-160563.
- [5] I. Carbone *et al.*, “Herpes virus in Alzheimer’s disease: relation to progression of the disease,” *Neurobiol. Aging*, vol. 35, no. 1, pp. 122–129, Jan. 2014, doi: 10.1016/j.neurobiolaging.2013.06.024.
- [6] H. C. Jha *et al.*, “Gammaherpesvirus Infection of Human Neuronal Cells,” *mBio*, vol. 6, no. 6, Dec. 2015, doi: 10.1128/mBio.01844-15.
- [7] D. Tiwari, S. Jakhmola, D. K. Pathak, R. Kumar, and H. C. Jha, “Temporal *In Vitro* Raman Spectroscopy for Monitoring Replication Kinetics of Epstein–Barr Virus Infection in Glial Cells,” *ACS Omega*, vol. 5, no. 45, pp. 29547–29560, Nov. 2020, doi: 10.1021/acsomega.0c04525.
- [8] S. Jakhmola and H. C. Jha, “Glial cell response to Epstein-Barr Virus infection: A plausible contribution to virus-associated inflammatory reactions in the brain,” *Virology*, vol. 559, pp. 182–195, Jul. 2021, doi: 10.1016/j.virol.2021.04.005.
- [9] C. Traylen *et al.*, “Identification of Epstein-Barr Virus Replication Proteins in Burkitt’s Lymphoma Cells,” *Pathogens*, vol. 4, no. 4, pp. 739–751, Oct. 2015, doi: 10.3390/pathogens4040739.
- [10] J. Fleischmann, E. Kremmer, J. S. Greenspan, F. A. Grässer, and G. Niedobitek, “Expression of viral and human *dUTPase* in Epstein-Barr virus-associated diseases: Expression of EBV and Human *dUTPase*,” *J.*

- Med. Virol.*, vol. 68, no. 4, pp. 568–573, Dec. 2002, doi: 10.1002/jmv.10234.
- [11] A. Arvin *et al.*, Eds., *Human Herpesviruses: Biology, Therapy, and Immunoprophylaxis*. Cambridge: Cambridge University Press, 2007. Accessed: Mar. 25, 2022. [Online]. Available: <http://www.ncbi.nlm.nih.gov/books/NBK47376/>
- [12] R. Chen, H. Wang, and L. M. Mansky, “Roles of uracil-DNA glycosylase and *dUTPase* in virus replication,” *J. Gen. Virol.*, vol. 83, no. 10, pp. 2339–2345, Oct. 2002, doi: 10.1099/0022-1317-83-10-2339.
- [13] L. Freeman, M. Buisson, N. Tarbouriech, A. Van der Heyden, P. Labbé, and W. P. Burmeister, “The Flexible Motif V of Epstein-Barr Virus Deoxyuridine 5'-Triphosphate Pyrophosphatase Is Essential for Catalysis,” *J. Biol. Chem.*, vol. 284, no. 37, pp. 25280–25289, Sep. 2009, doi: 10.1074/jbc.M109.019315.
- [14] N. Tarbouriech, M. Buisson, J.-M. Seigneurin, S. Cusack, and W. P. Burmeister, “The Monomeric *dUTPase* from Epstein-Barr Virus Mimics Trimeric *dUTPases*,” *Structure*, vol. 13, no. 9, pp. 1299–1310, Sep. 2005, doi: 10.1016/j.str.2005.06.009.
- [15] R. S. Leang *et al.*, “The Anti-interferon Activity of Conserved Viral *dUTPase* ORF54 is Essential for an Effective MHV-68 Infection,” *PLoS Pathog.*, vol. 7, no. 10, p. e1002292, Oct. 2011, doi: 10.1371/journal.ppat.1002292.
- [16] M. Williams, B. Cox, and M. Ariza, “Herpesviruses *dUTPases*: A New Family of Pathogen-Associated Molecular Pattern (PAMP) Proteins with Implications for Human Disease,” *Pathogens*, vol. 6, no. 1, p. 2, Dec. 2016, doi: 10.3390/pathogens6010002.
- [17] R. Glaser *et al.*, “EBV-encoded *dUTPase* induces immune dysregulation: Implications for the pathophysiology of EBV-associated disease,” *Virology*, vol. 346, no. 1, pp. 205–218, Mar. 2006, doi: 10.1016/j.virol.2005.10.034.
- [18] M.-E. Ariza, R. Glaser, P. T. P. Kaumaya, C. Jones, and M. V. Williams, “The EBV-Encoded *dUTPase* Activates NF- κ B through the TLR2 and MyD88-Dependent Signaling Pathway,” *J. Immunol.*, vol. 182, no. 2, pp. 851–859, Jan. 2009, doi: 10.4049/jimmunol.182.2.851.

- [19] M. E. Ariza, P. Rivaille, R. Glaser, M. Chen, and M. V. Williams, “Epstein-Barr Virus Encoded *dUTPase* Containing Exosomes Modulate Innate and Adaptive Immune Responses in Human Dendritic Cells and Peripheral Blood Mononuclear Cells,” *PLOS ONE*, vol. 8, no. 7, p. 14, 2013.
- [20] M. V. Williams PhD, B. Cox, W. P. Lafuse PhD, and M. E. Ariza, “Epstein-Barr Virus *dUTPase* Induces Neuroinflammatory Mediators: Implications for Myalgic Encephalomyelitis/Chronic Fatigue Syndrome,” *Clin. Ther.*, vol. 41, no. 5, pp. 848–863, May 2019, doi: 10.1016/j.clinthera.2019.04.009.
- [21] M. V. Williams PhD, B. Cox, W. P. Lafuse PhD, and M. E. Ariza, “Epstein-Barr Virus *dUTPase* Induces Neuroinflammatory Mediators: Implications for Myalgic Encephalomyelitis/Chronic Fatigue Syndrome,” *Clin. Ther.*, vol. 41, no. 5, pp. 848–863, May 2019, doi: 10.1016/j.clinthera.2019.04.009.
- [22] J. Fleischmann, E. Kremmer, J. S. Greenspan, F. A. Grässer, and G. Niedobitek, “Expression of viral and human *dUTPase* in Epstein-Barr virus-associated diseases: Expression of EBV and Human *dUTPase*,” *J. Med. Virol.*, vol. 68, no. 4, pp. 568–573, Dec. 2002, doi: 10.1002/jmv.10234.
- [23] Lindahl, Abraham, Hess, and V. D. Spoel, “GROMACS 2021 Manual,” Jan. 2021, doi: 10.5281/ZENODO.4457591.
- [24] M. J. Abraham and J. E. Gready, “Optimization of parameters for molecular dynamics simulation using smooth particle-mesh Ewald in GROMACS 4.5,” *J. Comput. Chem.*, vol. 32, no. 9, pp. 2031–2040, Jul. 2011, doi: 10.1002/jcc.21773.
- [25] B. R. Miller, T. D. McGee, J. M. Swails, N. Homeyer, H. Gohlke, and A. E. Roitberg, “*MMPBSA.py*: An Efficient Program for End-State Free Energy Calculations,” *J. Chem. Theory Comput.*, vol. 8, no. 9, pp. 3314–3321, Sep. 2012, doi: 10.1021/ct300418h.
- [26] M. S. Valdés-Tresanco, M. E. Valdés-Tresanco, P. A. Valiente, and E. Moreno, “*gmx_MMPBSA*: A New Tool to Perform End-State Free Energy Calculations with GROMACS,” *J. Chem. Theory Comput.*, vol. 17, no. 10, pp. 6281–6291, Oct. 2021, doi: 10.1021/acs.jctc.1c00645.

- [27] O. Indari, M. F. Sk, S. Jakhmola, N. A. Jonniya, H. C. Jha, and P. Kar, “Decoding the Host–Parasite Protein Interactions Involved in Cerebral Malaria Through Glares of Molecular Dynamics Simulations,” *J. Phys. Chem. B*, vol. 126, no. 2, pp. 387–402, Jan. 2022, doi: 10.1021/acs.jpcc.1c07850.
- [28] D. Hwang, M. Kang, C. Kang, and G. Kim, “Kaempferol-3-O- β -rutinoside suppresses the inflammatory responses in lipopolysaccharide-stimulated RAW264.7 cells via the NF- κ B and MAPK pathways,” *Int. J. Mol. Med.*, Oct. 2019, doi: 10.3892/ijmm.2019.4381.
- [29] T. Liu, Y. Song, and A. Hu, “Neuroprotective mechanisms of mangiferin in neurodegenerative diseases,” *Drug Dev. Res.*, vol. 82, no. 4, pp. 494–502, Jun. 2021, doi: 10.1002/ddr.21783.
- [30] A. Dar *et al.*, “Analgesic and Antioxidant Activity of Mangiferin and Its Derivatives: the Structure Activity Relationship,” *Biol. Pharm. Bull.*, vol. 28, no. 4, pp. 596–600, 2005, doi: 10.1248/bpb.28.596.
- [31] M. S. Zheng and Z. Y. Lu, “Antiviral effect of mangiferin and isomangiferin on herpes simplex virus,” *Chin. Med. J. (Engl.)*, vol. 103, no. 2, pp. 160–165, Feb. 1990.
- [32] P. Kashyap, K. Muthusamy, M. Niranjana, S. Trikha, and S. Kumar, “Sarsasapogenin: A steroidal saponin from *Asparagus racemosus* as multi target directed ligand in Alzheimer’s disease,” *Steroids*, vol. 153, p. 108529, Jan. 2020, doi: 10.1016/j.steroids.2019.108529.
- [33] Y.-N. Zhang, Y.-F. Yang, and X.-W. Yang, “Blood-brain barrier permeability and neuroprotective effects of three main alkaloids from the fruits of *Euodia rutaecarpa* with MDCK-pHaMDR cell monolayer and PC12 cell line,” *Biomed. Pharmacother. Biomedecine Pharmacother.*, vol. 98, pp. 82–87, Feb. 2018, doi: 10.1016/j.biopha.2017.12.017.
- [34] R. N. Azizah, Suharti, and Yahmin, “A molecular docking study of dehydroevodiamine as an inhibitor of epstein-barr virus protease,” *IOP Conf. Ser. Mater. Sci. Eng.*, vol. 833, no. 1, p. 012006, May 2020, doi: 10.1088/1757-899X/833/1/012006.
- [35] K. Sargsyan, C. Grauffel, and C. Lim, “How Molecular Size Impacts RMSD Applications in Molecular Dynamics Simulations,” *J. Chem.*

- Theory Comput.*, vol. 13, no. 4, pp. 1518–1524, Apr. 2017, doi: 10.1021/acs.jctc.7b00028.
- [36] L. Martínez, “Automatic Identification of Mobile and Rigid Substructures in Molecular Dynamics Simulations and Fractional Structural Fluctuation Analysis,” *PLOS ONE*, vol. 10, no. 3, p. e0119264, Mar. 2015, doi: 10.1371/journal.pone.0119264.
- [37] A. Choubey, B. Dehury, S. Kumar, B. Medhi, and P. Mondal, “Naltrexone a potential therapeutic candidate for COVID-19,” *J. Biomol. Struct. Dyn.*, vol. 40, no. 3, pp. 963–970, Feb. 2022, doi: 10.1080/07391102.2020.1820379.
- [38] S. Singh, G. Sablok, R. Farmer, A. K. Singh, B. Gautam, and S. Kumar, “Molecular Dynamic Simulation and Inhibitor Prediction of Cysteine Synthase Structured Model as a Potential Drug Target for Trichomoniasis,” *BioMed Res. Int.*, vol. 2013, pp. 1–15, 2013, doi: 10.1155/2013/390920.
- [39] S. Kumar *et al.*, “Novel insight into the molecular interaction of catalase and sucrose: A combination of *in-silico* and in planta assays study,” *Comput. Electron. Agric.*, vol. 151, pp. 258–263, Aug. 2018, doi: 10.1016/j.compag.2018.06.005.
- [40] S. Jakhmola, N. A. Jonniya, M. F. Sk, A. Rani, P. Kar, and H. C. Jha, “Identification of Potential Inhibitors against Epstein–Barr Virus Nuclear Antigen 1 (EBNA1): An Insight from Docking and Molecular Dynamic Simulations,” *ACS Chem. Neurosci.*, vol. 12, no. 16, pp. 3060–3072, Aug. 2021, doi: 10.1021/acchemneuro.1c00350.
- [41] K. Girdhar *et al.*, “Novel insights into the dynamics behavior of glucagon-like peptide-1 receptor with its small molecule agonists,” *J. Biomol. Struct. Dyn.*, vol. 37, no. 15, pp. 3976–3986, Oct. 2019, doi: 10.1080/07391102.2018.1532818.
- [42] S. Ekins, J. Mestres, and B. Testa, “*In silico* pharmacology for drug discovery: methods for virtual ligand screening and profiling: *In silico* pharmacology for drug discovery,” *Br. J. Pharmacol.*, vol. 152, no. 1, pp. 9–20, Sep. 2007, doi: 10.1038/sj.bjp.0707305.
- [43] S. Jakhmola, A. Upadhyay, K. Jain, A. Mishra, and H. C. Jha, “Herpesviruses and the hidden links to Multiple Sclerosis

- neuropathology,” *J. Neuroimmunol.*, vol. 358, p. 577636, Sep. 2021, doi: 10.1016/j.jneuroim.2021.577636.
- [44] D. Tiwari *et al.*, “Indication of Neurodegenerative Cascade Initiation by Amyloid-like Aggregate-Forming EBV Proteins and Peptide in Alzheimer’s Disease,” *ACS Chem. Neurosci.*, vol. 12, no. 20, pp. 3957–3967, Oct. 2021, doi: 10.1021/acchemneuro.1c00584.
- [45] J. A. Schiff, J. A. Schaefer, and J. E. Robinson, “Epstein-Barr virus in cerebrospinal fluid during infectious mononucleosis encephalitis,” *Yale J. Biol. Med.*, vol. 55, no. 1, pp. 59–63, Feb. 1982.
- [46] C. Grose, W. Henle, G. Henle, and P. M. Feorino, “Primary Epstein–Barr-Virus Infections in Acute Neurologic Diseases,” *N. Engl. J. Med.*, vol. 292, no. 8, pp. 392–395, Feb. 1975, doi: 10.1056/NEJM197502202920804.
- [47] C. Kerepesi *et al.*, “Life without *dUTPase*,” *Front. Microbiol.*, vol. 7, Nov. 2016, doi: 10.3389/fmicb.2016.01768.
- [48] C. H. Park *et al.*, “Dehydroevodiamine·HCl Prevents Impairment of Learning and Memory and Neuronal Loss in Rat Models of Cognitive Disturbance,” *J. Neurochem.*, vol. 74, no. 1, pp. 244–253, Dec. 2001, doi: 10.1046/j.1471-4159.2000.0740244.x.
- [49] K. Y. Shin, K. Y. Kim, and Y.-H. Suh, “Dehydroevodiamine·HCl enhances cognitive function in memory-impaired rat models,” *Korean J. Physiol. Pharmacol.*, vol. 21, no. 1, p. 55, 2017, doi: 10.4196/kjpp.2017.21.1.55.
- [50] P. T. Francis, A. M. Palmer, M. Snape, and G. K. Wilcock, “The cholinergic hypothesis of Alzheimer’s disease: a review of progress,” *J. Neurol. Neurosurg. Psychiatry*, vol. 66, no. 2, pp. 137–147, Feb. 1999, doi: 10.1136/jnnp.66.2.137.
- [51] R. M. Lane, S. G. Potkin, and A. Enz, “Targeting acetylcholinesterase and butyrylcholinesterase in dementia,” *Int. J. Neuropsychopharmacol.*, vol. 9, no. 01, p. 101, Aug. 2005, doi: 10.1017/S1461145705005833.
- [52] R. A. Hansen, G. Gartlehner, A. P. Webb, L. C. Morgan, C. G. Moore, and D. E. Jonas, “Efficacy and safety of donepezil, galantamine, and rivastigmine for the treatment of Alzheimer’s disease: a systematic review and meta-analysis,” *Clin. Interv. Aging*, vol. 3, no. 2, pp. 211–225, 2008.
- [53] H.-H. Wang, C.-J. Chou, J.-F. Liao, and C.-F. Chen, “Dehydroevodiamine attenuates β -amyloid peptide-induced amnesia in mice,” *Eur. J.*

Pharmacol., vol. 413, no. 2–3, pp. 221–225, Feb. 2001, doi: 10.1016/S0014-2999(00)00913-4.

[54] J.-H. Peng, C.-E. Zhang, W. Wei, X.-P. Hong, X.-P. Pan, and J.-Z. Wang, “Dehydroevodiamine attenuates tau hyperphosphorylation and spatial memory deficit induced by activation of glycogen synthase kinase-3 in rats,” *Neuropharmacology*, vol. 52, no. 7, pp. 1521–1527, Jun. 2007, doi: 10.1016/j.neuropharm.2007.02.008.

[55] O. Indari, R. Chandramohanadas, and H. C. Jha, “Epstein–Barr virus infection modulates blood–brain barrier cells and its co-infection with *Plasmodium falciparum* induces RBC adhesion,” *Pathog. Dis.*, vol. 79, no. 1, p. ftaa080, Jan. 2021, doi: 10.1093/femspd/ftaa080.

Chapter 7

Conclusion and future perspective

Despite the ever-increasing global burden, AD remains among yet unsolved enigmas. Various theories have been proposed to explain disease causation and progression, including the A β hypothesis, tau hyperphosphorylation hypothesis, genetic predisposition hypothesis, and viral hypothesis. Our study attempts to investigate the role of Human Herpesvirus-4, often called the Epstein-Barr virus, in the pathogenesis of AD. The neurotropic potential of HHV-4 is relatively recently discovered; thereby, only limited studies exist exploring its implication in AD.

Our initial investigation proposes the possibility of EBV infection playing a crucial role in developing AD pathophysiology via the viral peptides. These peptides are generated due to cellular proteasomal activity and could be involved in causing neurodegeneration in amalgamation with other infection-induced events. *In-silico* analysis of viral proteins identified multiple candidates among virus-generated peptides with aggregate formation tendency. Furthermore, *in-vitro* experiments on a screened 11-amino-acid-long peptide generated from the proteasomal processing of EBV-gM₁₄₇₋₁₅₆ corroborated the hypothesis. A correlation between aggregate formation and viral infection is depicted by the concentration and time-dependent evolution of fluorescence. Besides, Raman signals and cytotoxicity data analysis strongly suggest the possibility mentioned above. Based on these results, a mechanism for viral protein processing inside the host cell leading to the formation of proteinaceous aggregates has been proposed and explained. This operational insight provides a novel outlook on how the infection of EBV could lead to the characteristic neurodegenerative pathology of AD.

After establishing the amyloidogenic potential of an EBV-derived peptide and its cytotoxic effect on the neurons, we went ahead in pursuit of checking the effect of EBV on the cells surrounding the neurons, i.e., the glial cells (microglia). To examine the same, time-dependent *in-vitro* spatial Raman spectroscopy was carried out on different regions of the microglial cells. Our

investigation showed the temporal evolution of EBV infection, enabling one to understand the virus influencing mechanism. In brief, the study directed us to believe that EBV enters the glial cells probably in the first two hpi by utilizing PIP-dependent signaling pathways, whereas further processing of the virus differs slightly among microglial and astroglial cells. Reaching inside and manipulating the nuclear microenvironment of microglial cells takes up to 6 for the virus. During its nuclear hijack process from 6 to 12 hpi, the virus manipulates glycogen and amino acid metabolism in the microglial cells. Later, during 12-24 hpi, the replication and cellular transport processes are still carried on in the cells. Only after 24 hpi viral packaging and egress are initiated in microglial cells. Furthermore, our observations directed toward the probable involvement of molecules related to lipid metabolism in glial cells in EBV-mediated insult on the neural milieu.

Thus, the study aided us in furthering our understanding of the involvement of different biomolecules at various stages of EBV infection progression in the glial cells. With further advances in technology in the future, the application of RS could extend to differentiating the viral infection stages in clinical settings and help in noninvasive and early disease diagnosis. The recent outbreak of SARS-CoV2 has brought forth the importance of such rapid diagnostic tools in detecting virus infection. The temporal and spatial Raman spectroscopic technique appears to be a step toward understanding the viral biology after infection in host cells and also assisting in a comparative analysis of replication kinetics in different cells on infection with multitrophic viruses such as EBV.

Lipid metabolism is one of the cornerstones of CNS functioning. Disturbances in the lipid profile of neuronal or glial cells could cause the brain to behave absurdly, manifesting as various neurological manifestations. As observed in our previous study and recorded through literature, EBV can very well disrupt the lipid metabolism of infected cells. Thus, we tried to study the repercussions of EBV-mediated lipid metabolism manipulation and its probable implications in AD. Though the involvement of EBV in AD development is still debated in the scientific community, recent evidence suggests otherwise. Still, as mentioned previously, the current knowledge about EBV's involvement in mediating AD lacks mechanistic understanding. Besides, an interesting report linking the two implicates ApoE, a well-known genetic risk factor for AD, as a possible element

modulating the outcome of EBV infection in an individual. Interestingly, ApoE is also involved in clearing amyloid- β fragments from the brain, and its defective functioning is linked with disease development. Additionally, several population-based studies have suggested that persistent EBV infection and its timely reactivation increase AD development chances in individuals at later stages of life. Nonetheless, the precise interplay happening between ApoE and EBV is unexplored.

Therefore, in this study, we attempted to examine the possibility of interaction between ApoE and various EBV proteins. For this analysis, we chose to examine the interactions of EBV proteins with ApoE3, the healthy isoform. The current investigation evaluates the interaction of various viral proteins at both the binding sites on ApoE: RBD at the N-terminal and LBD at the C-terminal regions. Our analysis showed that EBV proteins BZLF-1 and EBNA-1 have a higher affinity toward the ligand-binding region at the CTD of ApoE3. Based on our findings, we propose that this interaction of EBV proteins might interfere with ApoE's A β binding capability and hinder its normal functioning. Defective amyloid- β clearance from the brain by ApoE3 could increase the chances of plaque deposition, thereby initiating AD pathogenesis. For the first time, our study suggests a novel interaction between EBV and the host protein strongly implicated in AD development, i.e., ApoE. The current investigation opens up novel avenues of exploration to determine the role of EBV, which has been so far considered only a bystander in AD development.

Though the definitive role of EBV in AD development is still ambiguous, the unavailability of such studies does not necessarily imply a lack of association between the two. Therefore, it is imperative to explore strategies to inhibit the viral life cycle and address the ever-looming threat of its reactivation leading to lethal outcomes. In one of our studies, we investigated and found a phytochemical DHED capable of binding with the viral *dUTPase* enzyme, potentially hindering the viral life cycle. Though, the *in-vitro* potential of the phytochemical is yet to be evaluated.

Conclusively, our studies have successfully established EBV as a potential threat to the CNS, which may converge into AD-associated neurodegenerative changes in the brain in amalgamation with various other factors. We have studied multiple mechanistic aspects of EBV infection, including the virus and virus-

derived peptides mediating the degeneration. The amyloidogenic property of the EBV-derived peptide must be explored further to ascertain its role in AD. Additionally, the biomolecules observed to be manipulated by EBV infection at the cellular level should be evaluated biochemically. In our study, we have come up with a phytochemical with a potential inhibitory effect on an essential EBV enzyme that could halt the viral replication. However, the *in-vitro* efficacy of the same needs to be evaluated.

APPENDIX A

Supplementary Figures

Figure S3.1 Atomic Force Microscopic (AFM) image of the EBV-gM₁₄₆₋₁₅₇ at 250 μ M

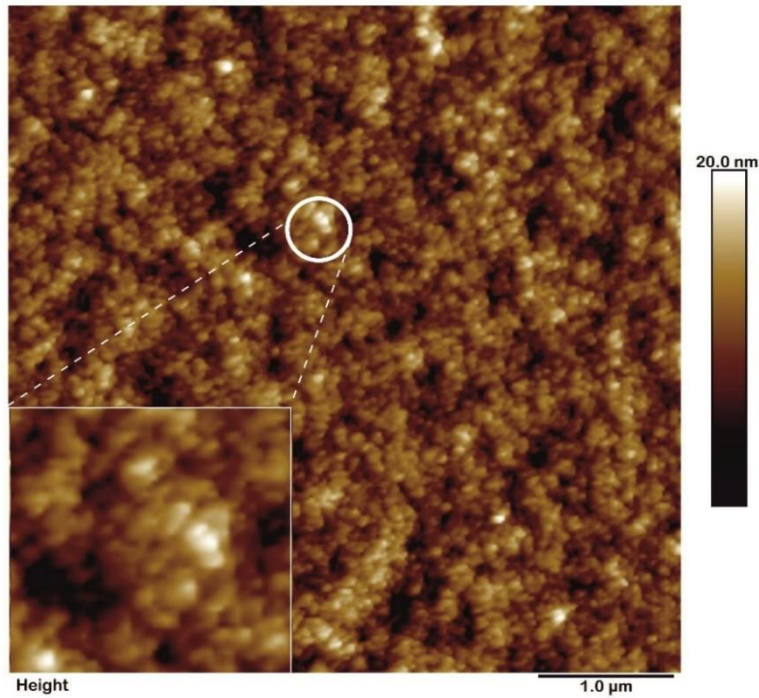


Figure S3. 1 Atomic Force Microscopic (AFM) image of EBV-gM₁₄₆₋₁₅₇ aggregates formed at 250 μ M concentration. The AFM image of the aggregates showing spheroid oligomers formed at 1 μ m scale bar. The inset at lower left corner shows magnified image of the spheroid oligomers.

Figure S3.2 Cytotoxicity of EBV-gM at 48 hours

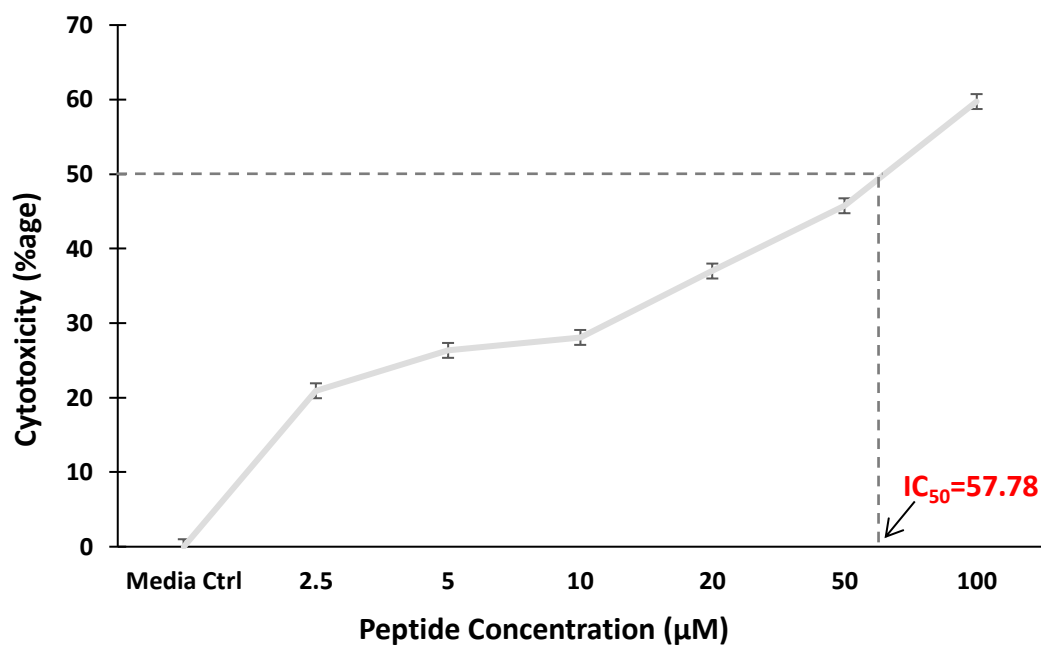
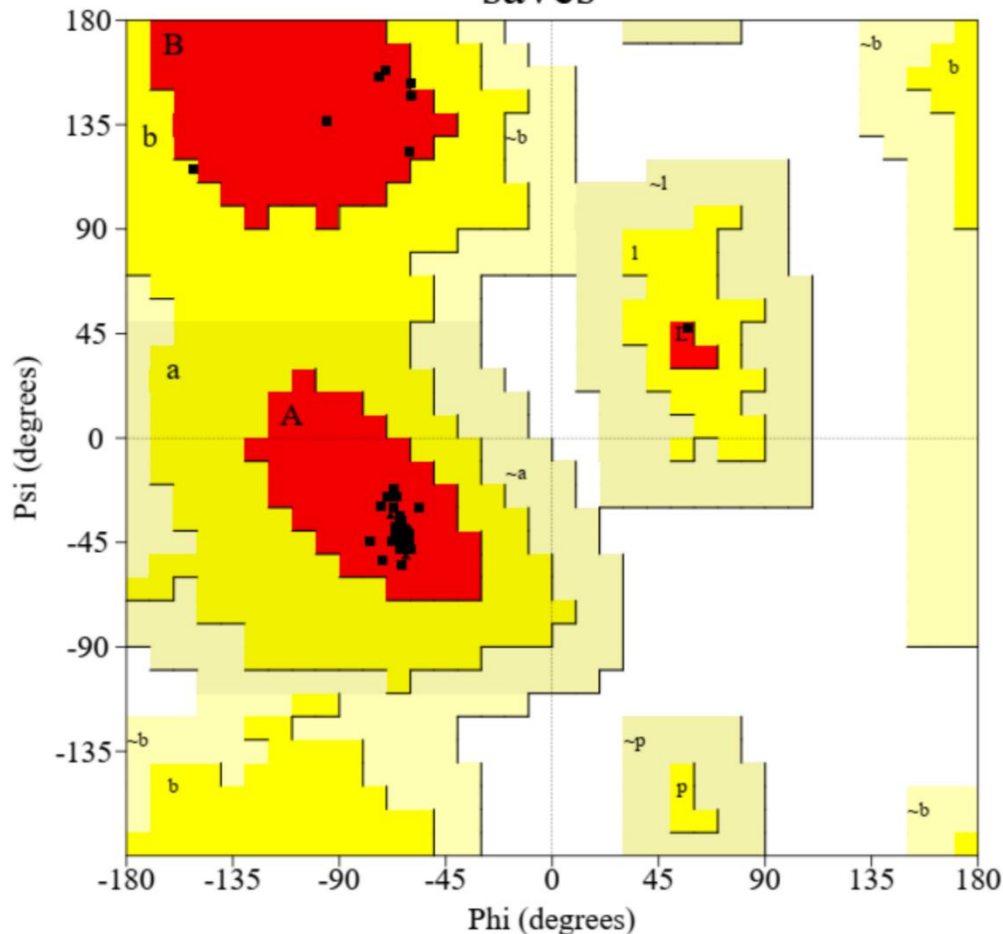


Figure S3. 2 Cytotoxicity of EBV-gM₁₄₆₋₁₅₇ against neuroblastoma cells IMR-32 after 48 hours of incubation. The cytotoxicity analysis using MTT dye revealed TD₅₀ of EBV-gM₁₄₆₋₁₅₇ to be ~58 μM upon 48 hours of incubation.

Ramachandran Plot

saves



Plot statistics

Residues in most favoured regions [A,B,L]	111	99.1%
Residues in additional allowed regions [a,b,l,p]	1	0.9%
Residues in generously allowed regions [-a,-b,-l,-p]	0	0.0%
Residues in disallowed regions	0	0.0%

Number of non-glycine and non-proline residues	112	100.0%
Number of end-residues (excl. Gly and Pro)	1	
Number of glycine residues (shown as triangles)	9	
Number of proline residues	5	

Total number of residues	127	

Based on an analysis of 118 structures of resolution of at least 2.0 Angstroms and R-factor no greater than 20%, a good quality model would be expected to have over 90% in the most favoured regions.

Figure S5. 1. The graph shows almost 99% of the residues lying in the favoured region, implying the acceptability of the modeled structure.

Supplementary Tables

Table S3.1 Average aggregation score of EBV protein sequences, positive and negative control as calculated by TANGO and AGGRESCAN

UniProt ID	Protein Name	TANGO Average aggregation score	AGGRESCAN Average aggregation score
Q9Q2P0	Potein RPMS1	0.00	0.01
Q777D8	Tegument protein G45	0.00	0.01
P03181	BHLF1 early reading frame	0.00	0.00
Q9Q2P1	Protein A73	0.02	0.07
Q8AZK7	EBNA-LP protein	0.03	0.00
Q777F1	Virion protein G52	0.04	0.04
Q8AZJ3	Protein BNLF2b	0.05	0.06
Q777D3	Myristylated tegument protein	0.11	0.14
Q66541	Capsid scaffold protein	0.18	0.04
Q9QCF1	BSLF2 protein	0.19	0.03
	Deoxyuridine 5'-triphosphate nucleotidohydrolase	0.29	0.11
P03195	Deoxyuridine triphosphatase	0.29	0.11
Q777F3	EBNA3C (EBNA 4B) latent protein	0.57	0.04
P03204	Nuclear antigen EBNA-3C	0.57	0.04
Q777E7	Protein G10	0.75	0.11
Q8AZJ5	Protein BLLF2	0.92	0.05
Q777E9	EBNA-2 nuclear protein	1.14	0.05
P12978	Tegument protein UL88	1.17	0.16
Q777C1	Virion protein BBRF1	1.21	0.12
P03213	Capsid portal protein	1.21	0.12
Q777D6	Capsid maturation protease	1.52	0.07
Q777B6	Multifunctional expression regulator	1.66	0.12
Q8AZJ9	Protein SM	1.67	0.12
Q3KSU1.2	Nuclear antigen EBNA-3A	1.73	0.06
Q8AZJ8	Ribonucleoside-diphosphate reductase large chain	1.76	0.12
P03190	Ribonucleotide reductase subunit 1	1.76	0.12
Q777G1	BMLF1 protein	1.80	0.13
Q04360	Capsid assembly protein	1.84	0.10
P03189	Tegument protein UL37	1.84	0.10
Q777G3	Single-stranded DNA-binding protein	1.88	0.11
Q777A7	BZLF1	2.01	0.07
Q777E5	Protein Zta	2.01	0.07
Q777E5	BRLF1	2.05	0.09
Q777E4	Protein Rta	2.05	0.09
Q777E4	Large tegument protein	2.22	0.16
P03186	Large tegument protein deneddylase	2.22	0.16
Q3KSU8.1	DNA polymerase catalytic subunit	2.40	0.13
Q777B1	BBRF2 protein	2.49	0.14
P29882	Tegument protein UL7	2.49	0.14
Q777D5	DNA packaging tegument protein		
Q777C7	UL17	2.51	0.12
Q777G2	Capsid triplex subunit 1	2.68	0.14
Q777G5	Capsid protein VP26	2.71	0.05
P03203	EBNA3B (EBNA4A) latent protein	2.75	0.06

Q777E8	Nuclear antigen EBNA-3B	2.77	0.06
Q777H3	Tegument protein G75	2.78	0.12
Q3KSV4.1	Protein p140	2.81	0.12
P03191	Early antigen protein D	3.00	0.11
Q777F9	DNA polymerase processivity subunit	3.00	0.11
Q777E2	Tegument protein G48	3.09	0.11
Q777G9	BFLF2 protein	3.10	0.13
Q777G9	Nuclear egress lamina protein	3.10	0.13
Q777F0	Glycoprotein 350	3.17	0.08
Q777F0	Envelope glycoprotein gp350	3.17	0.08
Q777G8	DNA packaging protein UL32	3.64	0.17
Q777G8	BFLF1	3.65	0.17
Q777D0	Protein UL95	3.78	0.13
Q777A8	DNA packaging terminase subunit 2	3.79	0.12
Q777F5	Helicase/primase complex protein	3.97	0.15
Q777F4	BSRF1 protein	4.05	0.12
Q777F4	Tegument protein UL51	4.05	0.12
Q777F5	Helicase-primase primase subunit	4.06	0.15
Q777C3	Capsid triplex subunit 2	4.19	0.20
Q777D1	Tegument serine/threonine protein kinase	4.19	0.12
Q8AZJ7	Helicase-primase subunit	4.32	0.12
P03217	Alkaline exonuclease	4.41	0.14
Q777E3	Protein G49	4.52	0.16
P0C722.1	BRRF1	4.52	0.16
Q8AZJ6	Protein UL87	4.74	0.13
Q777G6	BFRF2	5.11	0.14
Q777G6	Protein UL49	5.11	0.14
Q777D7	Helicase-primase helicase subunit	5.17	0.13
Q777B8	Nuclear protein UL24	5.26	0.12
Q777B7	DNA packaging tegument protein UL25	5.91	0.12
P0C706.1	Capsid vertex component 2	5.92	0.12
Q777C4	Envelope glycoprotein 48	6.35	0.15
Q777B0	Envelope glycoprotein B	6.61	0.12
Q777D9	Uracil-DNA glycosylase	6.68	0.15
Q777D9	Uracil-DNA glycosylase	6.68	0.15
P03180	BCRF1 protein precursor	7.35	0.16
Q777H2	Interleukin-10 BCRF1	7.35	0.16
Q777A5	Protein BARF1	7.40	0.20
Q777C8	Tegument protein UL16	7.93	0.18
Q777C6	Protein UL92	8.80	0.21
P0CAP6	Ribonucleoside-diphosphate reductase small chain	8.92	0.17
Q777G0	Ribonucleotide reductase subunit 2	8.92	0.17
Q777E6	Envelope glycoprotein 42	9.28	0.22
Q777G7	BFRF1 protein	9.45	0.14
Q777G7	Nuclear egress membrane protein	9.45	0.14
Q777C9	DNA packaging terminase subunit 1	10.00	0.17
Q777C0	Envelope glycoprotein H	10.28	0.23
Q777C5	Envelope glycoprotein 150	10.51	0.19
Q777A6	Apoptosis regulator BALF1	11.72	0.26
P03182	BHRF1	12.30	0.21
Q777B4	Membrane protein BILF2	12.77	0.23
P03212	Glycoprotein L precursor	14.69	0.29
Q777E0	Envelope glycoprotein L	14.69	0.29
Q777A4	Latent membrane protein LMP-1	25.40	0.37

P03215	Glycoprotein M (gM)	26.24	0.45
Q777F2	Glycoprotein N (gN)	27.36	0.41
Q8AZJ2	Protein BNLF2a	27.89	0.41
Q777F8	Protein BMRF2	29.46	0.49
Q777B2	Membrane protein BILF1	31.67	0.45
P13285	Terminal protein LMP2A	32.00	0.44
P13285	Terminal protein LMP2B	42.05	0.57
CONTROL PROTEINS			
P05067	A-beta 42	36.34	3.61
Q06787	FMRP-1	2.52	0.60

Table S3. 2 Distribution of predicted cleavage sites

UniProt ID, Protein name, prediction method	Residue No – Distribution of predicted cleavage sites	Distribution of the cleavage sites
P03215, EBV-gM, Pcleavage	1- MKSSKNDTFVYRTWVKT LVVYFVMFVMSAVVPITAMFPNLGYPCYFNALV 51- DY GALN L TNYN L AHHL TPTLYLEPPEMFVYITLVFIADCVAFIYYACGEV 101- ALIKARKKVSGLTDL SAW VS AVGS P TV LF LAILKLWSIQVFIQ VL SYKH V 151- FLSAFVYFLHFLASVLHACACVTRFSPVWVKAQDNSIPQDTFLWVVFY 201- LKPVV TNLYLGCLA LET LVFSLSVFLALGNSFYFVMGDMVLGAVNLFLIL 251- PIF WYILTEVWLASFLRHNF GFY CGMFIASIIILPLVRYEAVFVSAKLH 301- TT VAINVAIIPILCSVAMLIRICRIFKSMRQGT DYVPV SETVELELESEP 351- RPRPSRTPSPGRNRRRSSTSSSSSRSTRRQRPVST QALVSSVLPMTT DSE 401- EE I FP	Total cleavage sites = 78 Sites within aggregation prone region = 48 (62%) Sites outside aggregation prone region = 30 (38%)
P03215, EBV-gM, NetChop 3.1	1- MKSSKNDTFVYRTWVKTLVVYFVMFVMSAVVPITAMFPNLGYPCYFNALV 51- DY GALN L TNYN L AHHL TPTLYLEPPEMFVYITLVFIADCVAFIYYACGEV 101- ALIKARKKVSGLTDL SAW VS AVGS P TV LF LAILKLWSIQVFIQ VL SYKH V 151- FLSAFVYFLHFLASVLHACACVTRFSPVWVKAQDNSIPQDTFLWVVFY 201- LKPVV TN LYLGCLA LET LVFSLSVFLALGNSFYFVMGDMVLGAVNLFLIL 251- PIF WYILTEVWLASFLRHNF GFY CGMFIASIIILPLVRYEAVFVSAKLH 301- TT VAINVAIIPILCSVAMLIRICRIFKSMRQGT DYVPV SETVELELESEP 351- RPRPSRTPSPGRNRRRSSTSSSSSRSTRRQRPVSTQALVSSVLPMTT DSE 401- EE I FP	Total cleavage sites = 159 Sites within aggregation prone region = 82 (52%) Sites outside aggregation prone region = 77 (48%)

Table S3. 3 Analysis of aggregation prone consensus sequences as predicted by Amylpred2 in A β ₄₂ and EBV-gM₁₄₆₋₁₅₇

Analysis of Amyloid beta peptide (A β ₁₋₄₂) using Amylpred2

<i>myseq</i>	1	SEVKMDAEFRHDSGYEVHHQKLVFFAEDVGSNKGAIIGLMVGGVVIA	50
CONSENSUS5		-----#####-----#####	
AGGRESCAN		-----#####-----#####	
AmyloidMutants		-----#####-----#####	
Amyloidogenic Pattern		-----#####-----#####	
Average Packing Density		-----#####-----#####	
Beta-strand contiguity		-----#####-----#####	
Hexapeptide Conf. Energy		-----#####-----#####	
NetCSSP		#####-----#####	
Pafig		-----#####-----#####	
SecStr		-----#####-----#####	
TANGO		-----#####-----#####	

Analysis of EBV-gM peptide (EBV-gM₁₄₆₋₁₅₇) using Amylpred2

<i>myseq</i>	1	AILKLWSIQVFIQVLSYKHVFLSAFVYFLHFLASVLHACACVTRFSPVWV	50
CONSENSUS5		#####-----	
AGGRESCAN		#####-----	
AmyloidMutants		#####-----	
Amyloidogenic Pattern		-----#####	
Average Packing Density		#####-----	
Beta-strand contiguity		#####-----	
Hexapeptide Conf. Energy		#####-----	
NetCSSP		#####-----	
Pafig		#####-----	
SecStr		#####-----	
TANGO		#####-----	

*NOTE: “#” denotes the consensus amyloidogenic residues predicted by various algorithms

Table S6. 1 Detailed description of the phytochemicals with anti-viral and neuroprotective properties with binding affinities towards EBV-dUTPase based on molecular docking study.

Sr. No.	Class	Compound Name (mol. wt.)	Molecular formula	Compound identifier (PubChem)	Binding Energy (kCal/mol)
1	Anti-viral ^[1]	Berberine (336.4g/mol)	C ₂₀ H ₁₈ NO ₄ ⁺	CID-2353	-8.4
2	Anti-viral ^[2]	Betulin (442.7g/mol)	C ₃₀ H ₅₀ O ₂	CID-72326	-8.4
3	Anti-viral, anti-inflammatory ^[3] Neuroprotective ^[4]	Ursolic acid (456.7g/mol)	C ₃₀ H ₄₈ O ₃	CID-64945	-8.4
4	Neuroprotective ^[5]	Arjunolic acid (488.7g/mol)	C ₃₀ H ₄₈ O ₅	CID-73641	-8.3
5	Neuroprotective and Anti-viral ^[6]	Memantine (179.3g/mol)	C ₁₂ H ₂₁ N	CID-4054	-8.0
6	Neuroprotective ^[7] Anti-viral ^[8]	Aloe emodin (270.24g/mol)	C ₁₅ H ₁₀ O ₅	CID-10207	-7.7
7	Neuroprotective ^[9]	Huperzine A (242.32g/mol)	C ₁₅ H ₁₈ N ₂ O	CID-44461111	-7.7
8	Anti-inflammatory ^[10]	Rosmarinic acid (360.3g/mol)	C ₁₈ H ₁₆ O ₈	CID-5281792	-7.7
9	Anti-inflammatory ^[11]	Chelerythrine (348.4g/mol)	C ₂₁ H ₁₈ NO ₄ ⁺	CID-2703	-7.6

10	Anti-inflammatory ^[12]	Luteolin (286.24g/mol)	C ₁₅ H ₁₀ O ₆	CID-5280445	-7.6
11	Neuroprotective ^[13]	Morphine (285.34g/mol)	C ₁₇ H ₁₉ NO ₃	CID-5288826	-7.6
12	Anti-inflammatory ^[14] , Anti-viral ^[15] , Neuroprotective ^[16]	Quercetin (302.23g/mol)	C ₁₅ H ₁₀ O ₇	CID-5280343	-7.6
13	Neuroprotective ^[17] , Anti-inflammatory and Anti-viral ^[18]	Indirubin (262.26g/mol)	C ₁₆ H ₁₀ N ₂ O ₂	CID-10177	-7.5
14	Anti-inflammatory ^[19]	beta-Sitosterol (414.7g/mol)	C ₂₉ H ₅₀ O	CID-222284	-7.5
15	Anti-inflammatory ^[20]	Coronopilin (264.32g/mol)	C ₁₅ H ₂₀ O ₄	CID-257278	-7.5
16	Neuroprotective ^[21]	Myricetin (318.23g/mol)	C ₁₅ H ₁₀ O ₈	CID-5281672	-7.5
17	Anti-inflammatory ^[22]	Apigenin (270.24g/mol)	C ₁₅ H ₁₀ O ₅	CID-5280443	-7.4
18	Anti-inflammatory ^[23] , Neuroprotective ^[24]	Galangin (270.24g/mol)	C ₁₅ H ₁₀ O ₅	CID-5281616	-7.3
19	Neuroprotective ^[25]	Isoquercitrin (464.4g/mol)	C ₂₁ H ₂₀ O ₁₂	CID-5280804	-7.3
20	Neuroprotective, Anti-viral, Anti- inflammatory ^[26]	Wogonin (284.26g/mol)	C ₁₆ H ₁₂ O ₅	CID-5281703	-7.3
21	Anti-inflammatory ^[27]	Emodin (270.24g/mol)	C ₁₅ H ₁₀ O ₅	CID-3220	-7.2

22	Anti-inflammatory, Anti-viral, Neuroprotective ^[28]	Formononetin (268.26g/mol)	C ₁₆ H ₁₂ O ₄	CID-5280378	-7.1
23	Anti-viral ^[29]	Perivine (338.4g/mol)	C ₂₀ H ₂₂ N ₂ O ₃	CID-6473766	-7.1
24	Anti-viral ^[30]	Pentamethoxyflavone (PMF) (404.4g/mol)	C ₂₀ H ₂₀ O ₉	CID-13942677	-6.9
25	Neuroprotective ^[31]	Galanthamine (287.35g/mol)	C ₁₇ H ₂₁ NO ₃	CID-9651	-6.8
26	Anti-inflammatory ^[32]	Oxyresveratrol (244.24g/mol)	C ₁₄ H ₁₂ O ₄	CID-5281717	-6.7
27	Antiviral ^[33]	Harmine (212.25g/mol)	C ₁₃ H ₁₂ N ₂ O	CID-5280953	-6.5
28	Neuroprotective ^[34] , Anti-inflammatory and Anti-viral ^[35]	Curcumin (368.4g/mol)	C ₂₁ H ₂₀ O ₆	CID-969516	-6.4
29	Neuroprotective ^[36]	Hyperforin (536.8g/mol)	C ₃₅ H ₅₂ O ₄	CID-441298	-6.4
30	Antiviral ^[37]	Hypericin (504.4g/mol)	C ₃₀ H ₁₆ O ₈	CID- 3663	-6.4
31	Neuroprotective ^[38]	Tacrine (198.26g/mol)	C ₁₃ H ₁₄ N ₂	CID-1935	-6.3
32	Neuroprotective ^[39]	Resveratrol (228.24g/mol)	C ₁₄ H ₁₂ O ₃	CID-445154	-6.3
33	Antiviral ^[40]	Caffeic acid (180.16g/mol)	C ₉ H ₈ O ₄	CID-689043	-6.1

34	Anti-inflammatory ^[41]	Zingiberene (204.35g/mol)	C ₁₅ H ₂₄	CID-92776	-6.1
35	Anti-inflammatory ^[42]	Coumarin (146.14g/mol)	C ₉ H ₆ O ₂	CID-323	-6
36	Anti-inflammatory ^[43]	Embelin (294.4g/mol)	C ₁₇ H ₂₆ O ₄	CID-3218	-5.6
37	Neuroprotective ^[44]	Nicotine (162.23g/mol)	C ₁₀ H ₁₄ N ₂	CID-86594	-5.6
38	Anti-inflammatory ^[45]	Linalool (154.25g/mol)	C ₁₀ H ₁₈ O	CID-6549	-5
39	Anti-inflammatory ^[46]	Ajoene (234.4g/mol)	C ₉ H ₁₄ OS ₃	CID-5386591	-3.8
40	Antiviral ^[47]	Allicin (162.3g/mol)	C ₆ H ₁₀ OS ₂	CID-65036	-3.8
